INVESTIGATIONS ON BULK GLASS FORMING ABILITY OF TITANIUM BASED MULTICOMPONENT ALLOYS

A THESIS SUBMITTED TO
THE GRADUATE SCHOOL OF NATURAL AND APPLIED SCIENCES
OF
MIDDLE EAST TECHNICAL UNIVERSITY

BY

SILA SÜER

IN PARTIAL FULFILLMENT OF THE REQUIREMENTS FOR THE DEGREE
OF
MASTER OF SCIENCE
IN
METALLURGICAL AND MATERIALS ENGINEERING

JUNE 2008

Approval of the thesis:

INVESTIGATIONS ON BULK GLASS FORMING ABILITY OF TITANIUM BASED MULTICOMPONENT ALLOYS

Submitted by **SILA SÜER** in partial fulfillment of the requirements for the degree of **Master of Science in Metallurgical and Materials Engineering Department, Middle East Technical University** by,

Prof. Dr. Canan Özgen _____
Dean, Graduate School of **Natural and Applied Sciences**

Prof. Dr. Tayfur Öztürk _____
Head of Department, **Metallurgical and Materials Engineering**

Prof. Dr. Amdulla O. Mekhrabov _____
Supervisor, **Metallurgical and Materials Eng. Dept., METU**

Prof. Dr. M. Vedat Akdeniz _____
Co-supervisor, **Metallurgical and Materials Eng. Dept., METU**

Examining Committee Members:

Prof. Dr. C. Hakan GÜR _____
Metallurgical and Materials Eng. Dept., METU

Prof. Dr. Amdulla O. MEKHRABOV _____
Metallurgical and Materials Eng. Dept., METU

Prof. Dr. M. Vedat AKDENİZ _____
Metallurgical and Materials Eng. Dept., METU

Assist. Prof. Dr. Kazım TUR _____
Materials Eng. Dept., Atılım University

Assist. Prof. Dr. Caner DURUCAN _____
Metallurgical and Materials Eng. Dept., METU

Date: 19.06.2008

I hereby declare that all information in this document has been obtained and presented accordance with the academic rules and ethical conduct. I also declare that, as required by these rules and conduct, I have fully cited and referenced all material and results that are not original to this work.

Name, Last name : Sıla Süer

Signature :

ABSTRACT

INVESTIGATIONS ON BULK GLASS FORMING ABILITY OF TITANIUM BASED MULTICOMPONENT ALLOYS

Süer, Sıla

M.S., Department of Metallurgical and Materials Engineering

Supervisor : Prof. Dr. Amdulla O. Mekhrabov

Co-Supervisor: Prof. Dr. M. Vedat Akdeniz

June 2008, 156 pages

The aim of this study is to investigate the bulk glass forming ability (BGFA) of Ti-based alloy systems. These investigations were carried out in two main parts that are complementary to each other: theoretical and experimental.

For theoretical studies, which are based on electronic theory of alloys in pseudopotential approximation, Ti-Zr, Ti-Co and Ti-Cu alloys were chosen as the binary systems. Alloying element additions were performed to each binary for the investigation of the BGFA of multicomponent Ti-based alloys. Among the three studied binary systems, Ti-Cu was found to exhibit better BGFA, and Mn, Al and Ni elements were found to be suitable for improving the BGFA of Ti-Cu binary alloy system.

BGFA of Ti-Cu binary and Ti-Cu-(Mn, Al, Ni) multicomponent alloys were investigated with the experimental studies that were carried out with performing arc melting and centrifugal casting operations. The characterizations of these alloys were done with scanning electron microscopy, X-ray diffraction analysis and

differential scanning calorimetry. $Ti_{60}Cu_{35}Mn_5$, $Ti_{60}Cu_{35}Al_5$ and $Ti_{60}Cu_{35}Ni_5$ alloys were produced and characterized as examples for ternary systems. Among them, $Ti_{60}Cu_{35}Mn_5$ system was found to have better indications regarding to BGFA. Therefore, it was chosen as the main composition and multicomponent alloys of $Ti_{59}Cu_{35}Mn_5Al_1$, $Ti_{59}Cu_{35}Mn_5Ni_1$ and $Ti_{58}Cu_{35}Mn_5Al_1Ni_1$ were synthesized and characterized.

Keywords: Ti-Based Alloys, Bulk Metallic Glasses, Pseudopotential Theory, Glass Forming Ability, Critical Cooling Rate

ÖZ

TİTANYUM BAZLI ÇOK BİLEŞENLİ ALAŞIMLARIN
İRİ VE HACİMLİ CAM OLUŞTURMA EĞİLİMİNİN İNCELENMESİ

Süer, Sıla
Y. Lisans, Metalurji ve Malzeme Mühendisliği Bölümü
Tez Yöneticisi : Prof. Dr. Amdulla O. Mekhrabov
Ortak Tez Yöneticisi: Prof. Dr. M. Vedat Akdeniz

Haziran 2008, 156 sayfa

Bu çalışmanın amacı Ti-bazlı alaşım sistemlerinin iri ve hacimli cam oluşturma eğilimini incelemektir. Bu incelemeler teorik ve deneysel olacak şekilde birbirini tamamlayan iki kısımdan oluşmaktadır.

Alaşımların psödopotansiyel yaklaşımdaki elektronik teorisine dayanan teorik çalışmalar esnasında Ti-Zr, Ti-Co ve Ti-Cu ikili alaşım sistemleri incelenmiştir. Çok bileşenli Ti-bazlı alaşımların iri ve hacimli cam oluşturma eğilimini inceleyebilmek için her ikili sisteme çeşitli alaşım elementleri eklenmiştir. Çalışılmış olan sistemler arasında, Ti-Cu sisteminin en iyi iri ve hacimli cam oluşturma eğilimini sergilediği gözlemlenmiş ve bu sistemin cam oluşturma eğilimini arttırabilmek için Mn, Al ve Ni elementlerinin kullanılabileceği gösterilmiştir.

Ti-Cu ikili ve Ti-Cu-(Mn, Al, Ni) çoklu alaşımların iri ve hacimli cam oluşturma eğilimi, ark ile ergitme ve savurmalı döküm yöntemleriyle deneysel olarak incelenmiştir. Bu alaşımların karakterizasyonu ise taramalı elektron mikroskopisi, X-ışınları kırınımı ve termal analiz yöntemleriyle gerçekleştirilmiştir. $Ti_{60}Cu_{35}Mn_5$,

$Ti_{60}Cu_{35}Al_5$ ve $Ti_{60}Cu_{35}Ni_5$ alaşımları üçlü alaşımlara örnek olarak üretilmiş ve karakterize edilmiştir. Bu üç sistemin arasında $Ti_{60}Cu_{35}Mn_5$ alaşımının daha iyi iri ve hacimli cam oluşturma eğilimi gösterdiği belirlenmiştir. Bu sebeple bu üçlü sistem ana kompozisyon olarak seçilmiş ve $Ti_{59}Cu_{35}Mn_5Al_1$, $Ti_{59}Cu_{35}Mn_5Ni_1$ ve $Ti_{58}Cu_{35}Mn_5Al_1Ni_1$ çoklu alaşımları üretilmiş ve incelenmiştir.

Anahtar Kelimeler: Ti-Bazlı Alaşımlar, İri ve Hacimli Metalik Camlar, Psödopotansiyel Teori, Cam Oluşturma Eğilimi, Kritik Soğuma Hızı

To My Parents

ACKNOWLEDGEMENTS

I would like to express my sincere gratefulness to my supervisor Prof. Dr. Amdulla O. Mekhrabov and my co-supervisor Prof. Dr. M. Vedat Akdeniz for their guidance, patience, encouragement and valuable discussions.

I must thank to my friends from Noval Alloys Laboratory; Nagehan Duman for her friendship and kindness, Muratahan Aykol for his helps during experiments, Cem Topbaşı for his support and motivation, Mehmet Yıldırım for his suggestions and discussions, and Ozan Özkan for being helpful and kind. They made my lab days cheerful and bright. I must also thank to Selen N. Gürbüz and Sultan Aybar for their helps and encouragement.

I would also like to send my special thanks to my dear friends Yankı Başaran and Ali Erdem Eken for always cheering me up and helping me during the continuation of this study.

I am also grateful to my family and especially to Oray B. Güngör for their endless love and support. Without their presence, the completion of this thesis would not be possible.

TABLE OF CONTENTS

CHAPTER 1

INTRODUCTION

Metallic glasses are so called due to their glassy like crystal structure. Ordinary crystalline alloys exhibit periodicity in three dimensions, whereas metallic glasses have no long range order resulting in surpassing properties when compared to the crystalline counterparts. Hence, metallic glasses have begun to be the midpoint of interest.

The most crucial point in the formation of metallic glasses is the cooling rate. Fast cooling rates should be achieved to obtain the amorphous structure, since suppression of the crystalline phases is attained by limiting their formation time. Generally, metallic glasses are obtained with critical cooling rates on the order of 10^5-10^7 K/s. Due to the requirement for rapid cooling; metallic glasses were usually synthesized in a thin sheet form having a thickness below 0.05 mm. So, in order to overcome the restrictions in shape and dimensions of the alloys, scientists started to search for a new way. This was achieved by synthesizing the alloys in multicomponent forms. By using multicomponent alloys, maintenance period of the supercooled liquid state was extended for several thousand of a second which is 6 to 8 orders longer than that of the ordinary metallic glasses. As a result, critical cooling rates of the bulk metallic glasses were decreased to values ranging between as low as 0.100 K/s and several hundreds of K/s [1-3].

Since the discoveries of a series of glassy alloys with large glass forming ability in Ln-Al-TM, Mg-Ln-TM, Zr-Al-TM, Ti-Zr-TM, Hf-Al-TM, Ti-Zr-Al-Be-TM, and Ti-Zr-Be-TM (Ln = lanthanide metals, TM = transition metals) systems, bulk metallic glasses have attracted rapidly increasing interest because of the importance

in both the scopes of materials science and engineering applications [4-13]. Bulk metallic glasses have a wide range of interesting properties, including near theoretical strength, high hardness, extremely low damping characteristics, excellent wear properties, high corrosion resistance and low shrinkage during cooling. Titanium based bulk amorphous alloys especially began to attract the attention of the scientists and engineers recently due to their high specific strength, good corrosion resistance and high temperature properties [14-19].

In recent years, solidification behavior of alloys was shown to be important for the selection of the bulk glass forming alloys systems. Alloys containing a sequence of two successive endothermic reactions; eutectic and peritectic, with a high magnitude of reaction enthalpies ratio were indicated to be essential for high bulk glass forming ability [20].

This thesis study is consisted of two main parts that are complimentary to each other. First part is the theoretical studies that were performed to understand the bulk glass forming ability of multicomponent alloy systems, and the second part is the experimental investigations on the alloy systems that were predicted with the theoretical studies. Theoretical part of the thesis deals with glass forming ability of selected Ti-based binary alloys; Ti-Zr, Ti-Co and Ti-Cu, on the base of the electronic theory of alloys in pseudopotential approximation. Moreover, this part also includes the studies on the effects of ternary alloying element additions to the binary systems, as well as the computations of the related glass forming ability parameters.

The results of the theoretical studies for the mentioned binary alloy systems showed that Ti-Cu has the best glass forming ability when compared to the others, and Mn, Al and Ni elements have the most positive effects on the glass forming ability of Ti-Cu binary system. Hence, Ti-Cu binary system was chosen as the master alloy and Mn, Al and Ni elements additions were performed to this binary. Afterwards, bulk glass forming ability of these alloy systems was experimentally investigated. The

alloys were synthesized with using high purity elements via arc melting method to obtain a more uniform structure. In order to investigate the fast cooling conditions, all the arc melted alloys were cast into Cu-molds with using centrifugal casting method. For characterization of the alloys, SEM, EDS, XRD and DSC techniques were used and effects of fast and non-equilibrium cooling conditions on the bulk glass forming ability of the multicomponent alloys were investigated. The alloying elements that were obtained with the theoretical calculations were found to enhance the glass forming ability of Ti-Cu binary system.

This thesis is composed of five chapters. In the first chapter, a brief introduction to glass forming ability and bulk metallic glasses is presented. The second chapter contains information about the historical background of metallic glasses, their properties, theories of glass formation, order in binary and multicomponent liquid alloys, and pseudopotential theory. Third chapter is related to the procedures performed during the theoretical and experimental studies. Fourth chapter presents the results and discussions about the theoretical and also the experimental investigations. The last chapter, chapter five, points out the important conclusions drawn from this study.

CHAPTER 2

THEORY

2.1 Historical Background

Metallic glasses were first synthesized over four decades ago. The first metallic glass, Au-Si alloy, produced with fast cooling from liquid state was reported by Duwez in 1960 [21]. What was obtained from this study is that, preventing nucleation and growth of the crystalline phases could be achieved by using fast cooling rates on the order of 10^5-10^6 K/s. After the first synthesis of the Au-Si amorphous alloy, a great deal of interest focused on those materials. Cohen and Turnbull suggested that, in order to obtain a favorable condition for glass formation, alloy of a metal and a semimetal having a eutectic point at a rather low temperature compared to that of the metal should be used [22]. By considering this condition, Pd-Si alloy with Si concentration around 20 at % was chosen for investigation and amorphous Pd-Si alloy was produced [23]. In 1967, the first strongly ferromagnetic metallic glass, $Fe_{75}P_{15}C_{10}$ alloy, was synthesized [24]. Up to 1967 it was believed that a metal and a semimetal should be used in order to obtain a metallic glass. However by the studies of Ruhl et al., it was seen that using a semimetal is not a necessity; since the alloys of Nb and Ta with Ni have been reported to be amorphous [25]. During early 1970s, $Pd_{40}Ni_{40}P_{20}$ and $Pd_{76}Cu_6Si_{18}$ amorphous alloys were produced in the bulk form having diameters up to 3 mm and 0.3 mm respectively [26, 27]. In 1975, the first superconducting amorphous alloy, $La_{80}Au_{20}$ which exhibits a transition temperature of 3.5 K was produced [28].

In 1980s, Inoue's group discovered new amorphous alloy systems that mainly consist of rare earth elements. During studies of these systems, outstanding glass

forming ability (GFA) was found in La-Al-Ni and La-Al-Cu alloys [29]. Rod specimens having diameters that reach up to 5 mm were prepared by copper mold casting of $La_{55}Al_{25}Ni_{20}$ alloy. Afterwards, Inoue's group synthesized glassy alloys of Mg-Cu-Y and Mg-Ni-Y systems [7]. Moreover in the same year, they also found Zr-Al-Ni-Cu alloys to have high GFA with a critical section thickness ranging up to 15 mm [30].

In 1993, a well known quinary alloy was developed by Peker and Johnson [6]. $Zr_{41.2}Ti_{13.8}Cu_{12.5}Ni_{10}Be_{22.5}$ known as Vitreloy 1 (Vit 1) was cast with a critical casting thickness reaching up to several centimeters. In 1997, $Pd_{40}Ni_{40}P_{20}$ alloy system was studied by Inoue's group with the replacement of 30% Ni by Cu. This study made a great improvement in the BGFA of the alloy with increasing the critical casting thickness to 72 mm [31].

Table 2.1 demonstrates the bulk metallic glass systems together with their production years [8]. As seen, cheaper systems were produced in time with including more elements, since it was discovered that expensive elements are not necessary for the formation of bulk metallic glasses.

Table 2.1 Bulk metallic glasses and their production years [8].

BMG System	Year
Pd-Cu-Si	1974
Pt-Ni-P	1975
Au-Si-Ge	1975
Pd-Ni-P	1982
Mg-Ln-Cu (Ln = Lanthanide metal)	1988
Ln-Al-TM (TM = Transition group metal)	1989
Zr-Ti-Al-TM	1990
Ti-Zr-TM	1993
Zr-Ti-Cu-Ni-Be	1993
Nd(Pr)-Al-Fe-Co	1994
Zr-(Nb, Pd)-Al-TM	1995
Cu-Zr-Ni-Ti	1995
Fe-(Nb, Mo)-(Al, Ga)-(P, C, B, Si, Ge)	1995
Pd-Cu(Fe)-Ni-P	1996
Co-(Al, Ga)-(P, B, Si)	1996
Fe-(Zr, Hf, Nb)-B	1996
Co-Fe-(Zr, Hf, Nb)-B	1996
Ni-(Zr, Hf, Nb)-(Cr, Mo)-B	1996
Ti-Ni-Cu-Sn	1998
La-Al-Ni-Cu-Co	1998
Ni-Nb	1999
Ni-(Nb, Cr, Mo)-(P, B)	1999
Zr-based glassy composites	1999
Zr-Nb-Cu-Fe-Be	2000
Fe-Mn-Mo-Cr-C-B	2002
Ni-Nb-(Sn, Ti)	2003
Pr(Nd)-(Cu, Ni)-Al	2003

2.2 Bulk Metallic Glasses and Their Properties

Lately, metallic glasses gained considerable attention because of the invention of new metallic glass compositions having critical cooling rates less than 100 K/s and critical casting thicknesses on the order of centimeters. Metallic glasses show very high resistance to crystallization upon cooling, hence the development of these alloys give rise to essential study of bulk metallic glass formation.

Metallic glasses are similar to ordinary oxide glasses with having non-crystalline atomic arrangement and glass transition temperature. However, they differ from oxide glasses with their non-brittle and non-transparent behavior. Moreover, metallic glasses do not usually contain oxides as oxide glasses. Due to the high degree of atomic disorder in their structures, metallic glasses display unusual combinations of mechanical, physical, chemical and magnetic properties that generally result in superior features when compared to crystalline alloys.

Unlike traditional metals, metallic glasses do not display work hardening, hence exhibiting simultaneous yielding and fracture. They are not very ductile when exposed to tension (usually less than 1%), but they are highly ductile under bending conditions. Density of metallic glasses is about 2% lower, shear and Young's moduli are about 20-30% less than their crystalline counterparts and fracture toughness values are two orders of magnitude higher than those of oxide glasses [1].

Room temperature electrical resistivity of metallic glasses is about 200 μΩcm and they have small temperature coefficient which can be positive, negative, or even zero depending on the composition. Electrical resistivity of metallic glasses increases rapidly below a certain temperature which makes them an appropriate choice for low temperature thermometers. Moreover, due to having high and almost constant resistance with changing temperature, metallic glasses can also be used as resistance standards [1].

Magnetic properties of metallic glasses were deeply investigated by the researchers. It was found that, they can be easily magnetized at very low field strengths, have high saturation magnetization and very high permeability. Moreover they are extremely hard, which means they overcome the disadvantage of soft magnetic materials that are mechanically soft [1].

Metallic glasses are homogeneous single phase amorphous materials with having no crystal defects such as grain boundaries, dislocations and second phase particles. Due to this property, metallic glasses have a very high corrosion resistance, even higher than that of conventional stainless steels. They also have good wear resistance and high reactivity [1].

Brief comparison of the several properties of metallic glasses with traditional metals and glasses are present in Table 2.2 [1].

Table 2.2 Comparison of the properties of metallic glasses with traditional metals and traditional glasses [1].

Property	Traditional Metal	Traditional Glass	Metallic Glasses
Structure	Crystalline	Amorphous	Amorphous
Bonding	Metallic	Covalent	Metallic
Yield Stress	Non-ideal	Almost ideal	Almost ideal
Workability	Good, ductile	Poor, brittle	Good, ductile
Hardness	Low to high	Very high	Very high
UTS	Low to high	Low	High to very high
Optical Transmission	Opaque	Transparent	Opaque
Thermal Conductivity	Very good	Poor	Very good
Resistance	Very low	High	Very low
Corrosion Resistance	Poor to good	Very good	Very good
Magnetic Properties	Various	Non-existent	Various

In time, metallic glasses were started to be produced in bulk form, enabling easier measurements of various properties and usage in structural applications.

Up to now, several techniques were developed for producing bulk metallic glasses. Several guiding ideas were used in these techniques; one of which is using elements with different atomic sizes to obtain a more complex structure that resists crystallization [8]. Another idea is finding system compositions involving deep eutectics having liquids stable at relatively low temperatures [32]. Bulk metallic glasses can be produced by many techniques such as water quenching, copper mold casting, high pressure die casting, unidirectional melting, suction casting and squeeze casting.

Due to the superior properties of bulk metallic glasses, they can be used in various application fields as engineering materials. These expected application fields are listed in Table 2.3 [4].

Table 2.3 Some of the application fields of bulk metallic glasses that are expected to be used as engineering materials [4].

Fundamental Characteristic	**Application Field**
High fracture toughness	Die materials
High impact fracture energy	Tool materials
High fatigue strength	Cutting materials
High elastic energy	Electrode materials
High reflection ratio	Composite materials
High magnetostriction	Bonding materials
High frequency permeability	Sporting good materials
High wear resistance	Hydrogen storage materials
High strength	Machinery structural materials
High corrosion resistance	Corrosion resistant materials
Efficient electrode	Soft magnetic materials

2.2.1 Ti-Based Bulk Metallic Glasses and Their Properties

Great deal of attention was paid to Ti-based metallic glasses due to their high specific strength [33-36]. Improvement of Ti-based bulk metallic glasses having higher specific strength and lower density is necessary for the expansion of application fields of bulk metallic glasses. Moreover, these alloys possess relatively high corrosion resistance at room temperature. On the other hand, there is a major disadvantage of Ti-based metallic glasses; they are very reactive at elevated temperatures due to the nature of titanium. This property causes problems during the production of Ti-based metallic glasses by hindering the achievement of exact alloy composition.

First Ti-based metallic glass was reported as early as 1977 [33], whereas, first Ti-based bulk metallic glass was observed by Peker and Johnson in 1994 in Ti-Zr-Ni-Be system [37]. By considering main compositions, Ti-based bulk metallic glasses can be classified into three groups: Ti-Cu-Ni [38-40]; Ti-Cu-Ni-Sn [41] and Ti-Cu-Ni-Si-B [42]. Recently, Be has also been added into these Ti-based bulk metallic glass forming alloys [43, 44].

Generally, in order to obtain high glass forming ability in alloys, large undercooled liquid region, ΔT_x, is required; where ΔT_x is the temperature range between glass transition T_g and onset of crystallization T_x. Ti-rich amorphous alloys, showing an undercooled liquid region have been observed in several systems such as: Ti-Ni-Cu [45], Ti-Be-Zr [46] and Ti-Ni-Cu-Al [40]. However, magnitude of ΔT_x in those alloy systems was not large. In time, large values of ΔT_x (>50 K) were reported in Ti-Cu-Ni-Sn amorphous alloys. Zhang et al. declared a large value of ΔT_x (60 K) in the $Ti_{50}Cu_{25}Ni_{20}Sn_5$ amorphous alloy [41]. Fully amorphous $Ti_{50}Cu_{32}Ni_{15}Sn_3$ rod with diameter of 1 mm [47] and $Ti_{50}Cu_{25}Ni_{15}Sn_3Be_7$ rod with a diameter up to 3 mm [43] were fabricated by injection casting into a copper mold. In 2001, Zhang and Inoue modified this system and produced $Ti_{50}Ni_{24}Cu_{20}B_1Si_2Sn_3$ alloy with a diameter of 1 mm and a supercooled liquid region over 70 K [48]. In 2004, Kim et

al. replaced Cu by Be and Ti by Zr in Ti-Cu-Ni-Sn alloy with considering atomic sizes and interaction parameters between constituent elements [49]. They fabricated fully amorphous rods of diameters 2, 5 and 8 mm by injection casting $Ti_{50}Cu_{25}Ni_{15}Sn_3Be_7$, $Ti_{45}Cu_{25}Ni_{15}Sn_3Be_7Zr_5$ and $Ti_{40}Zr_{25}Ni_8Cu_9Be_{18}$ alloys respectively. These bulk amorphous alloys were found to exhibit high compressive strengths around 2500 MPa with good ductility. Table 2.4 summarizes the maximum diameter (d) and production method of recently produced Ti-based bulk metallic glasses.

Table 2.4 Recently produced examples of Ti-based bulk metallic glasses, together with the maximum diameter (d) and production method.

Alloy	d	Production Method	Ref. No.
$Ti_{50}Cu_{20}Ni_{24}B_1Si_2Sn_3$	1 mm	Copper Mold Casting	[48]
$Ti_{50}Cu_{32}Ni_{15}Sn_3$	1 mm	Injection Casting into Copper Mold	[47]
$Ti_{50}Cu_{25}Ni_{15}Sn_3Be_7$	3 mm	Injection Casting	[43]
$Ti_{45}Cu_{25}Ni_{15}Sn_3Be_7Zr_5$	5 mm	Injection Casting	[50]
$Ti_{40}Zr_{25}Ni_8Cu_9Be_{18}$	8 mm	Injection Casting	[49]
$Ti_{41.5}Zr_{2.5}Hf_5Cu_{42.5}Ni_{7.5}Si_1$	5 mm	Copper Mold Casting	[51]
$Ti_{53}Cu_{15}Ni_{18.5}Al_7Si_3Sc_3B_{0.5}$	2 mm	Copper Mold Casting	[52]
$Ti_{53}Cu_{15}Ni_{18.5}Al_7Si_3Hf_3B_{0.5}$	2 mm	Copper Mold Casting	[52]
$Ti_{53}Cu_{15}Ni_{18.5}Al_7Si_3Ta_3B_{0.5}$	2 mm	Copper Mold Casting	[52]
$Ti_{53}Cu_{15}Ni_{18.5}Al_7Si_3Nb_3B_{0.5}$	2 mm	Copper Mold Casting	[52]
$Ti_{53}Cu_{27}Ni_{12}Zr_3Al_7Si_3B_1$	2 mm	Ejection Casting into Copper Mold	[5]
$Ti_{50}Cu_{42}Ni_8$	2 mm	Copper Mold Casting	[16]
$(Ti_{40}Zr_{25}Be_{20}Cu_{12}Ni_3)_{99.5}Y_{0.5}$	5 mm	Injection Casting into Copper Mold	[53]
$Ti_{50}Cu_{25}Ni_{20}Sn_5$	-	Spark Plasma Sintering	[54]
$Ti_{45}Zr_5Cu_{45}Ni_5$	3 mm	Copper Mold Casting	[17]
$Ti_{41.5}Zr_{2.5}Hf_5Cu_{37.5}Ni_{7.5}Si_1Sn_5$	6 mm	Drop Casting into Copper Mold	[55]

2.3 Theory of Glass Formation

2.3.1 Glass Forming Ability & Related Parameters

Choosing correct elements in order to produce bulk metallic glasses is a necessary concept to be understood. By that correct choices, metallic glasses with critical cooling rates as low as 100 K/s can be obtained. Due to these slow cooling rates, larger pieces of metallic glasses can be manufactured. Hence, for understanding the origins of glass formation and designing and developing new bulk metallic glasses, glass forming ability (GFA) should be investigated. Glass forming ability is related to the critical cooling rate, which is the cooling rate necessary for preventing crystallization of the melt during solidification, hence obtaining an amorphous structure. For a better glass forming ability, critical cooling rate should be as low as possible. Figure 2.1 illustrates the schematic time temperature transformation (TTT) diagram of structure formation during quenching from liquid state [56]. If the critical cooling rates of systems could be obtained easily, it would be very beneficial for the determination of glass forming ability. However, it is very difficult to measure the critical cooling rate precisely. As a result, many related parameters were suggested to explain glass forming ability.

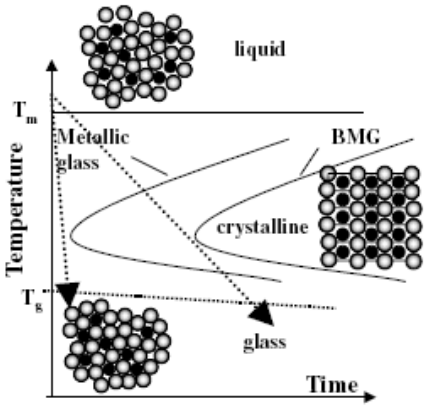

Figure 2.1 Schematic time temperature transformation diagram of structure formation during quenching from the melt [56].

2.3.1.1 Reduced Glass Transition Temperature (T_{rg})

Reduced glass transition temperature is the ratio of the glass transition temperature T_g to the liquidus temperature T_l:

$$T_{rg} = \frac{T_g}{T_l} \tag{2.1}$$

This ratio was proposed for the requirement that viscosity must be large at a temperature between T_g and T_l. The higher the ratio T_g/T_l, the higher is the viscosity at the nose of time temperature transformation (TTT) and continuous cooling transformation (CCT) curves, with the viscosity at T_g being constant. As a result, the smaller will be the critical cooling rate. This is said to be the reason of the high probability of glass formation near eutectic compositions. Values of T_{rg} are usually between 0.6 and 0.7 for bulk metallic glasses. The critical cooling rate and reduced glass transition temperature of conventional metallic glasses, silicate glasses and bulk metallic glasses are compared in Figure 2.2 [56].

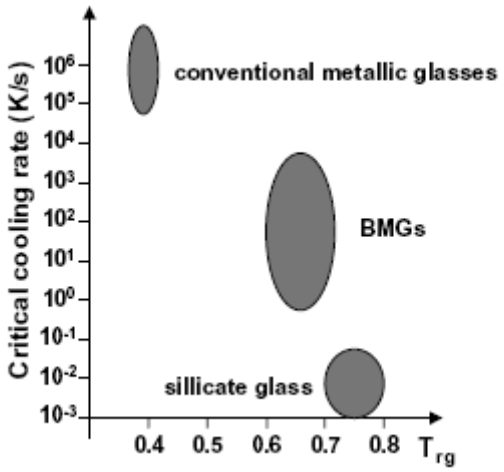

Figure 2.2 Critical cooling rate versus reduced glass transition temperature T_{rg} for conventional metallic glasses, silicate glasses and bulk metallic glasses [56].

2.3.1.2 Supercooled Liquid Region

Supercooled liquid region ΔT_x is the interval between the glass transition temperature T_g and onset crystallization temperature T_x [57]:

$$\Delta T_x = T_x - T_g \tag{2.2}$$

This temperature interval is considered as an empirical indicator of glass forming ability. ΔT_x is an indication about the devitrification tendency of a glass that is heated above T_g. A large ΔT_x value may point out that the supercooled liquid can exist in a wide interval without being crystallized and with having resistance to the nucleation and growth of any crystalline phase. Since crystallization and glass formation are opposing mechanisms, a large ΔT_x is expected for higher glass forming ability. Hence, in general, GFA is considered to increase as the temperature interval ΔT_x increases [58, 59].

2.3.1.3 γ Parameter

A new parameter depending on glass transition temperature T_g, liquidus temperature T_l and onset crystallization temperature T_x was defined:

$$\gamma = \frac{T_x}{T_g + T_l} \tag{2.3}$$

This parameter was defined by Lu and Liu [59] as a new indicator of glass forming ability. Crystallization processes during cooling and reheating of the supercooled liquid were taken into account during the proposal of γ parameter.

2.3.1.4 α Parameter

This parameter was suggested by Mondal and Murty [60] by using onset crystallization temperature T_x and liquidus temperature T_l:

$$\alpha = \frac{T_x}{T_l} \tag{2.4}$$

The reason to formulate such a parameter aroused from the need to include both the thermal stability of liquid with T_x and easiness of glass formation with T_l. Moreover, this parameter is useful for alloys that do not exhibit a distinct glass transition.

2.3.1.5 Reduced Crystallization Temperature (T_{rx})

Reduced crystallization temperature T_{rx} is another parameter suggested for the prediction of glass forming ability [61]:

$$T_{rx} = \frac{T_x}{T_s} \tag{2.5}$$

where T_x and T_s are onset temperature of crystallization and solidification respectively. T_{rx} parameter was suggested by considering both the amorphous phase's resistance to crystallization and undercooled liquid's stability against competing crystalline phase formation. T_{rx} is between T_{rg} and unity; $T_{rg} \leq T_{rx} \leq 1$. Higher the reduced crystallization temperature, higher will be the glass forming ability.

2.3.2 Approaches for Glass Formation

There exists mainly four approaches to glass formation; solidification behavior, semi-empirical, thermodynamic and kinetic approach. Brief explanations of the principles of these approaches are explained in the next sections.

2.3.2.1 Solidification Behavior Approach

Akdeniz et al. suggested that solidification behavior of alloys plays an important role in the determination of glass formation [20]. According to this approach, it was indicated that, alloys having a sequence of eutectic and peritectic reactions with a high magnitude of reaction enthalpies ratio are essential parameters for high BGFA. Figure 2.3 shows a schematic phase diagram and melting DSC curve for a hypothetical alloy that was stated to be a good glass former by considering solidification behavior approach.

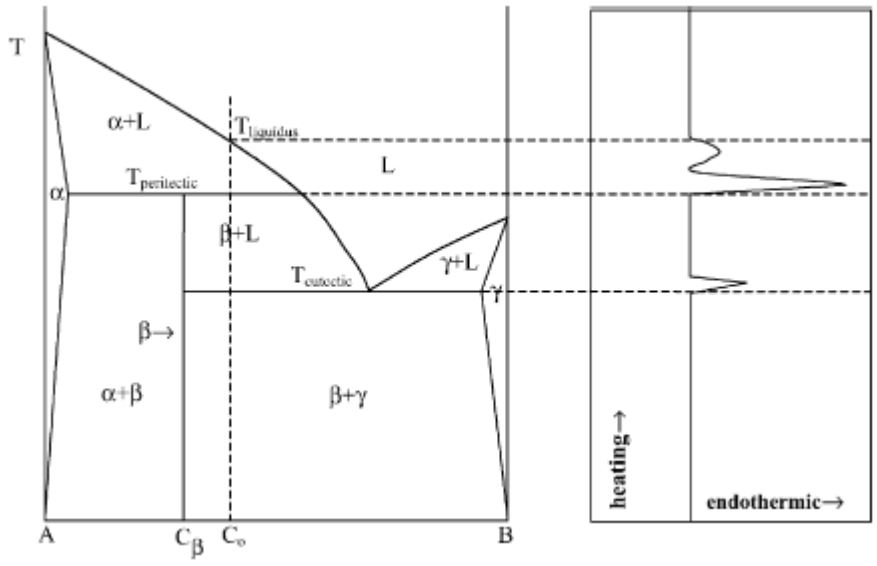

Figure 2.3 Schematic phase diagram and DSC curve for a hypothetical binary alloy which melts through a sequence of eutectic and peritectic reactions [20].

2.3.2.2 Semi Empirical Approach

When analyzed, most of the glass forming alloy systems were found to share three empirical rules. According to semi-empirical approach, for good glass forming ability:

1. Alloy should be a multicomponent system consisting of more than three elements,
2. There should be a significant difference in atomic size ratios above about 12% among the three main constituent elements, and
3. Heat of mixing between the three main constituent elements should be negative.

First and second rules indicate the importance of topology in glass formation, where third rule is supported by the experimental fact that the glass formation composition range generally coincides with a eutectic region [52, 62].

Amorphous alloy systems having the above features were found to contain higher degrees of dense randomly packed atomic configurations, new local atomic configurations that are different from those of the corresponding crystalline phases, and a homogeneous atomic configuration of the multicomponents on a long-range scale.

This approach states that, formation of liquid with new atomic configurations and multicomponent interactions on a short-range scale leads to an increase in the solid/liquid interfacial energy, difficulties in atomic rearrangement, and a necessity of atomic rearrangement on a long range scale for crystallization. Increase in the solid/liquid interfacial energy results in the suppression of nucleation of crystalline phases. Due to the difficulties in atomic rearrangement, atomic diffusivity decreases and viscosity increases. Atomic rearrangement on a long range scale for crystallization results in the suppression of growth of the crystalline phases.

Altogether, those changes in the system cause higher glass transition temperatures and lower melting temperatures. Hence, T_g/T_m and ΔT_x increases, therefore glass forming ability enhances. Figure 2.4 outlines the mechanisms of glass formation according to semi empirical approach [4].

2.3.2.3 Thermodynamic Approach

When analyzed from thermodynamic point of view, the ease of obtaining amorphous solids, which are indeed undercooled liquids, depends upon two main factors [63]:

1. The difference in free energy between undercooled liquid and more stable solid phases at the temperature of freezing, should be comparatively small or negative, and
2. The rate of formation of the crystalline phases should be smaller than that of the amorphous phases.

These conditions have two fundamental effects; they limit the composition range in which the glass state can be obtained and limit the choices of the components and compositions that will lead to the desired properties [63].

Solidification analysis generally necessitates the knowledge of the difference in energy between solid and liquid states, G^L-G^S. However, it is impossible to find the accurate energies as a function of composition and temperature for multicomponent alloy systems. On that account, the following assumption was suggested; G^L-G^S at a composition is proportional to the free energy of mixing ΔG of the liquid phase [64]. Critical cooling rate for multicomponent systems can be calculated based on that assumption. More detailed information about the calculation principles of critical cooling rate depending on the stated assumption will be given later on.

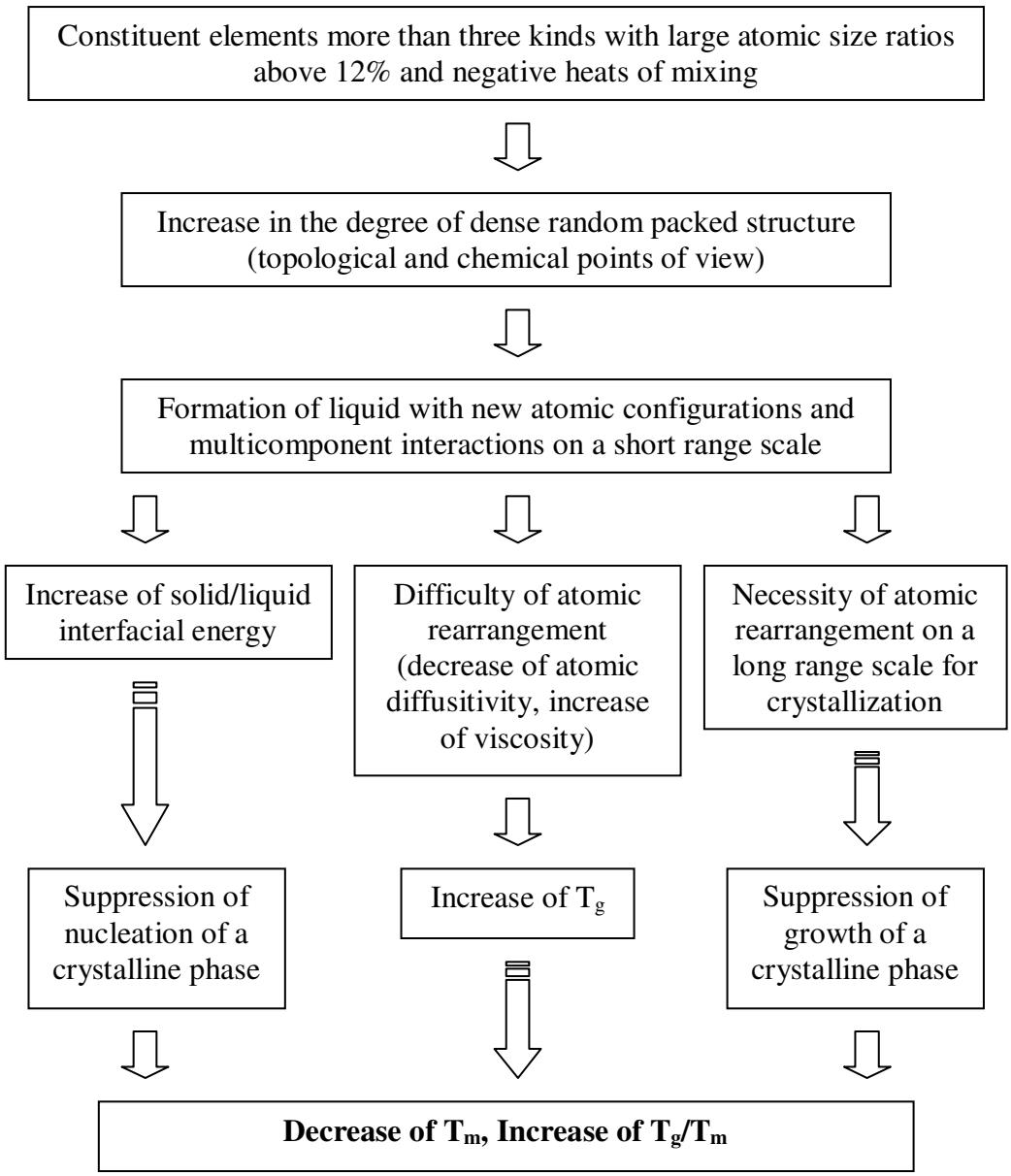

Figure 2.4 Mechanisms for the stabilization of supercooled liquid and high glass forming ability for the multicomponent alloys which satisfy the rules of semi empirical approach [4].

2.3.2.4 Kinetic Approach

When a liquid is cooled from a temperature higher than the liquidus temperature T_l to a temperature below glass transition temperature T_g at a constant cooling rate R, the time dependent volume of crystalline phase X can be formulated based on the non-isothermal crystallization kinetics as follows [59]:

$$X(T) = \frac{4\pi}{3R^4} \int_{T_l}^{T_g} I(T') \left[\int_{T'}^{T_g} U(T'')dT'' \right]^3 dT' \qquad \textbf{(2.6)}$$

where, I and U are the steady state nucleation frequency and crystal growth rate respectively.

The nucleation frequency and crystal growth rate can be expressed based on the common crystallization theory [59]:

$$I = \frac{10^{35}}{\eta} \exp\left[\frac{-16\pi}{3} \cdot \frac{\Delta S_f \alpha_m^3 T^2}{N_A k (T_l - T)^2} \right] \qquad \textbf{(2.7)}$$

and

$$U = \frac{kT}{3\pi a_0^2 \eta} \left[1 - \exp\left(-\frac{(T_l - T)\Delta S_f}{RT} \right) \right] \qquad \textbf{(2.8)}$$

Here, η, k, α_m, a_0, N_A, ΔS_f and R are viscosity, Boltzman constant, dimensionless parameter related to the liquid/solid interface energy, mean atomic diameter, Avogadro's number, molar fusion entropy and gas constant respectively. It is know that, critical cooling rate decreases with decreasing liquidus temperature, increasing activation energy for viscous flow, fusion entropy and viscosity of the supercooled liquid. It is also possible to calculate the fraction $X(T)$ of precipitated phases in

amorphous solids when the glass is reheated from a certain temperature T_0 to a temperature T with a constant heating rate β. According to non-isothermal transformation theory $X(T)$ will be [59]:

$$X(T) = \frac{4\pi}{3\beta^4} \int_{T_0}^{T} I(T') \left[\int_{T'}^{T} U(T'') dT'' \right]^3 dT' \qquad \textbf{(2.9)}$$

However, the above equation can only be used when $X(T)$ is small compared with unity.

The strong liquid behavior indicates high viscosity and sluggish kinetics in the supercooled liquid state. This behavior delays the formation of stable nuclei in the melt. Due to the poor mobility of the constituents, growth of the thermodynamically favored phases will be inhibited. Since the nucleation and growth of crystalline phases in the supercooled liquid state is very difficult, glass forming ability and thermal stability of the supercooled liquid will increase [8].

The formation of amorphous structure occurs with quenching from the liquid state as previously mentioned, Figure 2.1. Hence the atomic ordering in liquid state plays an important role in the formation of amorphous structure. As a result, the mechanisms behind this subject should be understood.

2.4 Order in Binary Liquid Alloys

When analyzed from the point of view of interatomic interactions, a binary alloy is either:

a. An ordered alloy, where unlike atoms are preferred as nearest neighbors over like atoms, or
b. A segregated alloy, where like atoms are preferred to pairs as nearest neighbors over unlike atoms.

Unluckily, constituent atoms cannot be distinguished in a direct way; hence the identification of a nearest neighbor pair of atoms is problematic. In this situation, either the structural data or the observed thermodynamic functions (such as activity, heat of mixing, excess Gibbs energy of mixing, excess heat capacity, etc) or other thermophysical data (such as viscosity, diffusivity, density, surface tension, electrical resistivity, etc) are considered to extract information associated with interatomic interactions. There exist some empirical criteria as well as microscopic parameters to identify ordered alloys. According to these suggestions, ordered alloys have the following properties [65]:

a. They are alloys that exhibit negative deviations from Raoult's law,
b. They have negative heat of formation and excess Gibbs energy of mixing,
c. Their concentration fluctuation in the long wavelength limit (S_{cc} (0)) is less than the ideal value,
d. If $V_{AB}(r)$ (i, j=A, B) are the effective interatomic potential, then one can define the radial form of the order potential, i.e.

$$W_{AB}(r) = V_{AB}(r) - \frac{V_{AA}(r) + V_{BB}(r)}{2} \qquad \textbf{(2.10)}$$

For ordered alloys, it is required that W_{AB} (r) > 0 around the nearest-neighbor distances [65].

e. In the framework of regular solution theory, the interchange energy ω $\left(= -\frac{Z}{2} W_{AB}\right)$ is less than zero,
f. The Warren–Cowley short range order parameter α needs to be less than 0. $(-1 \le \alpha \le 0)$

2.4.1 Atomistic Approach to Binary Liquid Alloys

Consider an alloy in which two liquid metals, say A and B, were mixed together at their standard states. On mixing, if A and B atoms prefer to remain self-coordinated (A–A pair or B–B pair) over the heterocoordinated (A–B pair), then it is called a segregating alloy. Phase separation is a severe condition of segregation. In order to quantify it, the Warren–Cowley short range order parameter should be investigated. Warren–Cowley short range order parameter, α_1, for the first coordination shell, is defined in terms of the conditional probability;

$$P_{A,B} = c_A(1-\alpha_1) \tag{2.11}$$

$P_{A,B}$ defines the probability that an A atom exists at site 2 as a nearest neighbor of a given B atom at site 1. Equation (2.11) supplies a direct insight to the local arrangement of atoms in the mixture. For random distribution of atoms, where $P_{A,B}=c_A$, the Warren–Cowley short range order parameter becomes zero, $\alpha_1=0$. However, if $\alpha_1 < 0$, A–B pairs of atoms are preferred over A–A or B–B pairs as nearest neighbors. Approaching the problem in a probabilistic way shows that the limiting values of α_1 lie in the following ranges;

$$-\frac{c_A}{c_B} \le \alpha_1 \le 1 \qquad \text{for } c_A \le \frac{1}{2} \tag{2.12}$$

$$-\frac{c_B}{c_A} \le \alpha_1 \le 1 \qquad \text{for } c_A = \frac{1}{2} \tag{2.13}$$

$$-1 \le \alpha_1 \le 1 \qquad \text{for } c_A = c_B = \frac{1}{2} \tag{2.14}$$

The minimum possible value $\alpha_{1,min} = -1$, means complete ordering of A–B pairs in the melt, whereas the maximum value, $\alpha_{1,max} = 1$, suggests total segregation of A–A and B–B pairs in the melt. For ordered alloys, α_1 ranges from -1 to 0.

Another important parameter, configurational partition function Q can be given as [65];

$$Q = \sum_r g_r e^{-E_r/k_B T} \tag{2.15}$$

Here, g_r stands for degeneracy of the state, where E_r is the configuration energy. The basic task is to obtain g_r and E_r for a binary alloy consisting of $N_A \left(= N_{c_A}\right)$ atoms of element A and $N_B \left(= N_{c_B}\right)$ atoms of element B.

As a starting point, two approximations were made;

1. The constituent atoms A and B are sufficiently similar in size and shape so that they are interchangeable on the lattice and
2. All configurations of atoms, whether in pure state A or pure state B, or in the alloy A–B, have equal energy. It is equivalent to saying that the mixing of atoms leaves this energy unchanged, i.e. there is no energetic effect. Therefore;

$$Q_A = Q_B \tag{2.16}$$

$$V_{AB} = \frac{V_{AA} + V_{BB}}{2} \tag{2.17}$$

where V_{ij} is the mutual energy of a pair of nearest neighbors.

Within these approximations, g_r can be expressed as;

$$g_r = \frac{N!}{N_A! + N_B!} \tag{2.18}$$

$$E_r = c_A(N_{AA}V_{AA}) + c_B(N_{BB}V_{BB}) \quad \textbf{(2.19)}$$

The terms in the brackets in Equation (2.19) represent the energy of pure substances A and B, respectively. For solid and liquid phases;

$$F \approx G = -k_B T \ln Q \quad \textbf{(2.20)}$$

then,

$$\Delta G^M = c_A(N_{AA}V_{AA}) + c_B(N_{BB}V_{BB}) + RT\sum_i c_i \ln c_i \quad \textbf{(2.21)}$$

or,

$$\Delta G^M = RT\sum_i c_i \ln c_i \quad \textbf{(2.22)}$$

$$\Delta S^M = -\left(\frac{\partial G^M}{\partial T}\right) = -R\sum_i c_i \ln c_i \text{ , } \Delta H^M = 0 \quad \textbf{(2.23)}$$

and,

$$S_{cc}(0) = RT\left(\frac{\partial^2 G^M}{\partial c^2}\right)^{-1} = c_A c_B \quad \textbf{(2.24)}$$

where, ΔG^M, ΔS^M, ΔH^M and $S_{cc}(0)$ are the Gibbs free energy of mixing, entropy of mixing, enthalpy of mixing and concentration fluctuations, respectively. By considering these approximations, $S_{cc}(0)$ were found to be a well behaved function that is always symmetrical at $c_A = c_B = 1/2$ and is independent of any physical constraints. It is also important to note that, systems will behave as an ideal mixture when there will not be any size and enthalpic effects.

When the energetic effect is considered as well, it is obvious that there will be contributions to the potential energy from A–B pairs of neighbors as well as from A–A and B–B pairs. In contrast to approximation (2.17), interatomic potential is now given as;

$$V_{AB} = \frac{V_{AA} + V_{BB}}{2} + \frac{1}{2}W \qquad \textbf{(2.25)}$$

where W is usually known as the ordering energy. In effect A–A, B–B and A–B pairs of atoms are now energetically distinguishable. Therefore the configurational energy, E_r , becomes,

$$E_r = c_A\left(N_{AA}V_{AA}\right) + c_B\left(N_{BB}V_{BB}\right) - \frac{1}{2}\overline{N}_{AB}W \qquad \textbf{(2.26)}$$

Where $\overline{N}_{AB}$ corresponds to the equilibrium or average value of A–B pairs of atoms. With the simplest approximation, where the atoms N_A and N_B are distributed completely randomly, N_{AB} can be expressed as,

$$\overline{N}_{AB} = \frac{N_A N_B}{N_A + N_B} \qquad \textbf{(2.27)}$$

By substituting these values into Equations (2.15) and (2.20),

$$\Delta G^M = RT\sum_i c_i \ln c_i - \frac{1}{2}Nc_A c_B W \qquad \textbf{(2.28)}$$

$$\Delta S^M = -R\sum_i c_i \ln c_i + \frac{1}{2}Nc_A c_B\left(\frac{dW}{dT}\right) \qquad \textbf{(2.29)}$$

$$\Delta H^M = -\frac{N}{2} c_A c_B W + T c_A c_B \frac{N}{2}\left(\frac{dW}{dT}\right) \quad \textbf{(2.30)}$$

Those equations were based on the assumption that constituent atoms A and B are sufficiently similar in size and shape, thus they are interchangeable on the lattice. However, further derivations for enthalpy and entropy of mixing were constructed that considers the size difference between the atoms. Following sections describe the calculations of enthalpy and entropy of mixing, critical cooling rate, viscosity and short range order parameter by taking the size difference into account.

2.4.1.1 ΔH^M and ΔS^M Calculations for Binary Liquid Alloys

ΔG^M is expressed in terms of enthalpy of mixing, ΔH^M and entropy of mixing ΔS^M as:

$$\Delta G^M = \Delta H^M - T\Delta S^M \quad \textbf{(2.31)}$$

If N_A occupy a group of γ_A –lattice sites and N_B occupy γ_B –lattice sites, for all possible arrangements of atoms (if there is no energetic effect, $\Delta H^M=0$) the entropy of mixing was derived by Sommer, Singh and Witusiewicz [66] as,

$$\frac{\Delta S^M}{R} = -\frac{\Delta G^M}{RT} = -c_A \ln\left(\frac{c_A}{c_A + \gamma c_B}\right) - c_B \ln\left(\frac{\gamma c_B}{c_A + \gamma c_B}\right) - 1/2\, z q_A c_A \ln\left(\frac{c_A + \gamma c_B}{c_A + q c_B}\right) - 1/2\, z q_B c_B \ln\left(\frac{c_B + \frac{c_A}{\gamma}}{c_B + \frac{c_A}{q}}\right) \quad \textbf{(2.32)}$$

where, γ and q parameters can be given as,

$$\gamma = \frac{\gamma_B}{\gamma_A} = \frac{\Omega_B}{\Omega_A} \tag{2.33}$$

$$q = \frac{q_B}{q_A} \tag{2.34}$$

$$\frac{1}{2} z(\gamma_i - q_i) = \gamma_i - 1, \quad i = A, B \tag{2.35}$$

As seen in Equation (2.33), γ involves the size difference between the A and B atoms since Ω_i is the atomic volume. There is an important point for the calculation of γ; Ω_B should be higher than Ω_A, so that, the atom with larger atomic radius is B. The parameter q can be calculated by the use of Equation (2.34), where q_A and q_B can be obtained by Equation (2.35), substituting z (coordination number), and γ_A (=Ω_A) and γ_B (=Ω_B), respectively.

On the other hand, if the energetic effect is taken into account $\left(\Delta H^M \neq 0\right)$ [66],

$$\frac{\Delta H^M}{N k_B T} = \frac{2 c_A c_B q_A q_B}{(h+1)(c_A q_A + c_B q_B)} \left(\frac{\omega_{AB}}{k_B T} \right) \tag{2.36}$$

$$\Delta H^M = N \frac{2 c_A c_B q_A q_B}{(h+1)(c_A q_A + c_B q_B)} \omega_{AB} \tag{2.37}$$

where,

$$h = \left[1 + \frac{4 c_A c_B q_A q_B}{(c_A q_A + c_B q_B)^2} \left(k^2 - 1 \right) \right]^{1/2} \tag{2.38}$$

$$k = \exp\left(\frac{\omega}{zk_BT}\right) \tag{2.39}$$

$$\omega = \frac{z}{2}\left(V_{AB} - \left(V_{AA} + V_{BB}\right)\right) \tag{2.40}$$

Here, ω is the interchange energy and V_{ij} are the energies of *ij* pairs of atoms [66]. In this study, interchange energy will be denoted as ω_{ij} and ordering energy will be denoted as W_{ij} to avoid confusion between these two terms, although they can be used in the same meaning in literature.

Substitution of Equations (2.32) and (2.37) into Equation (2.31), enables the calculation of the Gibbs free energy of mixing.

2.4.1.2 Critical Cooling Rate Calculations for Binary Liquid Alloys

Critical cooling rate R_c is a very important parameter for the analysis of glass forming ability. Hence its calculation is an important deal. For calculation of critical cooling rate, Inoue et al. proposed the following formula [64];

$$R_c = Z\frac{k_BT_m^2}{a^3\eta_{T=T_m}}\exp\left(\frac{\Delta G}{RT}\right) \tag{2.41}$$

where Z is the constant of 2 x 10^{-6} which was determined by the analysis of R_c for NaCl, k_B is the Boltzmann constant, T_m is the melting temperature, a is the interatomic distance and $\eta_{T=T_m}$ is the viscosity at the melting temperature. $\eta_{T=T_m}$ can be expressed by modified Andrade's equation [67];

$$\eta_{T=T_m} = C_A\frac{\sqrt{AT_m}}{V^{2/3}} \tag{2.42}$$

where, C_A is a constant of 1.85 x 10^{-7} (J/K.mol$^{1/3}$)$^{1/2}$, A is the atomic weight $\left(A = A_A c_A + A_B c_B\right)$ and V is the molar volume $\left(V = V_A c_A + V_B c_B\right)$.

2.4.1.3 Viscosity Calculations for Binary Liquid Alloys

Viscosities of liquid metals have been investigated deeply by many scientists. It was found that viscosity affects the glass forming ability of alloys. Glass forming ability is promoted by a rapid increase of viscosity on undercooling [67]. The change in viscosity of liquid metal can be represented as [68],

$$\frac{\Delta\eta}{\eta_0} = -\frac{\Delta H^M}{RT} \tag{2.43}$$

where R is the ideal gas constant. It should be noted that $\Delta\eta/\eta_0$ is positive for ordered alloys since ΔH^M is always negative for glass forming alloys.

2.4.1.4 Short Range Order Parameter Calculations for Binary Liquid Alloys

Concentration fluctuation, $S_{cc}(0)$, can be defined for binary alloys as [65];

$$\frac{S_{cc}(0)}{c_A c_B} = 1 + \sum_l Z_l \alpha_l \tag{2.44}$$

where, Z_l and α_l are the coordination number and short range order parameters for the l^{th} shell. Here, l varies from first-neighbor shells to higher shells.

Afterwards, short range order parameter for the first coordination shell was expressed by Bhatia and Singh by using the lattice model theory [65];

$$\alpha_1 = \frac{s-1}{s+1} \tag{2.45}$$

So,

$$S_{cc}(0) = \frac{c_A c_B}{1+\frac{1}{2}Z\left(\frac{1}{s-1}\right)} \tag{2.46}$$

with

$$s = \left[1+4c_A c_B\left(e^{2\omega/Zk_BT}-1\right)\right]^{1/2} \tag{2.47}$$

For $\omega/k_BT \to 0$, Equation (2.45) suggests that $\alpha_1 = 0$, meaning random distribution of atoms in the alloy. If $\omega/k_BT > 0$, α_1 is positive, exhibiting a tendency of like atoms (A-A or B-B) to pair as nearest neighbors. However, if $\omega/k_BT < 0$, α_1 is negative, showing a preference for unlike atoms (A-B) to pair in the alloy.

By combining Equation (2.45) and Equation (2.46), an explicit relationship between $S_{cc}(0)$ and α_1 can be obtained for the first coordination shell;

$$\frac{S_{cc}(0)}{c_A c_B} = \frac{1+\alpha_1}{1-(Z-1)\alpha_1} \tag{2.48}$$

2.5 Order in Multicomponent Liquid Alloys

2.5.1 ΔH^M and ΔS^M Calculations for Multicomponent Liquid Alloys

Accurate estimation of energies as a function of composition and temperature is not possible for multicomponent alloy systems. Hence, G^l - G^s at a composition can be assumed to be proportional to the free energy of mixing ΔG^M of the liquid phase [64].

If entropy of mixing is analyzed with including the effects of atomic size, it can be expressed as a combination of ideal configurational entropy ΔS^{ideal} and mismatch term of entropy S_σ [64];

$$\Delta S^M = \Delta S^{ideal} + S_\sigma \tag{2.49}$$

According to the regular solution model, ΔH^M and ΔS^{ideal} are defined as followings for the multicomponent systems with N elements [64];

$$\Delta H^M = \sum_{i=1, i\neq j}^{N} \omega_{ij} c_i c_j \tag{2.50}$$

$$\Delta S^{ideal} = -R \sum_{i=1}^{N} \left(c_i \ln c_i \right) \tag{2.51}$$

where ω_{ij} is the regular solution interaction parameter between *i* and *j* elements, and R is the gas constant.

Mismatch term of entropy S_σ, was defined by an equation of state for the mixture of hard spheres [64];

$$S_\sigma = k_B\left\{\frac{3}{2}(\zeta^2-1)y_1+\frac{3}{2}(\zeta-1)^2 y_2-\left[\frac{1}{2}(\zeta-1)(\zeta-3)+\ln\zeta\right](1-y_3)\right\} \quad \textbf{(2.52)}$$

where $\zeta=(1-\gamma)^{-1}$ and γ is the packing fraction. y_1, y_2 and y_3 are parameters having a relation of $y_1+y_2+y_3 = 1$, Following relations were derived for the multicomponent systems with *N* elements [64]:

$$y_1=\frac{1}{\sigma^3}\sum_{j>i=1}^{N}(d_i+d_j)(d_i-d_j)^2 c_i c_j \quad \textbf{(2.53)}$$

$$y_2=\frac{\sigma^2}{(\sigma^3)^2}\sum_{j>i=1}^{N} d_i d_j (d_i-d_j)^2 c_i c_j) \quad \textbf{(2.54)}$$

$$y_3=\frac{(\sigma^2)^3}{(\sigma^3)^2} \quad \textbf{(2.55)}$$

$$\sigma^k=\sum_{i=1}^{N} c_i d_i^k \quad \textbf{(2.56)}$$

where d_i is the atomic diameter of the *i* element and $k = 2,\ 3$.

2.5.2 Critical Cooling Rate Calculations for Multicomponent Liquid Alloys

Critical cooling rate plays an important role in the determination of the bulk glass forming ability. Thus, evaluation of this parameter will provide easiness with annihilating the time consuming, difficult and expensive experiment steps. In the present study, for the calculation of critical cooling rate following equation was used [64]:

$$R_c = \psi \frac{k_B T_m^2}{a^3 \eta_{T=T_m}} \exp\left[f_1 \left(\frac{\Delta H - T_m \Delta S^{ideal}}{300R} \right) - f_2 \left(\frac{T_m S_\sigma}{300R} \right) \right] \quad \textbf{(2.57)}$$

where ψ is a constant $\left(2 \times 10^{-6}\right)$, k_B is the Boltzmann constant, T_m is the melting temperature, $\eta_{T=T_m}$ is the viscosity at the melting temperature, a is the interatomic distance and f_1 and f_2 are the fitting parameters. Fitting parameters of f_1 and f_2 were calculated as 0.75 and 1.2 respectively by using the method of least-squares for 300 K [64].

2.6 Pseudopotential Theory

2.6.1 Principles of One-Electron Theory

Discovering the properties of a crystal structure by solving Schrödinger's equation for a system of interacting nuclei and electrons that form the crystal structure is possible in principle. However, this is a very complicated problem to be solved, hence some simplifications are required. Following are the assumptions of the one electron theory [69];

1. Generally, the nuclei are assumed to be too massive to follow the rapidly changing spatial distribution of the electrons (the adiabatic approximation). As a result, two Schrödinger's equations will be considered, one for the electrons and the other for the nuclei. In the following, the one with the behavior of electrons will be concerned.

2. It is further assumed that instead of treating the electronic subsystem as a whole, it is possible to consider separately the motions of individual electrons. Each of them is then thought of as moving in the effective field of the (stationary) nuclei and all the other electrons (hence the name – the

effective field approximation). Accordingly, the total electron wave function is expressed in terms of individual electron wave functions, ψi.

3. Further approximations are made in the actual evaluation of the total function and in the consequent determination of the effective potential as seen by a single electron (Pauli-exclusion principle). It is customary to use Slater's determinant which automatically incorporates the Pauli Exclusion Principle. This leads to a system of one-electron Schrödinger equation in the Hartree-Fock approximation including both Coulomb and exchange interactions between the electrons.

The one electron theory is the primitive or basis. It has been worked detail by several times, however it will be surveyed in some detail through, first of all, nearly-free electron model.

2.6.2 Nearly-Free Electron Model

According to nearly-free electron model, a structure is considered as a spatial lattice of ions embedded in an electron gas. While in linear combination of atomic orbital the perturbation in the Eigen-value problem is the departure of the true potential from the atomic potential, in this model it is the departure from zero. For a zero potential (i.e. in vacuum), an electron wave function is a plane wave normalized to all space. In a structure, the normalization integral may be conveniently presented as the sum of contributions from all the structural sites. In the following, more complicated effective potentials (pseudopotentials) will be introduced with form factors dependent both on $\vec{q}$ (any vector) and $\overrightarrow{K}$ (wave vector). These form factors and potentials are called to be non-local.

In addition, it is necessary to consider the perturbation theory as well. It is assumed that the flat-bottomed potential well of free electron theory is a good approximation to the real potential in a metal.

Additionally, in the Fermi free-electron gas model, the structure formation process is as follows: N neutral isolated atoms are each stripped of z outer (valance) electrons. The resulting ions are then brought together to form a structural lattice, with a volume of Ω_0 per ion. An electron gas is then allowed into the lattice, its spatial distribution being assumed uniform, so that its density is z / Ω_0. If the fact that the lattice potential is not constant is ignored, the electron dispersion law is simply $E = K^2$. The energy levels occupied by the electrons range from zero to a maximum, which is known as the Fermi level of a free electron gas:

$$E_F^0 = \left(\frac{3\pi^2 z}{\Omega_0} \right)^{2/3} = K_F^2 \qquad \textbf{(2.58)}$$

To calculate the total structure energy in the nearly-free electron model, the dispersion laws are summed over all the occupied states. This is achieved by integrating the perturbation theory expansion in the Rayleigh-Schrödinger form over all the wave vectors within the Fermi sphere. As a result, the total structure energy $\sum_{str}$ is expressed as;

$$\sum_{str} = U_0 + U_{bs} + U_{lattice} \qquad \textbf{(2.59)}$$

where $U_{lattice}$ includes the Coulomb repulsion between the ion cores; U_0 and U_{bs} are respectively the volume and structure-dependent electronic contributions to the total energy:

$$U_0 = -2\frac{\Omega}{(2\pi)^3}\int_{\substack{inside\\fermi\\sphere}}\left(K^2 + \left\langle \vec{K}\middle|V\middle|\vec{K}\right\rangle\right)d^3K \qquad \textbf{(2.60)}$$

$$U_{bs} = -2\frac{\Omega}{(2\pi)^3}\sum_q \left|S\left(\vec{q}\right)\right|^2 \int_{\substack{inside\\fermi\\sphere}} \frac{\left|\left\langle \vec{K}+\vec{q}\middle|V\middle|\vec{K}\right\rangle\right|^2}{\left(\vec{K}+\vec{q}\right)^2 - K^2} d^3K - U_{el}^{\text{int}} \qquad \textbf{(2.61)}$$

The g_n vectors are replaced by the ordinary position vectors $\vec{q}$. The wave vector is designates as K, where Ω and V stands respectively for volume of the crystal and crystal potential. U_0 term describes a "free" electron gas with the inclusion of electron-electron interaction. U_{bs} is related to band characteristics and is therefore called the band-structure energy. If a potential V is local, its form-factor is $\vec{K}$-independent and can be taken out of the $\vec{K}$ integral that appears then in U_{bs} is known as Lindhard's function [70]:

$$\chi\left(\vec{q}\right) = -2\frac{\Omega}{(2\pi)^3}\frac{1}{N}\int_{\substack{inside\\fermi\\sphere}} \frac{d^3K}{\left(\vec{K}+\vec{q}\right)^2 - \vec{K}^2} \qquad \textbf{(2.62)}$$

If Fermi surface is assumed spherical, then the Equation (2.62) becomes;

$$\chi(q) = -\frac{Z}{4}\left(\frac{2}{3}E_F^0\right)^{-1}\left(1 + \frac{1-x^2}{2x}\ln\left|\frac{1+x}{1-x}\right|\right) \qquad \textbf{(2.63)}$$

In this equation, $x = k/2k_F$ and $E_F^0 = \left(3\pi^2 z/\Omega_0\right)^{2/3}$.

The electron-electron interaction energy U_{el}^{int} can be expressed [71] as a result of interactions between non-uniform part of the crystal electron density and the

potential, which is the difference between the crystal potential, ϑ^{cr} and the initial potential ϑ^{ion} of the system of ions. U_{el}^{int} can also be expressed based on the form factor $V^{cr}(q)$, given that a function $\alpha(\vec{q}) = \vartheta^{ion}/\vartheta^{cr}$ is used for the characterization of this potential.

$$U_{el}^{\text{int}} = \sum_{q} |S(q)|^2 |V(q)|^2 \chi(q)(1-\alpha(q)) \qquad \textbf{(2.64)}$$

and

$$U_{bs} = \sum_{q} |S(q)|^2 |V(q)|^2 \chi(q) - U_{el}^{\text{int}} = \sum_{q} |S(q)|^2 |V(q)|^2 \chi(q)\alpha(q) \qquad \textbf{(2.65)}$$

where $S(q) = \frac{1}{N}\sum_{i} e^{-iqt_i}$.

The structure potential is composed of the ionic potentials, which is related to the screening mechanism. $\chi(q)$ is a function arising from perturbation theory whereas $\alpha(\vec{q})$ is the ratio of the original potential of the ions to the crystal potential. A frequently used characteristic function $\Phi_{bs}(q)$ is defined as;

$$\Phi_{bs}(q) = |V(q)|^2 X(q)\alpha(q) \qquad \textbf{(2.66)}$$

The interatomic interaction potential is given with the following form;

$$\Phi_{(r)} = \frac{z^2 e^2}{r} + \frac{2\Omega}{(2\pi)^3} \sum_{q} \int_{\substack{inside \\ fermi \\ sphere}} \frac{\left|\left\langle \vec{K}+\vec{q} \middle| V \middle| \vec{K} \right\rangle\right|^2}{(\vec{K}+\vec{q})^2 - K^2} d^3K - U_{el}^{\text{int}}$$

$$= \frac{z^2 e^2}{r} + \frac{2\Omega}{(2\pi)^3} \int [W^{str}(q)]^2 X(q)\varepsilon^*(q) e^{i\vec{q}\vec{r}} d^3q \qquad \textbf{(2.67)}$$

It is considered that the simplest pseudopotential, namely the Coulomb potential $(-ze^2/r)$ with a form factor, can be shown as;

$$V(q) = -\frac{4\pi z e^2}{\Omega_0}\frac{1}{q^2} \tag{2.68}$$

2.6.3 Pairwise Interatomic Interactions and Ordering Energy Calculations for Ternary Alloys

When the electronic theory of ternary alloys in the pseudopotential approximation is considered, the partial ordering potential, $W_{\alpha\beta}(R_i)$, can be written as a function of interatomic distance, R_i [72-76];

$$W_{\alpha\beta}(R_i) = V_{\alpha\alpha}(R_i) + V_{\beta\beta}(R_i) - 2V_{\alpha\beta}(R_i) \tag{2.69}$$

and

$$W_{\alpha\beta}(R_i) = \frac{2}{N}\sum_{q}^{l} F_p(q) e^{i\vec{q}\vec{R}_i} \tag{2.70}$$

or

$$W_{\alpha\beta}(R_i) = \frac{\bar{\Omega}}{\pi^2}\int dq \cdot q^2 F_p(q)\frac{SinqR_i}{qR_i} \tag{2.71}$$

where

$$\begin{aligned} F_p(q) &= \frac{\bar{\Omega}}{8\pi}\left|W_\alpha^o(q) - W_\beta^o\right|^2 q^2 \frac{1-\varepsilon(q)}{\varepsilon^*(q)} + \frac{2\pi}{\bar{\Omega}}(\Delta z)^2 \frac{1}{q^2}\exp\left(-\frac{q^2}{4\lambda}\right) \\ &= F_{bs}(q) + F_{es}(q) \end{aligned} \tag{2.72}$$

$F_p(q)$ is the characteristic function of partial ordering energy. $W_\alpha^o(q)$ and $W_\beta^o(q)$ are the form factor of an unscreened pseudopotential of α and β ions, respectively (α, β ≡ A, B and C). ε(q) is the dielectric constant in the Hartree approximation; ε*(q) is the modified dielectric constant on the basis of the correlation and exchange effects; λ is the Ewald parameter; z is the effective valancy of atoms; $\overline{\Omega}$ is the average atomic volume of the alloy, and can be written as:

$$\overline{\Omega} = c_A\Omega_A + c_B\Omega_B + c_C\Omega_C \qquad \textbf{(2.73)}$$

Pairwise interatomic interaction potentials in the ternary alloys can be calculated as;

$$V_{\alpha\beta}(R_i) = \frac{\overline{\Omega}}{\pi^2}\int_0^\infty F_{\alpha\beta}^1(q)\frac{\sin qR_i}{qR_i}q^2dq \qquad \textbf{(2.74)}$$

where

$$F_{\alpha\beta}^1(q) = -\frac{\overline{\Omega}}{8\pi}\left|W_\alpha^o(q)W_\beta^o(q)\right|q^2\frac{\varepsilon(q)-1}{\varepsilon^*(q)} + \frac{2\pi}{\overline{\Omega}}\left|z_\alpha^* z_\beta^*\right|\frac{1}{q^2}\exp\left(-\frac{q^2}{4\lambda}\right) \qquad \textbf{(2.75)}$$

CHAPTER 3

EXPERIMENTAL PROCEDURE

This study consists of two main parts as stated previously. First part includes the theoretical studies carried out for the determination of bulk glass forming ability of alloys. Second part is the experimental studies performed for the synthesis and characterization of the selected alloy systems.

3.1 Theoretical Studies for Ti-Based Systems

First part of this chapter deals with the theoretical studies performed for achieving the bulk glass forming alloy systems. Three different binary Ti-based systems were chosen for investigation; Ti-Zr, Ti-Co and Ti-Cu. Several compositions were taken to be analyzed in each system. The basic idea behind the computational studies carried out is finding ternary alloying elements that will increase the bulk glass forming ability of its corresponding binary alloy. Hence, several elements were added to all the chosen binary systems.

3.1.1 Alloy Systems Selection

During selection of the alloy systems, several parameters were taken into account. First of all, a broad literature review was done to obtain information about the systems used and the criteria applied during the selection stage. While determination of the compositions of the master alloys, phase diagrams were consulted to. Binary phase diagrams for the systems that were chosen to be analyzed during this thesis study are present in Appendix A. The alloy system

selection was performed according to the approach described in section 2.3.2.1. Master binary alloys were selected by considering the requirements described above. Afterwards, ternary alloys were selected by using the electronic theory of alloys in pseudopotential approximation. To be able to use that theory, calculation of the ordering energies should be carried out. Details of ternary alloy selection and the calculations of its key parameters will be given in the following sections.

3.1.2 Calculation of Ordering Energies

Electronic theory of alloys in pseudopotential approximation relates the parameters needed to define bulk glass forming ability such as, viscosity, enthalpy and entropy of mixing, critical cooling rate, etc with the ordering energies of the alloys obtained from the interatomic potentials. In this study, calculation of interatomic potentials and ordering energies for the selected candidate bulk glass forming alloy systems was aimed. These potentials and energies were afterwards used for the calculation of bulk glass formation parameters.

Ordering energy calculations were carried out by using the Fortran Programs, MEH 1, MEH 2, MEH 3 and MEH 7 written by Prof. Dr. Amdulla O. Mekhrabov. These programs are available at the Metallurgical and Materials Engineering Department of the Middle East Technical University.

Each program gives the ordering energies between the desired atoms. These programs operate based on the Equations (2.67) to (2.75). MEH 7 program deals with the interactions between atoms for the binary systems. However during the calculations of ordering energies for the ternary alloys, interactions caused by the third alloying element are also needed to be taken into account. Hence the programs MEH 1, MEH 2 and MEH 3 were written for the compensation of this need.

MEH 7 program was used to obtain the ordering energies between the atoms of the binary alloy, whereas MEH 1 was utilized to get the ordering energies between the

atoms of the binary alloy upon addition of the ternary alloying element. MEH 2 and MEH 3 gives the ordering energies between the first atoms of the binary alloy and the atoms of the ternary alloying element, and between the second atoms of the binary alloy and the atoms of the ternary alloying element, respectively.

For the calculation of the ordering energies in the ternary alloys, 1 at % of third alloying element additions were performed either in the place of first or second constituent elements of the binary alloy. In addition to the ordering energies, interchange energies between the selected atoms were also calculated with the help of Equation (2.40).

The systems, binary alloys and ternary alloys analyzed during this study are listed in Table 3.1. All the compositions are given in terms of atomic percent.

Table 3.1 Binary and ternary alloys analyzed for the chosen Ti-based alloy systems where X is the third alloying element.

System	Binary Alloy	Ternary Alloy
Ti - Zr	$Ti_{40}Zr_{60}$	$Ti_{40}Zr_{59}X_1$
		$Ti_{39}Zr_{60}X_1$
	$Ti_{50}Zr_{50}$	$Ti_{50}Zr_{49}X_1$
		$Ti_{49}Zr_{50}X_1$
	$Ti_{60}Zr_{40}$	$Ti_{60}Zr_{39}X_1$
		$Ti_{59}Zr_{40}X_1$
Ti - Cu	$Ti_{65}Cu_{35}$	$Ti_{65}Cu_{34}X_1$
		$Ti_{64}Cu_{35}X_1$
Ti - Co	$Ti_{68}Co_{32}$	$Ti_{68}Co_{31}X_1$
		$Ti_{67}Co_{32}X_1$

3.1.3 Calculations of ΔH^M, ΔS^M, Viscosity, Short Range Order Parameter and Critical Cooling Rate

After the calculations of ordering energies, key parameters for bulk glass formation such as enthalpy and entropy of mixing, viscosity, short range order parameter and critical cooling rate became easy to calculate with using proper definitions.

Definitions and equations used for the calculations of these parameters were presented in the previous chapter. ΔH^M and ΔS^M were calculated with the help of Equations (2.49) to (2.55). Viscosity was investigated with using Equation (2.43). Short range order parameter and critical cooling rate were obtained by using Equations (2.44) to (2.47) and Equations (2.41) and (2.57), respectively.

3.2 Experimental Studies for Ti-Based Systems

After the completion of theoretical studies for the selected possible bulk glass forming alloy systems, experimental studies were performed for the production and characterization of these alloys.

Syntheses of the alloys were performed in three steps as follows:

1. Weighing and physically mixing the nearly pure elements with a proper ratio needed for the production of the alloy,
2. Arc melting of the nearly pure elements,
3. Centrifugal casting of the arc melted alloy.

All of the alloys selected with the theoretical studies were synthesized by following the above production route. After the synthesis of the alloys, characterization studies were performed.

The alloys were characterized by consulting to the following methods:

1. X-Ray Diffraction (XRD),
2. Scanning Electron Microscopy (SEM),
3. Differential Scanning Calorimetry (DSC).

The synthesis and characterization studies that were carried out will be thoroughly described in the following sections.

3.2.1 Alloy Preparation

All the alloys examined in this study were prepared by using nearly pure elements. The form and purity of the elements used are given in Table 3.2. The component elements of the alloys were weighed according to the desired composition with SARTORIUS precision weighing balance, and physically mixed for the production. Following sections describe the production methods used after weighing and physically mixing the nearly pure elements.

Table 3.2 Form and purity of elements that were used during the experimental studies.

Element Name	Form	Purity
Titanium	Wire	99.7%
Copper	Shot	99.9%
Manganese	Pieces	99.9%
Aluminum	Shot	99.9%
Nickel	Pieces	99.9%

3.2.1.1 Arc Melting

Homogeneity throughout the alloy plays an important role for the production of the bulk metallic glasses. All the elements should melt and form a homogeneous alloy. Hence, using arc melting is crucial for the aim of this study. By using arc melting,

the elements were melted. The melting processes were done for multiple times in order to achieve the homogeneous structure throughout the specimen.

BUEHLER Arc Melting machine was used for the melting processes. This machine can go up to 4000°C and down to 10^{-6} mbar pressure. Hence, melting of all the elements used in this study was successfully achieved with avoiding contamination with atmosphere. This is crucial for titanium alloys, since they are highly reactive.

3.2.1.2 Centrifugal Casting

After obtaining a homogeneous specimen with the help of arc melting, alloys were centrifugally cast into copper molds in order to obtain non-equilibrium cooling conditions which could lead to amorphous phase formation. Main idea behind the centrifugal casting operation is to push the melt metal into the copper mold placed on the rotating arm by means of centrifugal forces.

For this process, MANFREDI multihertz neutromag digital centrifugal casting machine was used. This machine is capable of melting alloys that have melting temperatures lower than 2000°C. Casting process can be done under three different atmospheres; natural, neutral (argon gas) atmosphere or vacuum, with the help of the special selector of the machine.

During the melting process in centrifugal casting machine, alloys were placed inside of alumina crucibles. Heating of the alumina crucible is done by means of the induction coil under vacuumed condition that was created by flowing argon gas. The alloys are heated until they melt. The temperature of the alloy is monitored by using the pyrometer present on the casting machine. At the casting process, alloy that melted inside alumina crucible flows to the copper mold present at the rotating arm. Details of crucibles and molds used in this study are given in the following sections.

3.2.1.2.1 Crucible Preparation

Alumina crucibles coated with yttrium (III) oxide, aerosol refractory paint were used during the centrifugal casting operation. Crucibles were chosen to be made from alumina, in order to benefit from the high temperature resistance of the alumina ceramic as well as to avoid contamination between the alloy and the crucible material. Coating with yttrium (III) oxide was performed to intensify the above properties. The raw alumina that was used for the production of the crucibles has the composition given in Table 3.3.

Table 3.3 Composition of the castable alumina

Compound	Weight %
Al_2O_3	~ 97.0
SiO_2	0.2 (max)
Fe_2O_3	0.1 (max)
CaO	1.6 (max)

Production of the crucibles was done by casting them into polyamide molds. Firstly, water was added into castable alumina. Afterwards, this mixture was stirred in a plastic cup to obtain good wetting and de-aeration. During this operation, conserving the size distribution of alumina particles was important, since it is known that large alumina particles result in binding effect, where small alumina particles improve thermal shock resistance. After preparing the desired slurry, casting into the polyamide mold was performed. Cast alumina was left in the mold for air drying for one day. Then, cast alumina was taken out of the mold and heat treatment was performed. Heat treatment of the crucible is desired for obtaining high strength and high thermal shock resistance. It was conducted in the controlled furnace with gradually increasing the temperature. Table 3.4 shows the heat treatment process applied to the cast alumina crucibles.

Table 3.4 Heat treatment operation for the alumina crucibles.

T_1	T_2	Time Interval
30°C	120°C	6 hr
120°C	150°C	2 hr
150°C	150°C	24 hr
150°C	330°C	6 hr
330°C	510°C	6 hr
510°C	600°C	3 hr
600°C	600°C	12 hr
600°C	900°C	6 hr
900°C	1200°C	6 hr
1200°C	30°C	Furnace Cooling

After the heat treatment of crucibles is completed, they were coated with yttrium (III) oxide for reinforcing the beneficial effects of alumina. Yttrium (III) oxide that was used is in the form of aerosol refractory paint with 99.9% purity. This paint is usable on graphite, ceramics and metals in all atmospheres to over 2000°C. The paint was sprayed to the inner parts of the alumina crucible and left for air drying. After those operations, crucibles were ready to use. Figure 3.1 presents a schematic view of the alumina crucibles used for this study.

Figure 3.1 Schematic view of the alumina crucibles.

3.2.1.2.2 Mold Design

During this study, wedge shaped copper molds were used in the centrifugal casting processes. The material of the molds was chosen as copper due to its high thermal conductivity which leads to higher cooling rates. The molds were designed as wedge shaped in order to obtain different cooling rates along the specimen. At the thicker sections of the specimen, cooling rate is lower, whereas at the thinner sections cooling rate is higher. Figure 3.2 is the schematic view of the copper mold used during the casting studies.

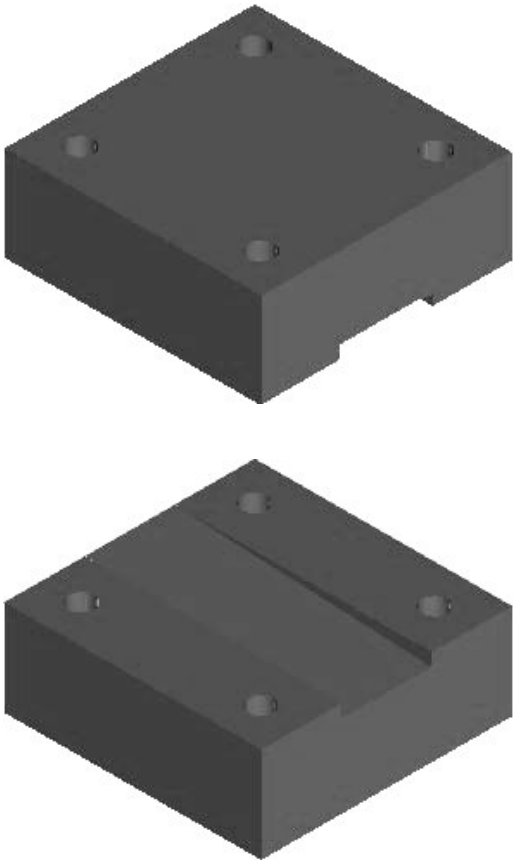

Figure 3.2 Schematic view of copper mold.

3.2.2 Structural Characterization

The alloys prepared by arc melting and centrifugal casting methods were characterized by metallographic examination, X-ray diffraction, scanning electron microscopy, energy dispersive spectroscopic analysis and differential scanning calorimetry. The details of each characterization method are given in the following sections.

3.2.2.1 Metallographic Examination

As the first step, a cross-sectional slice was cut by using Buehler Isomet 5000 Linear Precision Saw from the specimens. Afterwards, for easy handling, this slice was mounted into bakalite under 4040 psi pressure and 130°C temperature. Grinding and polishing steps followed each other after mounting is completed. Grinding was performed with silicon carbide emery papers under flowing water. Emery papers ranging from coarsest to finest were used until all the scratches except the ones that belong to the finest emery paper were annihilated. As a next step, polishing was accomplished with 1 μm Al_2O_3. This step is done until a scratch free surface is obtained. In the final step, specimens were etched with the following etchant: 60 vol % Lactic acid ($C_3H_6O_3$), 20 vol % HNO_3, 10 vol % HF and 10 vol % H_2O.

3.2.2.2 X-Ray Diffraction (XRD)

During the XRD studies, Rigaku Diffractometer was used where the specimens were investigated under Cu K_α radiation.

Both the arc melted and centrifugal cast specimens were investigated with the help of X-ray diffraction. Each peak present was identified and existence of amorphous structure was searched for.

3.2.2.3 Scanning Electron Microscope (SEM)

Microstructural analyses were conducted with JSM-6400 scanning electron microscope (JEOL) equipped with Noran System 6 X-ray Microanalysis System and Semafore Digitizer. In order to make sure about the composition of the alloys prepared, energy dispersive spectroscopic (EDS) analyses were also performed for the specimens. EDS analysis was also used for obtaining information about the compositions of the phases present. Most frequently used mode of SEM was secondary electron mode. Back scattered mode of the microscope was used where phases having different compositions were present.

3.2.2.4 Differential Scanning Calorimetry (DSC)

Thermal analysis of the specimens were conducted with Setsys System 16/18 DSC, which operates under high purity argon gas and a water cooling system attached to the machine.

The specimens to be analyzed should be small in amount for ensuring uniform temperature distribution and high resolution. For thermal analysis during this study, samples of 20-25 mg in weight were used. Those samples were placed into Al_2O_3 crucibles, which were coated with yttrium (III) oxide, and heated above the melting temperature with a 20°/min rate. Later on, they were cooled to room temperature with the same rate. By this process, it is possible to determine several properties of the samples such as melting temperature, crystallization temperature and glass transition temperature.

CHAPTER 4

RESULTS AND DISCUSSION

Results and discussion part of present thesis includes both the theoretical and experimental studies conducted for the Ti-based alloy systems. In the first part, results of theoretical studies are present. The aim of the theoretical studies is to determine the alloying elements that will increase the bulk glass forming ability of various Ti-based alloy systems. Those candidate elements were used during the experiments in order to justify the results of theoretical predictions as well as to establish a connection between theoretical and experimental studies.

4.1 Theoretical Studies on Bulk Glass Forming Ability of Ti-Based Alloys

For the determination of bulk glass forming ability of Ti-based alloys, theoretical modeling and simulation studies that are based on the atomistic and thermodynamic approach were carried out, and the results of these studies are given in this section. Three different Ti-based alloy systems were selected for the investigation: Ti-Zr, Ti-Co and Ti-Cu on the base of their phase diagrams as described in section 3.1.1. From each alloy system, several binary master alloys were chosen and 40 elements from periodic table were added as ternary alloying elements to each master alloy. On the base of the modeling and simulation studies, ordering energy values of binary and ternary alloys were computed and compared. Afterwards, the thermodynamic parameters that are important for bulk glass forming ability i.e., heat of mixing, entropy of mixing, Gibbs free energy of mixing, critical cooling rate, short range order parameter and viscosity were calculated based on the theories described in sections 2.4 and 2.5 for binary and multicomponent alloys, respectively. Variation of all of these parameters were taken into account during the

selection of ternary alloying elements that will increase the bulk glass forming ability of Ti-based alloys.

4.1.1 Calculation of Ordering Energies for Binary and Ternary Ti-based Alloys

Ordering energy calculations were carried out with the Fortran Programs described in section 3.1.2 for the alloy systems stated in Table 3.2. Magnitudes of ordering energies were determined for nearest neighbor interatomic distance between constituent element atoms, Table 4.1.

Table 4.1 Nearest neighbor interatomic distance for Ti-Zr, Ti-Co and Ti-Cu alloys.

Alloy	Interatomic Distance
Ti - Zr	3.0641A
Ti - Co	2.7125 A
Ti - Cu	2.7395 A

Nearest neighbor interatomic distances were found by summing up the radius values [77] of the constituent element atoms of each alloy system with the assumption that these atoms touch one another at the liquid state.

In this section, the results of modeling studies for Ti-Cu system, which was chosen for experimental investigations, are present. Tables 4.2 to 4.5 show the ordering energy (W_{ij}) and interchange energy (ω_{ij}) values for the binary and ternary alloys, where X indicates the ternary alloying element. The results of ordering energy simulations for Ti-Zr and Ti-Co systems are given in Appendix B. The calculated partial ordering energies, based on Equations (2.71) and (2.75), $W_{Ti\text{-}Cu}(R)$, $W_{Ti\text{-}X}(R)$ and $W_{Cu\text{-}X}(R)$ as a function of interatomic distance in $Ti_{64}Cu_{35}X_1$ alloy are given in Figure 4.1 for X=Ag, Au, Al, Ni and Mn as an example. The nearest neighbor

distance between Ti and Cu atoms in $Ti_{65}Cu_{35}$ binary alloy is labeled as R_{Ti-Cu} in Figure 4.1. In these calculations the non-local bare-pseudopotential form-factors and parameters of pseudopotentials for Ti, Cu and X ions proposed in [78-80] are used in quasi- on the Fermi sphere approximations and was screened using modified dielectric constant [81, 82]. However, during the calculations, the form of function responsible for the exchange and correlation effects in the interacting electron gas proposed in [83] was used. The value of Ewald Parameter in Equation (2.75) was taken as $\lambda = 0.7$.

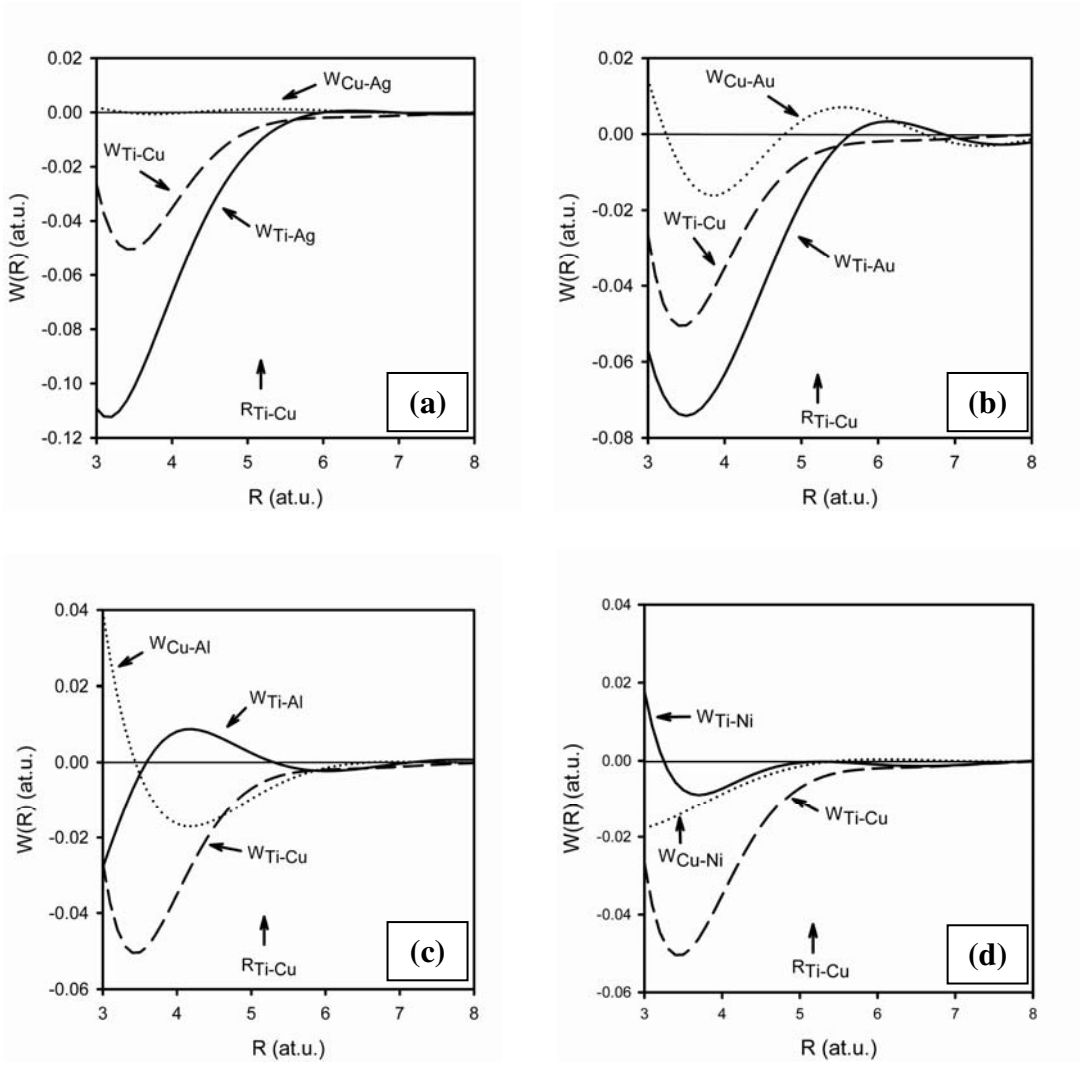

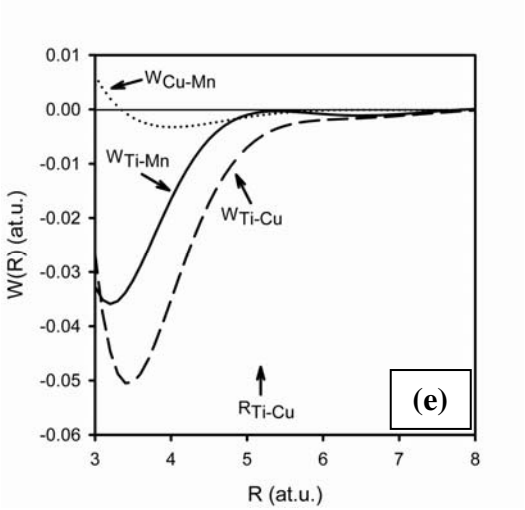

Figure 4.1 Partial ordering energies, W(R), between pair of constituting element atoms for (a) $Ti_{64}Cu_{35}Ag_1$, (b) $Ti_{64}Cu_{35}Au_1$, (c) $Ti_{64}Cu_{35}Al_1$, (d) $Ti_{64}Cu_{35}Ni_1$ and (e) $Ti_{64}Cu_{35}Mn_1$ ternary alloy systems. (R_{Ti-Cu}=5.1786 at.u.)

In Figure 4.1, it is obvious that ordering energies show an oscillating and sign changing character with changing interatomic distance. This well known feature for the metallic materials suggests that different pairs of atoms have different partial ordering energies as shown in Tables 4.2 to 4.5 for various X ternary alloying additions at nearest neighbor interatomic distance.

For a better glass formation, ordering energy of the system is desired to be increased. Hence, the ordering energy values of ternary and binary systems were compared. Table 4.6 and 4.7 show the alloying elements that were found to increase the ordering energy of the binary alloys.

Table 4.2 Ordering energy and interchange energy values for $Ti_{65}Cu_{34}X_1$ alloy (in atomic unit of energy).

$Ti_{65}Cu_{34}X_1$						
X	W_{Ti-Cu} at.u. (10^{-3})	W_{Ti-X} at.u. (10^{-3})	W_{Cu-X} at.u. (10^{-3})	ω_{Ti-Cu} at.u. (10^{-2})	ω_{Ti-X} at.u. (10^{-2})	ω_{Cu-X} at.u. (10^{-2})
None	-5.0447	-	-	-3.0268	-	-
Ag	-5.0818	-9.9975	1.2144	-3.0491	-5.9985	0.7286
Au	-5.0810	-10.9910	5.6115	-3.0486	-6.5946	3.3669
Zn	-5.0313	-1.5038	-0.0544	-3.0188	-0.9023	-0.0327
Cd	-5.0746	-3.3746	-0.7967	-3.0448	-2.0247	-0.4780
Co	-5.0037	-0.2124	-0.8197	-3.0022	-0.1275	-0.4918
Hg	-5.0880	-3.4636	5.8882	-3.0528	-2.0782	3.5329
Sc	-5.0622	0.7792	-3.2483	-3.0373	0.4675	-1.9490
Y	-5.1175	4.5112	-2.4472	-3.0705	2.7067	-1.4683
La	-5.1467	6.0931	2.6446	-3.0880	3.6559	1.5868
Hf	-5.0077	13.1476	3.6628	-3.0046	7.8885	2.1977
V	-4.9151	-0.9672	-12.1676	-2.9491	-0.5803	-7.3006
Nb	-4.9430	12.1814	-5.6926	-2.9658	7.3088	-3.4155
Cr	-4.9728	1.5554	-2.5915	-2.9837	0.9333	-1.5549
Mo	-4.8917	19.2176	0.7017	-2.9350	11.5305	0.4210
W	-4.8925	21.9689	2.4994	-2.9355	13.1813	1.4996
Mn	-5.0109	-0.4787	-1.0759	-3.0065	-0.2872	-0.6455
Re	-4.8494	14.3828	-9.1688	-2.9096	8.6297	-5.5013
Fe	-4.9728	0.8190	-3.4373	-2.9837	0.4914	-2.0624
Ru	-4.9492	13.4516	1.0998	-2.9695	8.0710	0.6599
Os	-4.9522	12.9893	3.5555	-2.9713	7.7936	2.1333
Zr	-5.0149	13.7485	1.2727	-3.0089	8.2491	0.7636
Ir	-4.9524	12.9536	3.5546	-2.9714	7.7721	2.1328
Ni	-5.0025	-0.2376	-0.7746	-3.0015	-0.1426	-0.4647
Pd	-5.0283	13.6941	5.8523	-3.0170	8.2164	3.5114
Pt	-5.0305	-2.7394	7.1817	-3.0183	-1.6436	4.3090
Li	-5.1105	-4.7320	1.4794	-3.0663	-2.8392	0.8877
Be	-4.9820	2.2527	-0.5102	-2.9892	1.3516	-0.3061
Mg	-5.0858	3.4808	-3.4060	-3.0515	2.0885	-2.0436
Al	-5.0037	0.8625	-7.7163	-3.0022	0.5175	-4.6298
Ga	-5.0241	-1.7266	-2.5305	-3.0145	-1.0360	-1.5183
In	-5.0694	1.0851	4.5422	-3.0416	0.6511	2.7253
Si	-4.9910	-0.9761	-10.3240	-2.9946	-0.5856	-6.1944
Ge	-5.0087	0.3342	-6.6560	-3.0052	0.2005	-3.9936
Sn	-5.0385	5.8465	-2.1212	-3.0231	3.5079	-1.2727
Pb	-5.0612	9.0533	10.8684	-3.0367	5.4320	6.5210
Sb	-5.0251	10.0213	2.3411	-3.0151	6.0128	1.4047
Te	-5.0127	6.3456	-8.1056	-3.0076	3.8073	-4.8634
B	-4.9407	10.6518	17.7016	-2.9644	6.3911	10.6210
C	-4.8935	4.1067	3.1521	-2.9361	2.4640	1.8913
P	-4.9684	-1.5553	-10.6782	-2.9810	-0.9332	-6.4069

Table 4.3 Ordering energy and interchange energy values for $Ti_{65}Cu_{34}X_1$ alloy (in SI units).

$Ti_{65}Cu_{34}X_1$						
X	W_{Ti-Cu} J/mol (10^3)	W_{Ti-X} J/mol (10^3)	W_{Cu-X} J/mol (10^3)	ω_{Ti-Cu} J/mol (10^4)	ω_{Ti-X} J/mol (10^4)	ω_{Cu-X} J/mol (10^4)
None	-13.2399	-	-	-7.9439	-	-
Ag	-13.3372	-26.2383	3.1871	-8.0023	-15.7430	1.9122
Au	-13.3351	-28.8456	14.7272	-8.0011	-17.3074	8.8363
Zn	-13.2046	-3.9467	-0.1429	-7.9228	-2.3680	-0.0857
Cd	-13.3182	-8.8565	-2.0910	-7.9909	-5.3139	-1.2546
Co	-13.1321	-0.5575	-2.1512	-7.8792	-0.3345	-1.2907
Hg	-13.3535	-9.0902	15.4535	-8.0121	-5.4541	9.2721
Sc	-13.2856	2.0450	-8.5251	-7.9714	1.2270	-5.1151
Y	-13.4307	11.8396	-6.4226	-8.0584	7.1037	-3.8536
La	-13.5076	15.9912	6.9407	-8.1045	9.5947	4.1644
Hf	-13.1426	34.5056	9.6129	-7.8855	20.7034	5.7677
V	-12.8996	-2.5385	-31.9338	-7.7398	-1.5231	-19.1603
Nb	-12.9727	31.9698	-14.9401	-7.7836	19.1819	-8.9641
Cr	-13.0511	4.0822	-6.8014	-7.8307	2.4493	-4.0809
Mo	-12.8381	50.4362	1.8417	-7.7029	30.2617	1.1050
W	-12.8402	57.6570	6.5596	-7.7041	34.5942	3.9358
Mn	-13.1510	-1.2564	-2.8236	-7.8906	-0.7538	-1.6942
Re	-12.7272	37.7475	-24.0634	-7.6363	22.6485	-14.4380
Fe	-13.0511	2.1494	-9.0211	-7.8307	1.2897	-5.4127
Ru	-12.9890	35.3036	2.8864	-7.7934	21.1821	1.7318
Os	-12.9969	34.0902	9.3313	-7.7981	20.4541	5.5988
Zr	-13.1615	36.0828	3.3402	-7.8969	21.6497	2.0041
Ir	-12.9975	33.9965	9.3290	-7.7985	20.3979	5.5974
Ni	-13.1289	-0.6237	-2.0329	-7.8773	-0.3742	-1.2197
Pd	-13.1967	35.9399	15.3592	-7.9180	21.5639	9.2155
Pt	-13.2026	-7.1894	18.8483	-7.9215	-4.3137	11.3090
Li	-13.4123	-12.4190	3.8827	-8.0474	-7.4514	2.3296
Be	-13.0753	5.9123	-1.3391	-7.8452	3.5474	-0.8035
Mg	-13.3477	9.1352	-8.9390	-8.0086	5.4811	-5.3634
Al	-13.1321	2.2637	-20.2514	-7.8792	1.3582	-12.1508
Ga	-13.1857	-4.5316	-6.6412	-7.9114	-2.7189	-3.9847
In	-13.3045	2.8479	11.9210	-7.9827	1.7087	7.1526
Si	-13.0989	-2.5617	-27.0952	-7.8593	-1.5370	-16.2571
Ge	-13.1452	0.8772	-17.4687	-7.8871	0.5263	-10.4812
Sn	-13.2236	15.3441	-5.5671	-7.9341	9.2065	-3.3402
Pb	-13.2830	23.7602	28.5239	-7.9698	14.2561	17.1143
Sb	-13.1883	26.3006	6.1442	-7.9130	15.7804	3.6865
Te	-13.1557	16.6538	-21.2731	-7.8934	9.9923	-12.7639
B	-12.9669	27.9556	46.4576	-7.7802	16.7734	27.8746
C	-12.8428	10.7779	8.2728	-7.7057	6.4667	4.9637
P	-13.0395	-4.0819	-28.0247	-7.8237	-2.4491	-16.8148

Table 4.4 Ordering energy and interchange energy values for $Ti_{64}Cu_{35}X_1$ alloy (in atomic unit of energy).

$Ti_{64}Cu_{35}X_1$						
X	W_{Ti-Cu} at.u. (10^{-3})	W_{Ti-X} at.u. (10^{-3})	W_{Cu-X} at.u. (10^{-3})	ω_{Ti-Cu} at.u. (10^{-2})	ω_{Ti-X} at.u. (10^{-2})	ω_{Cu-X} at.u. (10^{-2})
None	-5.0447	-	-	-3.0268	-	-
Ag	-5.1520	-10.1180	1.2007	-3.0912	-6.0708	0.7204
Au	-5.1520	-11.2465	5.4443	-3.0912	-6.7479	3.2666
Zn	-5.1005	-1.5202	-0.0727	-3.0603	-0.9121	-0.0436
Cd	-5.1447	-3.3794	-0.8192	-3.0868	-2.0276	-0.4915
Co	-5.0728	-0.2419	-0.8439	-3.0437	-0.1452	-0.5063
Hg	-5.1582	-3.5179	5.8182	-3.0949	-2.1108	3.4909
Sc	-5.1321	0.7594	-3.2825	-3.0793	0.4556	-1.9695
Y	-5.1876	4.5224	-2.4933	-3.1126	2.7134	-1.4960
La	-5.2175	6.0312	2.5504	-3.1305	3.6187	1.5303
Hf	-5.0766	13.1209	3.5639	-3.0460	7.8726	2.1383
V	-4.9830	-0.9950	-12.2839	-2.9898	-0.5970	-7.3703
Nb	-5.0109	12.2574	-5.7649	-3.0065	7.3545	-3.4590
Cr	-5.0420	1.5133	-2.6736	-3.0252	0.9080	-1.6042
Mo	-4.9594	19.1567	0.4739	-2.9756	11.4940	0.2844
W	-4.9596	21.9652	2.3365	-2.9758	13.1791	1.4019
Mn	-5.0808	-0.5044	-1.0881	-3.0485	-0.3027	-0.6528
Re	-4.9163	14.3627	-9.4023	-2.9498	8.6176	-5.6414
Fe	-5.0417	0.7984	-3.4737	-3.0250	0.4790	-2.0842
Ru	-5.0171	13.4881	1.0447	-3.0103	8.0929	0.6268
Os	-5.0203	12.9614	3.4564	-3.0122	7.7769	2.0738
Zr	-5.0838	13.7880	1.2199	-3.0503	8.2728	0.7319
Ir	-5.0211	12.9267	3.4553	-3.0127	7.7560	2.0732
Ni	-5.0716	-0.2681	-0.7978	-3.0430	-0.1609	-0.4787
Pd	-5.0982	13.5188	5.6916	-3.0589	8.1113	3.4149
Pt	-5.1005	-2.7907	7.1165	-3.0603	-1.6744	4.2699
Li	-5.1814	-4.7391	1.4606	-3.1088	-2.8435	0.8764
Be	-5.0512	2.2462	-0.5437	-3.0307	1.3477	-0.3262
Mg	-5.1557	3.5512	-3.4010	-3.0934	2.1307	-2.0406
Al	-5.0734	0.9101	-7.7405	-3.0440	0.5461	-4.6443
Ga	-5.0932	-1.7280	-2.5877	-3.0559	-1.0368	-1.5526
In	-5.1385	1.0205	4.4881	-3.0831	0.6123	2.6929
Si	-5.0600	-0.9506	-10.4034	-3.0360	-0.5704	-6.2421
Ge	-5.0776	0.3414	-6.7229	-3.0466	0.2049	-4.0337
Sn	-5.1085	5.8505	-2.1682	-3.0651	3.5103	-1.3009
Pb	-5.1303	8.9830	10.8332	-3.0782	5.3898	6.4999
Sb	-5.0940	9.9826	2.2385	-3.0564	5.9896	1.3431
Te	-5.0816	6.3290	-8.2556	-3.0490	3.7974	-4.9533
B	-5.0097	10.6558	17.6580	-3.0058	6.3935	10.5948
C	-4.9616	4.1149	3.1001	-2.9770	2.4689	1.8601
P	-5.0365	-1.5721	-10.8344	-3.0219	-0.9433	-6.5006

Table 4.5 Ordering energy and interchange energy values for $Ti_{64}Cu_{35}X_1$ alloy (in SI units).

$Ti_{64}Cu_{35}X_1$						
X	W_{Ti-Cu} J/mol (10^3)	W_{Ti-X} J/mol (10^3)	W_{Cu-X} J/mol (10^3)	ω_{Ti-Cu} J/mol (10^4)	ω_{Ti-X} J/mol (10^4)	ω_{Cu-X} J/mol (10^4)
None	-13.2399	-	-	-7.9439	-	-
Ag	-13.5212	-26.5546	3.1513	-8.1127	-15.9327	1.8908
Au	-13.5212	-29.5164	14.2886	-8.1127	-17.7098	8.5731
Zn	-13.3861	-3.9898	-0.1907	-8.0317	-2.3939	-0.1144
Cd	-13.5023	-8.8691	-2.1499	-8.1014	-5.3215	-1.2899
Co	-13.3135	-0.6349	-2.2147	-7.9881	-0.3810	-1.3288
Hg	-13.5376	-9.2328	15.2698	-8.1225	-5.5397	9.1619
Sc	-13.4691	1.9929	-8.6149	-8.0815	1.1957	-5.1689
Y	-13.6148	11.8690	-6.5437	-8.1689	7.1214	-3.9262
La	-13.6932	15.8287	6.6936	-8.2159	9.4972	4.0162
Hf	-13.3235	34.4357	9.3534	-7.9941	20.6614	5.6121
V	-13.0779	-2.6114	-32.2390	-7.8467	-1.5668	-19.3434
Nb	-13.1510	32.1694	-15.1300	-7.8906	19.3017	-9.0780
Cr	-13.2326	3.9716	-7.0168	-7.9395	2.3829	-4.2101
Mo	-13.0158	50.2765	1.2438	-7.8095	30.1659	0.7463
W	-13.0164	57.6475	6.1320	-7.8098	34.5885	3.6792
Mn	-13.3345	-1.3239	-2.8556	-8.0007	-0.7943	-1.7134
Re	-12.9028	37.6946	-24.6762	-7.7417	22.6168	-14.8057
Fe	-13.2320	2.0953	-9.1168	-7.9392	1.2572	-5.4701
Ru	-13.1673	35.3994	2.7418	-7.9004	21.2396	1.6451
Os	-13.1758	34.0171	9.0713	-7.9055	20.4103	5.4428
Zr	-13.3424	36.1865	3.2015	-8.0054	21.7119	1.9209
Ir	-13.1778	33.9260	9.0685	-7.9067	20.3556	5.4411
Ni	-13.3104	-0.7037	-2.0938	-7.9862	-0.4222	-1.2563
Pd	-13.3803	35.4798	14.9374	-8.0282	21.2879	8.9624
Pt	-13.3861	-7.3242	18.6771	-8.0317	-4.3945	11.2063
Li	-13.5985	-12.4378	3.8334	-8.1591	-7.4627	2.3001
Be	-13.2567	5.8952	-1.4268	-7.9540	3.5371	-0.8561
Mg	-13.5312	9.3201	-8.9259	-8.1187	5.5920	-5.3555
Al	-13.3150	2.3885	-20.3147	-7.9890	1.4331	-12.1888
Ga	-13.3672	-4.5351	-6.7915	-8.0203	-2.7211	-4.0749
In	-13.4860	2.6782	11.7789	-8.0916	1.6069	7.0674
Si	-13.2798	-2.4949	-27.3036	-7.9679	-1.4970	-16.3822
Ge	-13.3261	0.8961	-17.6441	-7.9957	0.5377	-10.5865
Sn	-13.4071	15.3546	-5.6904	-8.0442	9.2128	-3.4142
Pb	-13.4644	23.5758	28.4315	-8.0787	14.1455	17.0589
Sb	-13.3692	26.1992	5.8750	-8.0215	15.7195	3.5250
Te	-13.3366	16.6103	-21.6666	-8.0020	9.9662	-13.0000
B	-13.1478	27.9659	46.3431	-7.8887	16.7796	27.8059
C	-13.0217	10.7995	8.1363	-7.8130	6.4797	4.8818
P	-13.2183	-4.1259	-28.4347	-7.9310	-2.4755	-17.0608

Table 4.6 Elements increasing ordering energy in Ti-Zr based systems in descending order.

$Ti_{60}Zr_{39}X_1$	$Ti_{59}Zr_{40}X_1$	$Ti_{50}Zr_{49}X_1$	$Ti_{49}Zr_{50}X_1$	$Ti_{40}Zr_{59}X_1$	$Ti_{39}Zr_{60}X_1$
Re	Re	Ag	Re	Re	Re
C	C	Re	C	C	C
W	W	C	W	W	W
Mo	Mo	W	Mo	Mo	Mo
V	V	Mo	V	V	V
B	B	V	B	B	B
Nb	Nb	B	Nb	Nb	Nb
Ru	Ru	Nb	Ru	Ru	Ru
Os	Os	Ru	Os	Os	Os
Ir	Ir	Os	Ir	Ir	Ir
P	P	Ir	P	P	P
Cr	Cr	P	Cr	Cr	Cr
Fe	Be	Cr		Fe	
Be		Fe		Be	
Si		Be		Si	
Al		Si		Al	
Ni		Al		Ge	
Ge		Ni		Ni	
Co		Ge		Te	
Te		Co		Co	
Hf		Te		Hf	
Mn		Hf			

Table 4.7 Elements increasing ordering energy in Ti-Co and Ti-Cu based systems in descending order.

$Ti_{68}Co_{31}X_1$	$Ti_{67}Co_{32}X_1$	$Ti_{65}Cu_{34}X_1$	$Ti_{64}Cu_{35}X_1$
Re	Re	Re	Re
C	C	Mo	Mo
Mo	Mo	W	W
W	W	C	C
V	V	V	V
B	B	B	B
Nb	Nb	Nb	Nb
Ru	Ru	Ru	Ru
Os	Os	Os	Os
Ir	Ir	Ir	Ir
Zn	Cr	P	P
Cr	Fe	Cr	Fe
Fe	P	Fe	Cr
P	Be	Be	
Be		Si	
Si		Ni	
Ni		Co	
		Al	
		Hf	
		Ge	
		Mn	
		Te	
		Zr	
		Ga	
		Sb	
		Pd	
		Pt	
		Zn	
		Sn	

Ordering energy of the systems is an important parameter for glass formation. However there are several thermodynamic parameters that should be investigated for obtaining better information about the bulk glass forming ability of the systems. Following section presents the results of the thermodynamic parameters' calculations.

4.1.2 Calculation of Thermodynamic Parameters for Binary and Ternary Ti-based Alloys

Enthalpy and entropy of mixing, short range order parameter and critical cooling rate of the alloy systems are related to the ordering energy values. The calculation of each parameter for binary and multicomponent systems was discussed in sections 2.4 and 2.5 respectively. Entropy and enthalpy of mixing for the ternary alloys were computed by using Equations (2.49) and (2.50). Entropy of mixing contains two terms which are ideal configurational entropy ΔS^{ideal} and mismatch term of entropy S_σ. ΔS^{ideal} and S_σ terms were calculated by using Equations (2.51) to (2.56). For mismatch term of entropy, packing fraction γ was taken to be equal to 0.64 according to [84]. Equation (2.57) was used for the calculation of critical cooling rate.

Short range order parameter calculation for binary liquid alloys was presented in section 2.4.1.4. By using the equations listed in that section, short range order parameters for each binary alloy were computed. The results are shown in Table 4.8. As seen from the table, $Ti_{65}Cu_{35}$ binary system has the most negative short range order parameter, whereas $Ti_{68}Co_{32}$ alloy has the least negative short range order parameter. Hence, $Ti_{65}Cu_{35}$ binary alloy shows the highest tendency and $Ti_{68}Co_{32}$ alloy shows the least tendency for pairing up of unlike atoms.

Table 4.8 Short range order parameters for $Ti_{60}Zr_{40}$, $Ti_{50}Zr_{50}$, $Ti_{40}Zr_{60}$, $Ti_{68}Co_{32}$ and $Ti_{65}Cu_{35}$ binary liquid alloys.

	$Ti_{60}Zr_{40}$	$Ti_{50}Zr_{50}$	$Ti_{40}Zr_{60}$	$Ti_{68}Co_{32}$	$Ti_{65}Cu_{35}$
α_1	-0.1480	-0.1491	-0.1319	-0.0166	-0.2497

ΔH^M, ΔS^M, viscosity and critical cooling rate parameters were computed for each binary system. Afterwards, 1 at % of X elements was added to the binary alloys. Here, X denotes the ternary alloying element. Then, enthalpy, entropy and critical

cooling rate values were investigated for each ternary alloy. Tables 4.9 and 4.10 show the calculated values of enthalpy of mixing, mismatch term of entropy, ideal configurational entropy, entropy of mixing, viscosity change of liquid metal, and critical cooling rate of Ti-Cu system. Results for Ti-Zr and Ti-Co systems are given in Appendix C.

Table 4.9 ΔH^M, S^σ, ΔS^{ideal}, ΔS^M, $\Delta\eta/\eta_0$ and critical cooling rate for $Ti_{65}Cu_{34}X_1$ alloy (in SI units).

$Ti_{65}Cu_{34}X_1$						
X	**ΔH^M J/mol (10^4)**	**S^σ J/mol.K**	**ΔS^{ideal} J/mol.K**	**ΔS^M J/mol.K**	**$\Delta\eta/\eta_0$**	**R_c K/s (10^5)**
None	-1.8072	0.7044	5.3803	6.0847	1.6563	2.2140
Ag	-1.8643	0.6906	5.7576	6.4482	1.7087	1.6137
Au	-1.8507	0.6904	5.7576	6.4481	1.6962	1.6678
Zn	-1.7666	0.6896	5.7576	6.4472	1.6191	2.1753
Cd	-1.8048	0.7146	5.7576	6.4722	1.6541	1.9004
Co	-1.7479	0.7110	5.7576	6.4686	1.6019	2.2718
Hg	-1.7746	0.6993	5.7576	6.4570	1.6264	2.0843
Sc	-1.7711	0.7442	5.7576	6.5018	1.6232	2.0773
Y	-1.7478	0.8546	5.7576	6.6122	1.6019	2.0692
La	-1.7146	0.9320	5.7576	6.6896	1.5714	2.1677
Hf	-1.5885	0.7177	5.7576	6.4753	1.4559	3.6134
V	-1.7855	0.6970	5.7576	6.4547	1.6364	2.0480
Nb	-1.6260	0.6898	5.7576	6.4474	1.4902	3.3119
Cr	-1.7285	0.7115	5.7576	6.4691	1.5842	2.4088
Mo	-1.5019	0.6913	5.7576	6.4489	1.3765	4.8049
W	-1.4644	0.6909	5.7576	6.4486	1.3421	5.3366
Mn	-1.7545	0.6925	5.7576	6.4501	1.6080	2.2542
Re	-1.5895	0.6904	5.7576	6.4480	1.4568	3.6630
Fe	-1.7406	0.7136	5.7576	6.4713	1.5953	2.3189
Ru	-1.5788	0.6938	5.7576	6.4514	1.4470	3.8047
Os	-1.5714	0.6922	5.7576	6.4499	1.4402	3.8619
Zr	-1.5977	0.7270	5.7576	6.4847	1.4643	3.5229
Ir	-1.5718	0.6918	5.7576	6.4494	1.4406	3.8573
Ni	-1.7475	0.7124	5.7576	6.4700	1.6016	2.2727
Pd	-1.5784	0.6904	5.7576	6.4480	1.4466	3.8154
Pt	-1.7402	0.6898	5.7576	6.4474	1.5949	2.3264
Li	-1.8190	0.7013	5.7576	6.4589	1.6671	1.8546
Be	-1.7135	0.7543	5.7576	6.5119	1.5704	2.4632
Mg	-1.7525	0.7265	5.7576	6.4842	1.6062	2.2257
Al	-1.7738	0.6899	5.7576	6.4475	1.6257	2.1360
Ga	-1.7796	0.6896	5.7576	6.4473	1.6310	2.0907
In	-1.7288	0.7534	5.7576	6.5110	1.5844	2.3305
Si	-1.8022	0.7438	5.7576	6.5015	1.6517	1.8953
Ge	-1.7753	0.7140	5.7576	6.4716	1.6270	2.0855
Sn	-1.7050	0.7344	5.7576	6.4920	1.5626	2.5328
Pb	-1.6105	0.8118	5.7576	6.5694	1.4760	3.1789
Sb	-1.6337	0.7038	5.7576	6.4614	1.4973	3.1992
Te	-1.7229	0.6912	5.7576	6.4488	1.5790	2.4642
B	-1.5156	0.9343	5.7576	6.6920	1.3891	3.9857
C	-1.6440	0.9677	5.7576	6.7253	1.5068	2.6515
P	-1.8021	0.7864	5.7576	6.5441	1.6517	1.8447

Table 4.10 ΔH^M, S^σ, ΔS^{ideal}, ΔS^M, $\Delta\eta/\eta_0$ and critical cooling rate for $Ti_{64}Cu_{35}X_1$ alloy (in SI units).

$Ti_{64}Cu_{35}X_1$						
X	**ΔH^M J/mol (10^4)**	**S^σ J/mol.K**	**ΔS^{ideal} J/mol.K**	**ΔS^M J/mol.K**	**$\Delta\eta/\eta_0$**	**R_c K/s (10^5)**
None	-1.8072	0.7044	5.3803	6.0847	1.6563	2.2140
Ag	-1.9126	0.7029	5.8096	6.5125	1.7529	1.3547
Au	-1.9006	0.7027	5.8096	6.5123	1.7419	1.3932
Zn	-1.8148	0.7017	5.8096	6.5113	1.6633	1.8267
Cd	-1.8533	0.7274	5.8096	6.5370	1.6985	1.5938
Co	-1.7964	0.7227	5.8096	6.5324	1.6464	1.9062
Hg	-1.8228	0.7119	5.8096	6.5215	1.6706	1.7497
Sc	-1.8207	0.7573	5.8096	6.5669	1.6687	1.7360
Y	-1.7980	0.8687	5.8096	6.6783	1.6479	1.7252
La	-1.7655	0.9466	5.8096	6.7562	1.6181	1.8025
Hf	-1.6388	0.7305	5.8096	6.5401	1.5020	3.0142
V	-1.8354	0.7089	5.8096	6.5186	1.6821	1.7114
Nb	-1.6757	0.7020	5.8096	6.5116	1.5358	2.7680
Cr	-1.7779	0.7232	5.8096	6.5329	1.6295	2.0158
Mo	-1.5537	0.7033	5.8096	6.5129	1.4239	3.9919
W	-1.5152	0.7030	5.8096	6.5126	1.3887	4.4469
Mn	-1.8032	0.7045	5.8096	6.5141	1.6527	1.8899
Re	-1.6412	0.7025	5.8096	6.5121	1.5042	3.0438
Fe	-1.7895	0.7254	5.8096	6.5350	1.6401	1.9437
Ru	-1.6280	0.7058	5.8096	6.5154	1.4921	3.1855
Os	-1.6211	0.7042	5.8096	6.5139	1.4858	3.2284
Zr	-1.6475	0.7399	5.8096	6.5496	1.5100	2.9421
Ir	-1.6218	0.7038	5.8096	6.5134	1.4864	3.2226
Ni	-1.7960	0.7241	5.8096	6.5337	1.6461	1.9070
Pd	-1.6307	0.7024	5.8096	6.5121	1.4945	3.1648
Pt	-1.7880	0.7019	5.8096	6.5115	1.6387	1.9563
Li	-1.8673	0.7139	5.8096	6.5235	1.7114	1.5562
Be	-1.7621	0.7658	5.8096	6.5755	1.6149	2.0666
Mg	-1.8015	0.7395	5.8096	6.5491	1.6511	1.8633
Al	-1.8230	0.7021	5.8096	6.5117	1.6708	1.7880
Ga	-1.8282	0.7017	5.8096	6.5114	1.6756	1.7537
In	-1.7775	0.7666	5.8096	6.5762	1.6291	1.9525
Si	-1.8517	0.7554	5.8096	6.5651	1.6971	1.5856
Ge	-1.8246	0.7257	5.8096	6.5353	1.6723	1.7455
Sn	-1.7549	0.7474	5.8096	6.5570	1.6084	2.1146
Pb	-1.6594	0.8256	5.8096	6.6352	1.5208	2.6610
Sb	-1.6839	0.7164	5.8096	6.5260	1.5433	2.6694
Te	-1.7742	0.7035	5.8096	6.5131	1.6260	2.0501
B	-1.5624	0.9458	5.8096	6.7554	1.4319	3.3630
C	-1.6916	0.9792	5.8096	6.7888	1.5503	2.2321
P	-1.8521	0.7979	5.8096	6.6076	1.6975	1.5414

From Tables 4.9, 4.10 and Appendix C, it is seen that, $Ti_{65}Cu_{35}$ binary alloy has the lowest critical cooling rate compared to the other investigated alloys. For Ti-Cu and Ti-Zr systems, critical cooling rates are on the order of 10^5 K/s, whereas, Ti-Co system has the highest critical cooling rate that is on the order of 10^7 K/s. Among Ti-Zr binary system, three different master alloys were investigated. For these alloys, lowest critical cooling rate was observed at the mid titanium concentration, that is at $Ti_{50}Zr_{50}$ alloy. Lower critical cooling rates indicate better glass forming ability as stated previously. As a result, $Ti_{65}Cu_{35}$ binary alloy seems to be the best glass former among the studied systems.

Enthalpy of mixing is also important for glass formation; higher negative heats of mixing indicate better glass forming ability. All of the studied systems have enthalpy of mixing values on the order of 10^4 J/mol. But the one that has the most negative value among them is again the $Ti_{65}Cu_{35}$ binary system. For the other systems, enthalpy of mixing shows a similar trend as critical cooling rate.

Glass forming ability is promoted with a rapid increase of viscosity on undercooling. It should be noted that $\Delta\eta/\eta_0$ is positive for ordered alloys since enthalpy of mixing is always negative for glass forming alloys. So it is expected to have larger changes in viscosity of a liquid metal if it possesses better glass forming ability. Among the binary alloys studied in this thesis, $Ti_{65}Cu_{35}$ alloy has the highest $\Delta\eta/\eta_0$ value.

Hence it is important to investigate the behavior of the ternary alloys compared to its binary alloy in terms of critical cooling rate and enthalpy of mixing. For this purpose, Figures 4.2 and 4.3 were formed to show the effect of each ternary alloying element added to Ti-Cu binary system. Results for Ti-Zr and Ti-Co systems are present in Appendix D. Percent change in critical cooling rate and percent change in enthalpy of mixing are seen by addition of each ternary alloying element. Percent changes in critical cooling rate and enthalpy of mixing are given in Equations (2.76) and (2.77) respectively.

$$\%R_c = \frac{R_c^{ternary} - R_c^{binary}}{R_c^{binary}} \times 100 \quad \textbf{(2.76)}$$

$$\%\Delta H^M = \frac{\Delta H^{M,binary} - \Delta H^{M,ternary}}{\Delta H^{M,binary}} \times 100 \quad \textbf{(2.77)}$$

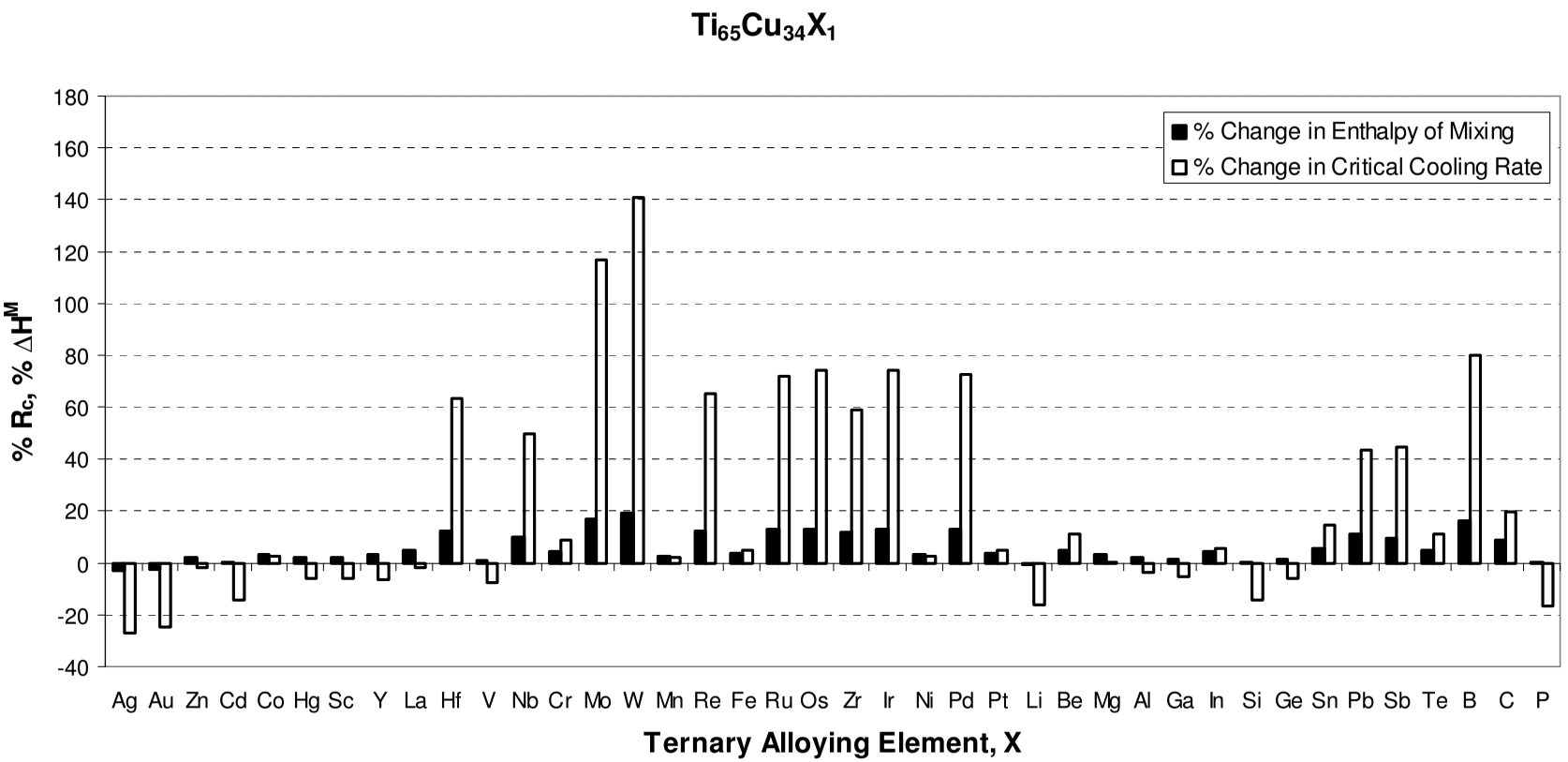

Figure 4.2 Percent changes in critical cooling rate and enthalpy of mixing for $Ti_{65}Cu_{35}$ binary alloy upon addition of 1 at % of X element instead of Cu.

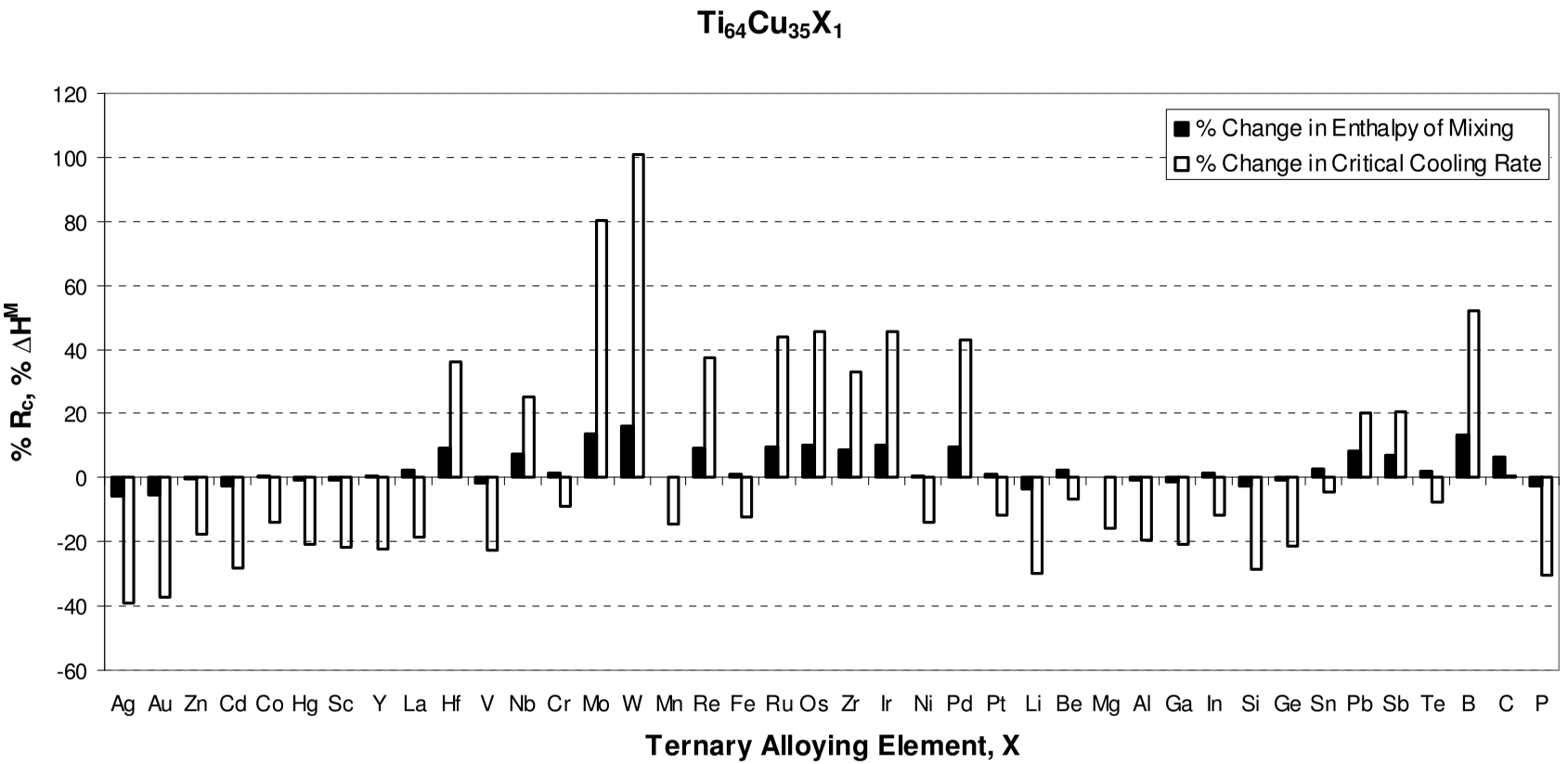

Figure 4.3 Percent changes in critical cooling rate and enthalpy of mixing for $Ti_{65}Cu_{35}$ binary alloy upon addition of 1 at % of X element instead of Ti.

Development of new multicomponent alloy systems having easy bulk glass formation and/or high bulk glass forming ability requires finding out appropriate alloying elements which tend to satisfy following criteria:

i. an increase in the negative enthalpy of mixing, ΔH^M
ii. a decrease in the critical cooling rate, R_c

relative to the given binary alloy. The satisfaction of both of these criteria simultaneously would be favored for effective improvement of BGFA. Although some alloying elements would decrease the negative enthalpy of mixing ΔH^M which is a function of only partial ordering energies of constituent element atoms, the critical cooling rate R_c however, could still be decreased relative to binary alloy due to the fact that R_c parameter is a function of both enthalpy of mixing ΔH^M and entropy of mixing ΔS^M in the liquid state.

For experimental studies, $Ti_{65}Cu_{35}$ binary system was selected due to the results of modeling studies. $Ti_{65}Cu_{35}$ binary alloy has the most negative enthalpy of mixing and short range order parameter, highest $\Delta\eta/\eta_0$, and lowest critical cooling rate. During the synthesis of the ternary system, third alloying element atoms were decided to be added in the place of titanium atoms, since $Ti_{64}Cu_{35}X_1$ systems were found to have lower critical cooling rates and higher negative enthalpy of mixing values compared to $Ti_{65}Cu_{34}X_1$ alloys. Moreover, there are more ternary alloying elements that satisfy criteria (i) and (ii) in $Ti_{64}Cu_{35}X_1$ alloys compared to $Ti_{65}Cu_{34}X_1$ alloys.

It is evident from Figure 4.2 and 4.3 that alloying elements with regard to their effect on BGFA of Ti-Cu-X alloys may be classified into two groups; X_I-group elements (Ag, Au, P, Li, Si, Cd, V, Sc, Ge, Hg, Ga, Al and Zn) satisfying criteria (i) and (ii) simultaneously and X_{II}-group elements (Y, La, Mg, Mn, Co, Ni, Fe, In, Pt, Cr, Te, Be and Sn) those satisfying only criterion (ii). Although X_I-group elements would be considered as potential candidate alloying elements obtaining high BGFA,

some of the X_{II}-group elements (i.e. Y, La) however, show significant decrease in the critical cooling rate which is comparable with the alloying elements those satisfying criteria (i) and (ii) simultaneously. Therefore, it appears that the critical cooling rate becomes the most important parameter for the prediction of candidate alloying elements for improving BGFA since it incorporates the contribution of both enthalpy of mixing and entropy of mixing all together as it was also pointed out by Inoue et al. [64, 85]. This would tend to suggest that not only X_I-group elements but also X_{II}-group elements should be taken into account to develop new Ti-Cu based multicomponent alloy systems having high BGFA.

This present prediction is consistent with experimental studies on the development of Ti-Cu based multicomponent BMGs in which some of the alloying elements have already been used from both X_I- and X_{II}-groups such as X_I = Ag, Al, Si, Zn and X_{II} = Ni, Co, Sn, Be [5, 14, 16-19, 41, 42, 48, 49, 86, 87].

Upon choosing the ternary alloying elements that are going to be added, critical cooling rate values together with binary phase diagrams of elements were considered. As a result Mn, Al and Ni elements were decided to be used in the multicomponent Ti-Cu based alloys. The binary phase diagrams of these elements with Ti and Cu are present in Appendix A.

Table 4.11 Elements decreasing enthalpy of mixing and critical cooling rate for Ti-Zr, Ti-Co and Ti-Cu systems.

Alloy	Elements Decreasing ΔH^M	Elements Decreasing R_c
$Ti_{60}Zr_{39}X_1$	Pd, Mo, B, Cr, C, W, Be Os, Ir, Hf, V, P, Ru, Si, Fe, Ni	Pd, C, B, Be, P, Cr, Mo, W, Os, Ir Si, V, Hf, Fe, La, Ni, Co, Ru, Ge, Re Al, Sc, Mn, Nb, Y, Sn, Ga, Zn, Sb Mg, Pt, Te, Pb, Hg, In, Cd, Cu, Li
$Ti_{59}Zr_{40}X_1$	Pd, B, Mo, Cr, C, Be, W, Os, Ir, V Hf, P, Ru, Si, Fe, Al, Ni, Co, Sc, Re	Pd, C, B, Be, P, Cr, Mo, W, Si, Os Ir, V, Fe, Hf, La, Ni, Co, Ru, Ge, Al Re, Sc, Mn, Nb, Sn, Y, Ga, Zn, Mg Sb, Pt, Te, Pb, Hg, Cd, In, Cu, Li
$Ti_{50}Zr_{49}X_1$	Pd, Ag, B, Be, Cr, C, Mo P, V, W, Si, Al, Os, Ir, Ni Fe, Co, Hf, Mg, Ru, Sc, Ge	Pd, C, B, Ag, Be, P, Cr, Si, Mo, V W, Fe, Ni, Co, Os, Ir, Al, Ge, Ru, Hf Mg, La, Sc, Mn, Re, Zn, Ga, Nb, Sn Y, Pt, Sb, Te, Cd, Li, Hg, Cu, In, Pb
$Ti_{49}Zr_{50}X_1$	Pd, Cd, Be, B, Cr, C, Mo, P, V, W Si, Al, Os, Ir, Ni, Co, Fe, Mg, Hf, Ru	Pd, C, B, Be, Cd, P, Cr, Si, Mo, V W, Ni, Fe, Co, Os, Ir, Al, Ge, Ru, Hf Mg, La, Sc, Mn, Re, Zn, Ga, Nb Sn, Y, Pt, Sb, Te, Li, Hg, Cu, In, Pb
$Ti_{40}Zr_{59}X_1$	Pd, Be, B, Cr, C, P, Al, Si Mg, V, Ni, Co, Mo, Fe, W, Os Ir, Ge, Sc, Hf, Ru, Zn, Ga, Mn	Pd, C, B, Be, P, Cr, Si, V, Al, Ni, Co Fe, Mg, Mo, Ge, W, Os, Ir, Ru, Mn Sc, Hf, Zn, Ga, La, Re, Nb, Pt, Sn Y, Au, Li, Cd, Te, Hg, Sb, Cu, In
$Ti_{39}Zr_{60}X_1$	Pd, Be, B, Cr, C, P, Al, Si Mg, V, Co, Ni, Mo, Fe, W	Pd, B, C, Be, P, Cr, Si, V, Al, Ni Co, Fe, Mg, Mo, Ge, W, Os, Ir, Ru Sc, Mn, Zn, Hf, Ga, La, Re, Nb Pt, Sn, Li, Y, Cd, Hg, Te, Sb, Cu
$Ti_{68}Co_{31}X_1$	W, Mo, Re, Os, Ir, Hf, Ru, Zr Pd, B, Nb, Pb, Sb, La, Te, Sn C, Y, In, Be, Cr, Fe, Mg, Pt, Sc, Ni	W, Mo, Re, B, Hf, Os, Ir, Zr, Ru Pb, Pd, Nb, Sb, La, C, Y, Te, Sn In, Be, Cr, Fe, Mg, Sc, Pt, Ni, Ge Mn, P, Hg, Zn, Al, Ga, V, Si, Cd
$Ti_{67}Co_{32}X_1$	W, Mo, Re, Os, Ir, Hf, Ru, Zr Pd, B, Nb, Pb, Sb, La, Te, Sn C, Y, In, Be, Cr, Fe, Pt, Mg, Sc	W, Mo, Re, B, Hf, Os, Ir, Zr, Ru Pb, Pd, Nb, Sb, La, C, Y, Te, Sn, In Be, Cr, Fe, Mg, Sc, Pt, Ni, Ge, Mn Hg, P, Zn, Al, Ga, V, Si, Cd, Cu, Au
$Ti_{65}Cu_{34}X_1$	Ag, Au, Li	Ag, Au, P, Li, Si, Cd, V Y, Sc, Hg, Ge, Ga, Al, La, Zn
$Ti_{64}Cu_{35}X_1$	Ag, Au, Li, Cd, P, Si V, Ga, Ge, Al, Hg, Sc, Zn	Ag, Au, P, Li, Si, Cd, V, Y, Sc Ge, Hg, Ga, Al, La, Zn, Mg, Mn Co, Ni, Fe, In, Pt, Cr, Te, Be, Sn

4.2 Experimental Studies on Bulk Glass Forming Ability of Ti-Based Alloys

4.2.1 Ti-Cu Binary Alloy

Upon the selection of binary alloy composition, a criterion which deals with the sequence of reactions that an alloy undergoes was consulted to. It was suggested that, the characteristic DSC pattern of melting involving a sequence of eutectic and peritectic like reactions with a high magnitude of reaction enthalpies ratio, ($\Delta H_p/\Delta H_e$), appears to be essential for high BGFA [20]. With considering this, the binary alloy composition was adjusted to $Ti_{65}Cu_{35}$. The alloy was prepared with arc melting and characterized with SEM, EDS, DSC and XRD. The arc melted $Ti_{65}Cu_{35}$ binary alloy was named as A1 and will be referred as so from this point on. The binary phase diagram of Ti-Cu system is given in Figure 4.4 and the alloy studied is marked on it for a better understanding of the reactions it is expected to undergo. The special points of Ti-Cu equilibrium phase diagram are given in Table 4.12. It is important to note that this phase diagram is valid for equilibrium conditions.

For $Ti_{65}Cu_{35}$ alloy, upon cooling from liquid state, first microstructural change is expected right after the liquidus line. Dendrites of Ti(β) are expected to form in the liquid after the temperature of the system decreases below liquidus temperature, which is approximately equal to 1040°C. When the system reaches peritectic temperature, which is 1005°C, peritectic reaction occurs; dendrites of Ti(β) react with liquid and form Ti_2Cu. At 960°C, eutectic reaction occurs and the remaining liquid transforms into two different solid phases which are Ti_2Cu and TiCu. So, one expects to see Ti(β) dendrites encapsulated by Ti_2Cu phase in a eutectic matrix of Ti_2Cu and TiCu at equilibrium cooling of $Ti_{65}Cu_{35}$ alloy.

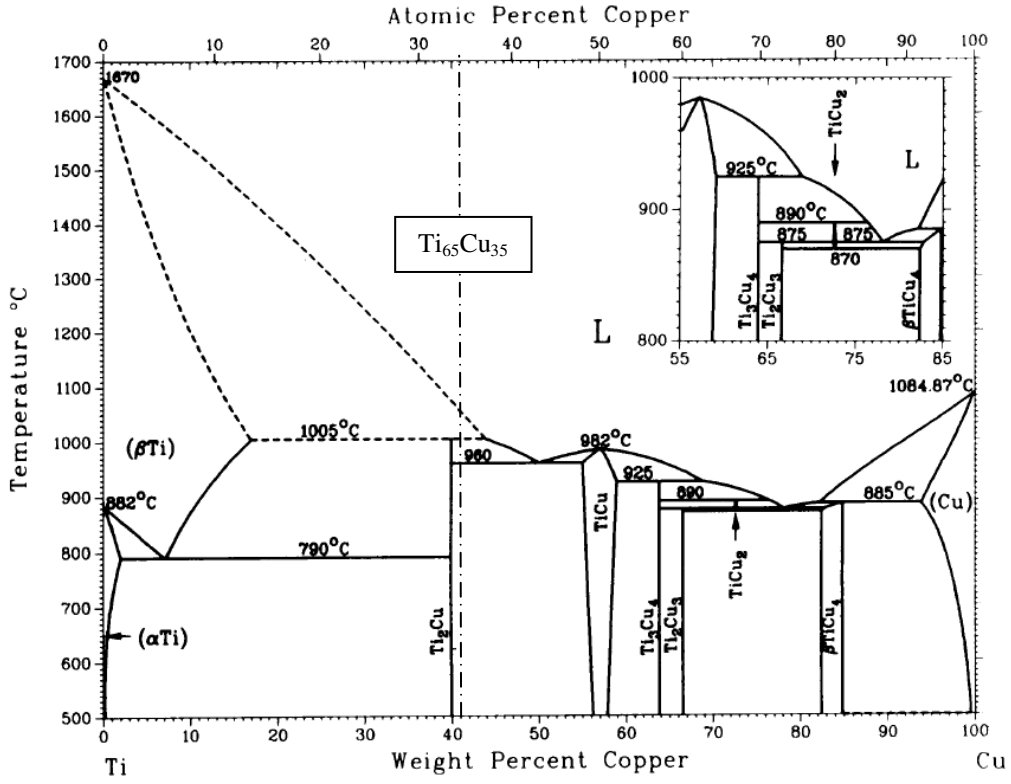

Figure 4.4 Equilibrium binary phase diagram of Ti-Cu.

Table 4.12 Special points of the Ti-Cu phase diagram.

Reaction	Compositions of the respective phases, at % Cu			Temperature, °C	Reaction type
$Ti(\beta)+L \leftrightarrow Ti_2Cu$	13.5	36.5	33.3	1005 ± 10	Peritectic
$Ti(\beta) \leftrightarrow Ti(\alpha)+Ti_2Cu$	5.4	1.6	33.3	790 ± 10	Eutectoid
$L \leftrightarrow Ti_2Cu+TiCu$	43	33.3	48	960 ± 5	Eutectic
$L \leftrightarrow TiCu$		50		985 ± 10	Congruent
$TiCu+L \leftrightarrow Ti_3Cu_4$	52	62.5	57.1	925 ± 10	Peritectic
$Ti_3Cu_4+L \leftrightarrow TiCu_2$	57.1	71	66.7	890 ± 10	Peritectic
$Ti_3Cu_4+TiCu_2 \leftrightarrow Ti_2Cu_3$	57.1	66.7	60	875 ± 10	Peritectoid
$L \leftrightarrow TiCu_2+\beta TiCu_4$	73	66.7	78	875 ± 10	Eutectic
$TiCu_2 \leftrightarrow Ti_2Cu_3+\beta TiCu_4$	66.7	60	78	870 ± 10	Eutectoid
$L+(Cu) \leftrightarrow \beta TiCu_4$	77	92	80.9	855 ± 10	Peritectic
$\beta TiCu_4 \leftrightarrow Ti_2Cu_3+\alpha TiCu_4$	~ 78	60	~ 78	~ 400	Eutectoid
$\beta TiCu_4 \leftrightarrow \alpha TiCu_4+(Cu)$	~ 80.9	~ 80.9	99.5	~ 500	Peritectoid
$Ti(\beta) \leftrightarrow Ti(\alpha)$		0		882	Allotropic Transformation
$L \leftrightarrow Ti(\beta)$		0		~ 1670	Melting Point
$L \leftrightarrow (Cu)$		100		1084.87	Melting Point

In order to investigate the microstructure of arc melted $Ti_{65}Cu_{35}$ alloy, A1 was metallographically prepared by using the methods described in section 3.2.2.1 and observed under SEM. The alloys prepared with arc melting may reveal different microstructures throughout its cross-section. The copper plate on which the elements are placed for melting has a water cooling system underneath it. Thus, the portion of the melted alloys that is in contact with the copper plate undergoes a faster cooling. As a result, different microstructures may be observed in different regions of arc melted specimens. Figure 4.5 schematically illustrates an arc melted sample, where region 1 is the portion that is in contact with the copper plate, hence it is the portion that has the highest cooling rate, region 2 and 3 are the parts that are free of contact to copper plate, and obviously, region 3 is the part that has the slowest cooling rate.

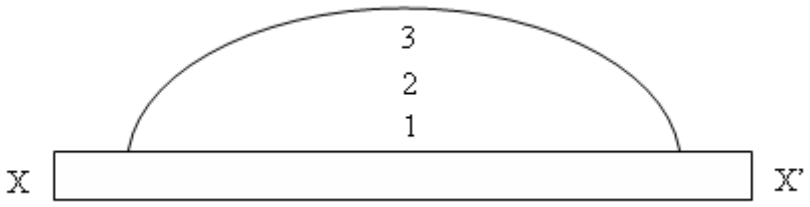

Figure 4.5 Schematic view of an arc melted sample. X-X' denotes the basal plane of the copper plate.

Figure 4.6 illustrates the SEM images of alloy A1 that were taken from section 1. This alloy revealed the same microstructure throughout its cross-section; hence microstructure pictures from one section are enough to generalize the alloy. Table 4.13 gives the EDS results obtained from the phases present in alloy A1.

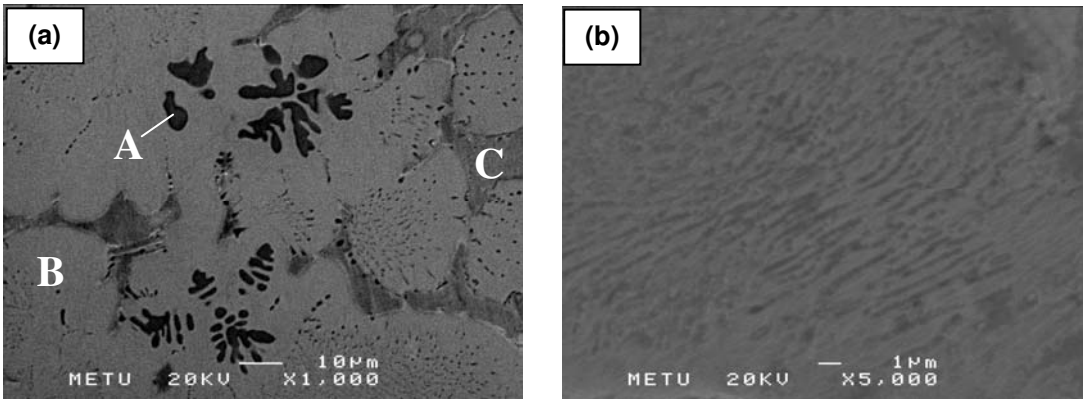

Figure 4.6 Microstructure of alloy A1 from region 1 at magnification of (a) 1000 and (b) 5000.

Table 4.13 EDS analysis for alloy A1.

A1	at% Ti	at% Cu
General	66.43	33.57
A	91.02	8.8
B	68.74	31.26
C	53.09	46.91

In Figure 4.6(a), black dendrites (A) were found to contain 91 at % Ti, indicating that these are the Ti(β) dendrites that were formed in the liquid above the peritectic temperature. Ti_2Cu phase is expected to be seen around these dendrites according to the equilibrium phase diagram. However there is no such structure seen in alloy A1. Peritectic reactions are slow reactions because they require diffusion in the solid phase, hence in most of the cases, peritectic reactions cannot be completed before reaching to eutectic temperature [88]. Moreover, the temperature difference between eutectic and peritectic reactions in Ti-Cu system is very small, 45°, supporting that it is even harder for this system to undergo peritectic reaction before eutectic transformation for non-equilibrium cooling conditions. So, solidification of the alloy after arc melting may be categorized as non-equilibrium cooling. The dendrites (B) present in Figure 4.6(a) were analyzed to contain 69 at % Ti and 31 at % Cu. When these dendrites were further analyzed at higher magnifications, Figure

4.6(b), the irregular eutectic structure present inside them was observed more clearly. The elements used during the experiments were high purity elements but they still contained impurities. It is known that, third impurity elements may cause two-phase instability and hence result in the formation of eutectic cells or even eutectic dendrites [88]. With the morphology seen in Figure 4.6(b), i.e. the eutectic dendrites, the alloy A1 may be attributed to have two-phase instability. If the binary off-eutectic alloy had contained dendrites of one phase and interdendritic two phase eutectic, it would be attributed to single-phase instability. The *C* phase present between the *B* dendrites was predicted to belong to TiCu intermetallic. However TiCu is not expected to form at the composition of alloy A1. The reason behind the occurrence of this phase is probably the skewed coupled zone phenomenon. A skewed coupled zone, Figure 4.7(a), is normally in correlation with irregular eutectic growth and is skewed towards the phase that has growth problems. The formation of eutectic or eutectic plus dendrites of primary phase depends on the competitive growth of these structures. This can be explained by their growth temperatures as a function of growth rate, Figure 4.7(c) and (d).

The phase growing with the highest tip/front temperature will be the phase that is going to take place in the structure. For a eutectic alloy, Figure 4.7(a) and (c), slow cooling rates will yield to eutectic phase mixture formation whereas higher cooling rates will result in eutectic and α phase formation. For an off-eutectic alloy, Figure 4.7(a) and (d), slow cooling rates will result in the formation of only eutectic phase mixture, moderate cooling rates will yield to eutectic and β phase formation, moderate to high cooling rates will cause only eutectic phase mixture formation and high cooling rates will yield to eutectic and α phase formation. The behavior of glass forming regions related to skewed coupled zone phenomena is present in Figure 4.7(b) [89]. In the case of alloy A1, eutectic dendrites and TiCu phase is present meaning that the phase diagram was skewed towards Ti_2Cu and cooling rate was high enough to cause the formation of eutectic together with TiCu.

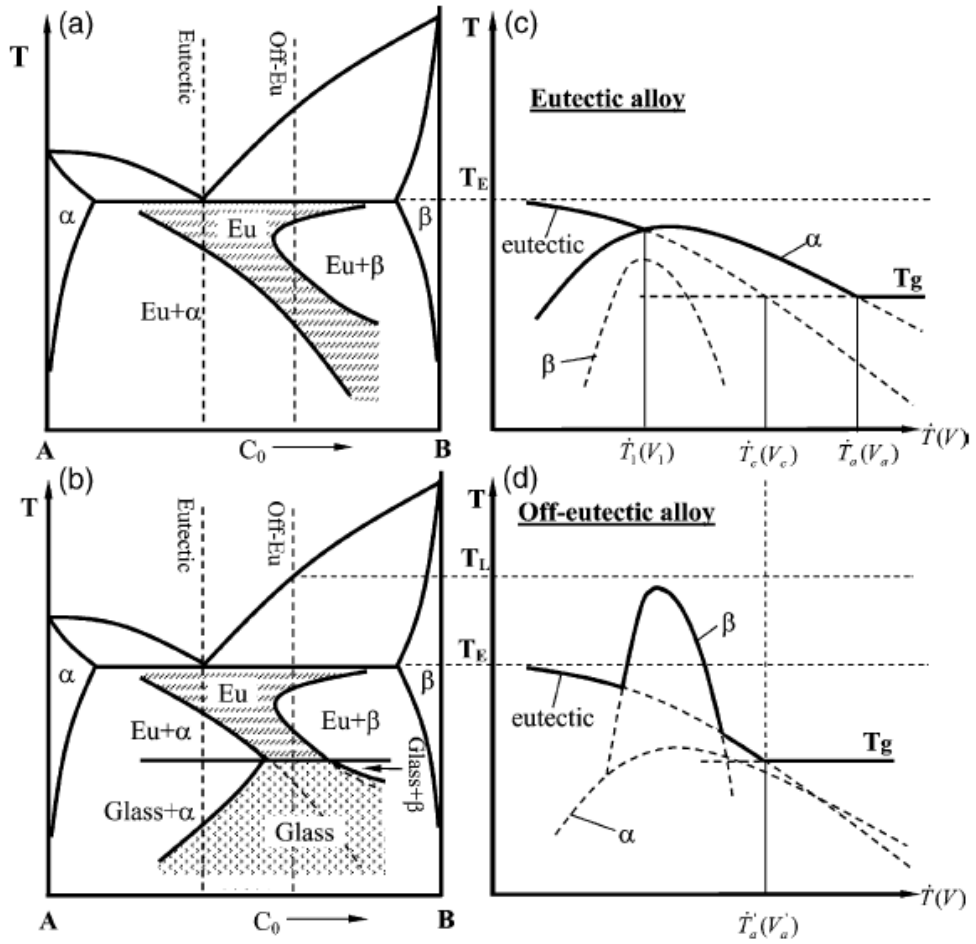

Figure 4.7 Schematic diagrams showing skewed eutectic coupled zone and its relation to the glass forming ability: (a) a eutectic system with a skewed coupled zone, (b) glass forming and composite forming regions related to the skewed coupled zone, (c) growth temperature of the constituents as a function of cooling rate (growth rate) for the eutectic alloy and (d) growth temperature of the constituents as a function of growth rate (cooling rate if temperature gradient is constant) for an off-eutectic alloy [89].

Afterwards, alloy A1 was thermally analyzed with DSC to investigate the reactions that the alloy will undergo with a heating rate of 20°C/min. Figure 4.8 shows the DSC trace of alloy A1 which includes two peaks having the thermal data given in Table 4.14. It is obvious from the DSC thermogram that two successive endothermic peaks on heating indicate that the alloy undergoes melting in two stages; eutectic reaction followed by a peritectic reaction.

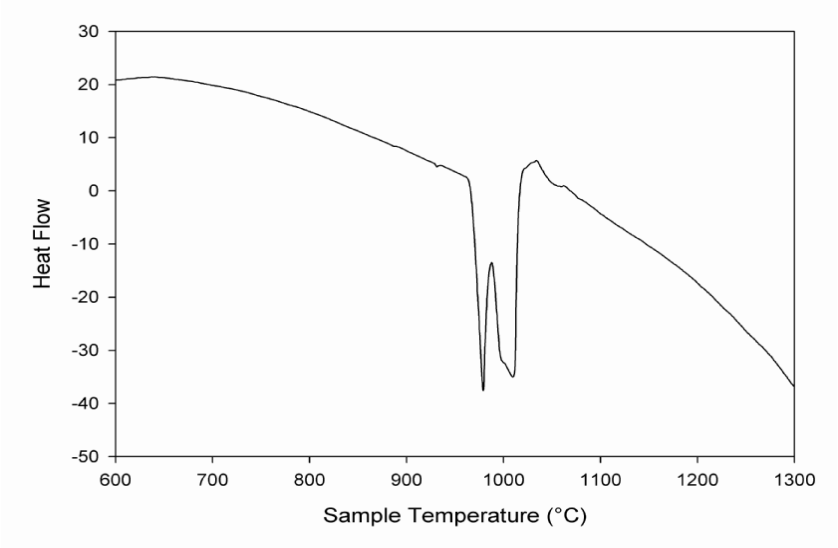

Figure 4.8 DSC heating curve for alloy A1 obtained with a heating rate of 20°C/min.

Table 4.14 Thermal analysis data for alloy A1. T_e denotes eutectic, T_p denotes peritectic temperatures. $\Delta H^{M,e}$ is the enthalpy for eutectic and $\Delta H^{M,p}$ is the enthalpy for peritectic reactions.

T_e (°C)	T_p (°C)	$\Delta H^{M,e}$ (J/gr)	$\Delta H^{M,p}$ (J/gr)
978.76	1003.11	34.7518	60.7447

Alloy A1 was further analyzed with XRD, Figure 4.9(a), to justify the predicted phases present in the structure. Ti_2Cu and Ti phases were also confirmed with XRD analysis. However the most intense peaks of TiCu phase could not have been observed. The peak that is referred as unknown actually belongs to TiCu, but did not name as so due to the absence of the highest intensity peaks of the phase. The reason behind the absence of TiCu peaks can be the relative amounts of Ti_2Cu and TiCu. Since the Ti_2Cu peaks were observed to be very intense, TiCu peaks might be missing in the diffractogram due to the small intensity of them. The reason of the appearance of unknown peak (which actually belongs to TiCu) can be attributed to the texturing of the (100) planes which gave diffraction to form the unknown peak in the diffractogram.

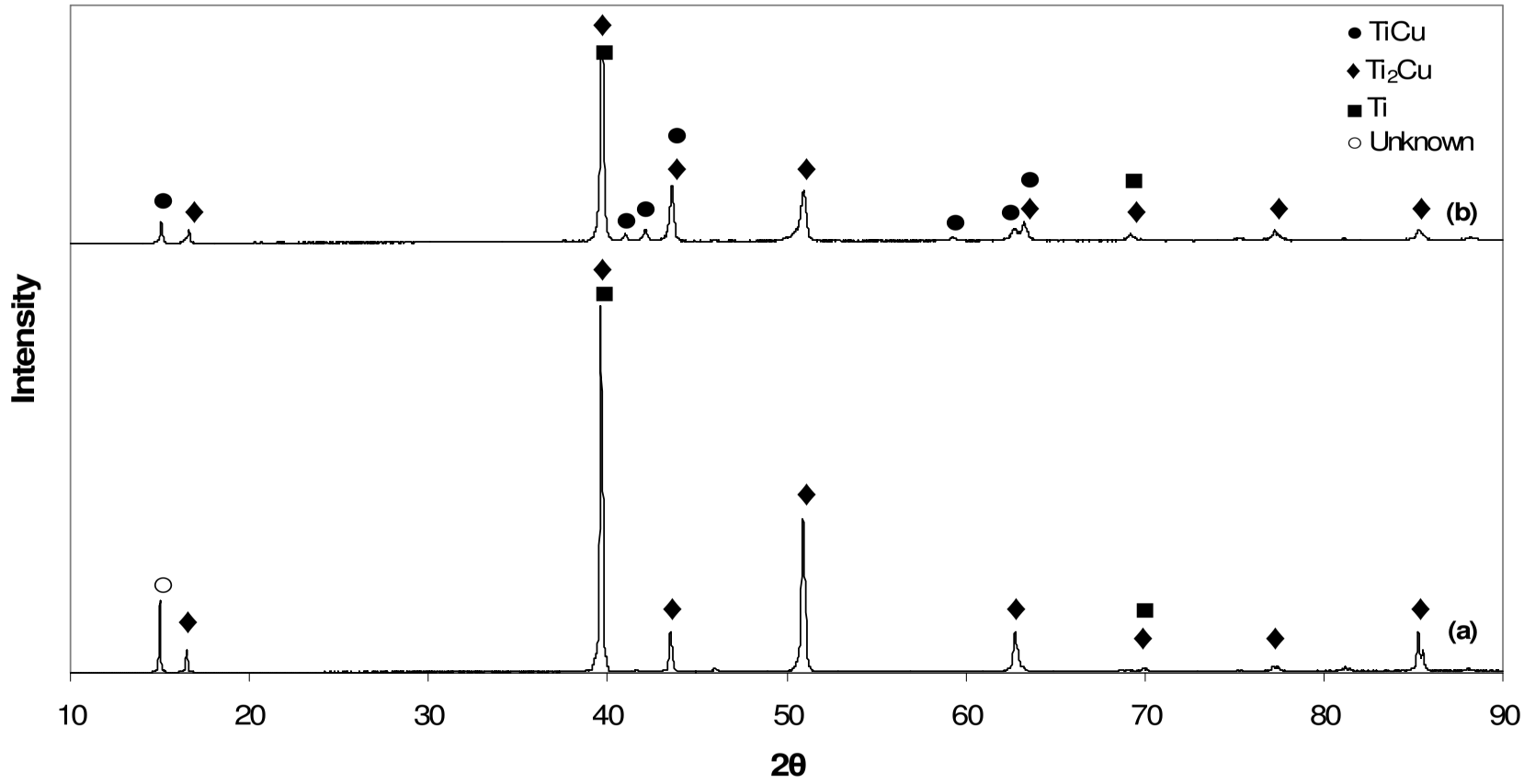

Figure 4.9 XRD pattern of (a) Alloy A1, (b) Alloy C1.

Alloy A1 was cast into Cu-molds at 1250°C with using a centrifugal casting machine in order to observe the effects of fast cooling conditions. The alloy prepared via fast cooling was named as alloy C1 and will be referred as so from now on. The Cu-molds used during the experiments have wedge shaped geometry, Figure 3.2, where thickness varies with length. Figure 4.10 illustrates a centrifugal cast sample having wedge shaped geometry. Obviously, thinner sections, indicated as X, have the highest cooling rate, whereas cooling rate decreases as the thickness of the section increases.

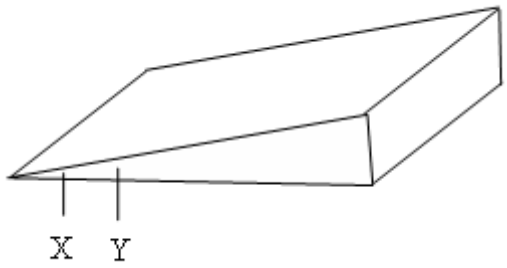

Figure 4.10 Shape of a centrifugally cast alloy. Thickness changes along the length of the specimen.

Alloy C1 was analyzed under SEM to observe the microstructural features present in the alloy and to compare them with the ones present in the arc melted alloy, A1. Figure 4.11 illustrates the structure of the thinnest part of alloy C1. Black dendrites indicated as *A*, were again found to be Ti(β) dendrites formed before peritectic reaction (see Table 4.15). Peritectic reaction product, Ti_2Cu, encapsulating the Ti(β) dendrites are not present here as well. But this is understandable; even arc melting was enough to skip peritectic reaction, it was not expected to imagine the reaction to occur at a faster cooling rate. *B* grains were found to contain almost same composition as the ones present in alloy A1. However, due to the fine structure of alloy C1, the inside of the grains could not be revealed to contain a eutectic phase mixture. *C* phase was again expected to be TiCu. So when compared to alloy A1, it

can be said that only difference is the size of the grains. All the phases present have formed with smaller sizes, which is an expected result since structures become finer as the cooling rate becomes higher.

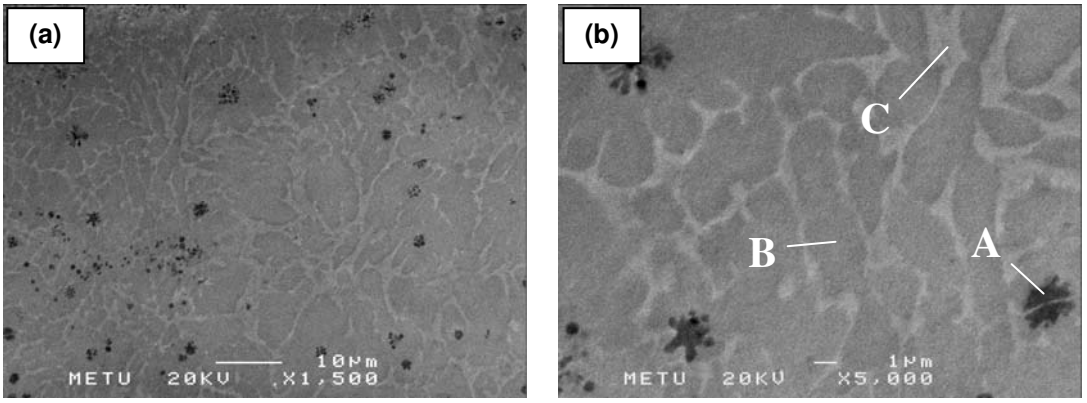

Figure 4.11 Microstructure of alloy C1 from region X at magnification of (a) 1500 and (b) 5000.

Table 4.15 EDS analysis for alloy C1.

C1	at.% Ti	at.% Cu
General	66.73	33.27
A	88.68	11.32
B	68.35	31.65
C	57.92	42.08

DSC analysis of alloy C1, Figure 4.12, includes the two endothermic peaks that were determined to belong to eutectic and peritectic reactions. When the data present in Table 4.16 is compared with the thermal data for alloy A1, it is seen that the peak temperatures for alloys A1 and C1 are almost same, suggesting that fast cooling of alloy A1 did not result in the amorphization of the alloy. This result is in good agreement with microstructral analysis, since no featureless matrix or a different phase that is present when compared to alloy A1 could have been observed in alloy C1.

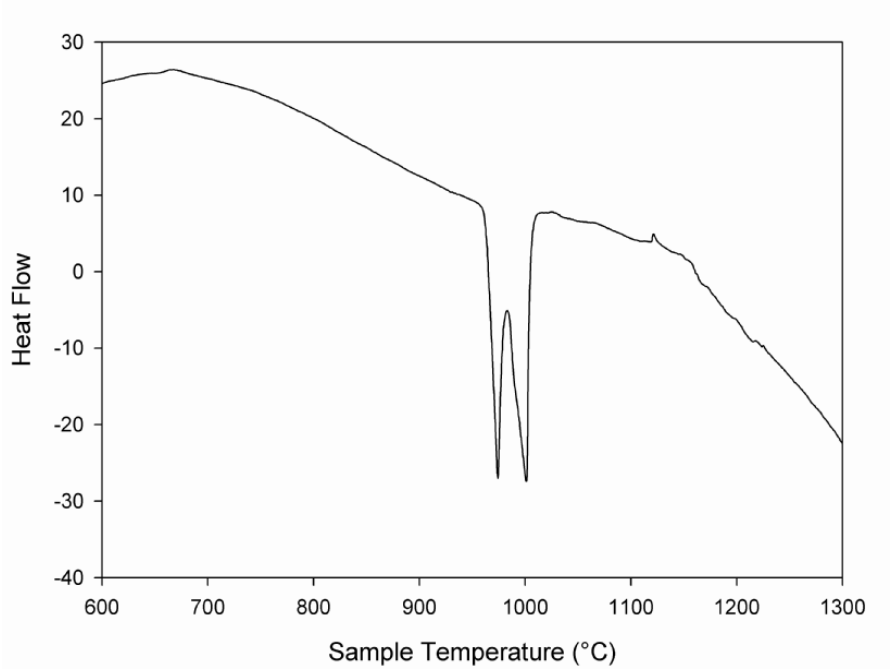

Figure 4.12 DSC heating curve for alloy C1 obtained with a heating rate of 20°C/min.

Table 4.16 Thermal analysis data for alloy C1. T_e denotes eutectic, T_p denotes peritectic temperatures. $\Delta H^{M,e}$ is the enthalpy for eutectic and $\Delta H^{M,p}$ is the enthalpy for peritectic reaction.

T_e (°C)	T_p (°C)	$\Delta H^{M,e}$ (J/gr)	$\Delta H^{M,p}$ (J/gr)
974.26	1001.36	43.6800	68.7258

XRD analyses were performed for the confirmation of the predicted phases in alloy C1, Figure 4.9(b). In addition to Ti_2Cu and Ti peaks, TiCu peaks were also observed in this alloy. So it can be concluded that XRD studies were found to be in good agreement with SEM and EDS analyses.

4.2.2 Effects of Alloying Element Additions to Ti-Cu Binary Alloy

Manganese, aluminum and nickel were chosen as candidate elements to increase the BGFA of $Ti_{65}Cu_{35}$ binary alloy with the help of the theoretical studies described in section 4.1. In order to observe the effects of each element on the Ti-Cu binary system, several alloys were prepared with both arc melting and centrifugal casting operations. For easier designation, each alloy that has been studied was given a name and will be referred as so from this point on, Table 4.17.

Table 4.17 Studied alloy systems.

Alloy Name	Composition	Production Method
A1	$Ti_{65}Cu_{35}$	Arc Melting
A2	$Ti_{60}Cu_{35}Mn_5$	Arc Melting
A3	$Ti_{60}Cu_{35}Al_5$	Arc Melting
A4	$Ti_{60}Cu_{35}Ni_5$	Arc Melting
A5	$Ti_{59}Cu_{35}Mn_5Al_1$	Arc Melting
A6	$Ti_{59}Cu_{35}Mn_5Ni_1$	Arc Melting
A7	$Ti_{58}Cu_{35}Mn_5Al_1N_{i1}$	Arc Melting
C1	$Ti_{65}Cu_{35}$	Centrifugal Casting
C2	$Ti_{60}Cu_{35}Mn_5$	Centrifugal Casting
C3	$Ti_{60}Cu_{35}Al_5$	Centrifugal Casting
C4	$Ti_{60}Cu_{35}Ni_5$	Centrifugal Casting
C5	$Ti_{59}Cu_{35}Mn_5Al_1$	Centrifugal Casting
C6	$Ti_{59}Cu_{35}Mn_5Ni_1$	Centrifugal Casting
C7	$Ti_{58}Cu_{35}Mn_5Al_1N_{i1}$	Centrifugal Casting

First of all, effects of Mn addition were investigated, and alloys A2 and C2 were produced, where the casting operation for alloy C2 was performed at 1250°C. Microstructures of each alloy were analyzed with SEM and EDS and are presented in Figure 4.13 and Table 4.18. As seen, alloy A2 was found to contain different microstructures in different regions Figure 4.13(a)-(d). However, recall that, this was not the case for alloy A1; it contained similar phases everywhere. This is an

indication that Mn addition caused different microstructures within each section of the alloy due to the variation of cooling rate. The structure of region 1 of alloy A2 is consisted of fine dendrites (A) that were found to have a composition indicated in Table 4.18, suggesting that these dendrites may belong to Ti_2Cu phase containing some Mn dissolved in it. As cooling rate decreased towards regions 2 and 3, different structures were observed. In region 2, lamellar grains (B) containing a white contrasted phase (C) at grain boundaries were seen, Figure 4.13(b). The lamellar grains were analyzed to have a composition which is very close to the composition of the alloy. The white contrasted phase was found to contain mainly Cu. Figure 4.13(c) and (d) show the microstructure at region 3. This region's structure resembles the structure of region 1 with some main differences. The structure in general is coarser in region 3 compared to region 1 due to the decreased cooling rate. The dendrites were again found to contain the same composition as the ones in first region and the matrix was observed more clearly compared to first region and was analyzed to have a composition that is nearly same as the lamellar grains' composition present in region 2. Moreover, there exist some other dendrites present on top of *A* dendrites as seen in parts (c) and (d). These dendrites, D, were analyzed better with using the back scattered electron mode of SEM, Figure 4.13(d). When their composition was investigated, it can be said that they probably belong to Ti dendrites. However when the SEM analysis were performed for alloy C2, it was found to contain a completely different microstructure than alloy A2, Figure 4.13(e) and (f). These pictures were taken from the thinnest section of the alloy, referred as region X. As seen, the matrix (F) could not be resolved, indicating that it has a very fine structure. EDS analysis from matrix showed that this part has a composition which is very close to the composition of the alloy, Table 4.18. The dendrites seen, E, may belong to Ti phase due to the very high amount of Ti detected in them. The microstructure of the alloy towards region Y was very similar to the structure of region X. Only difference was that region Y was found to contain more *E* dendrites. So, it can be said that, with fast cooling conditions, formation of Ti_2Cu dendrites, lamellar matrix and the Cu rich phase, which was named as *C*,

observed in alloy A2 was suppressed, whereas the same suppression could not have been obtained for Ti dendrites.

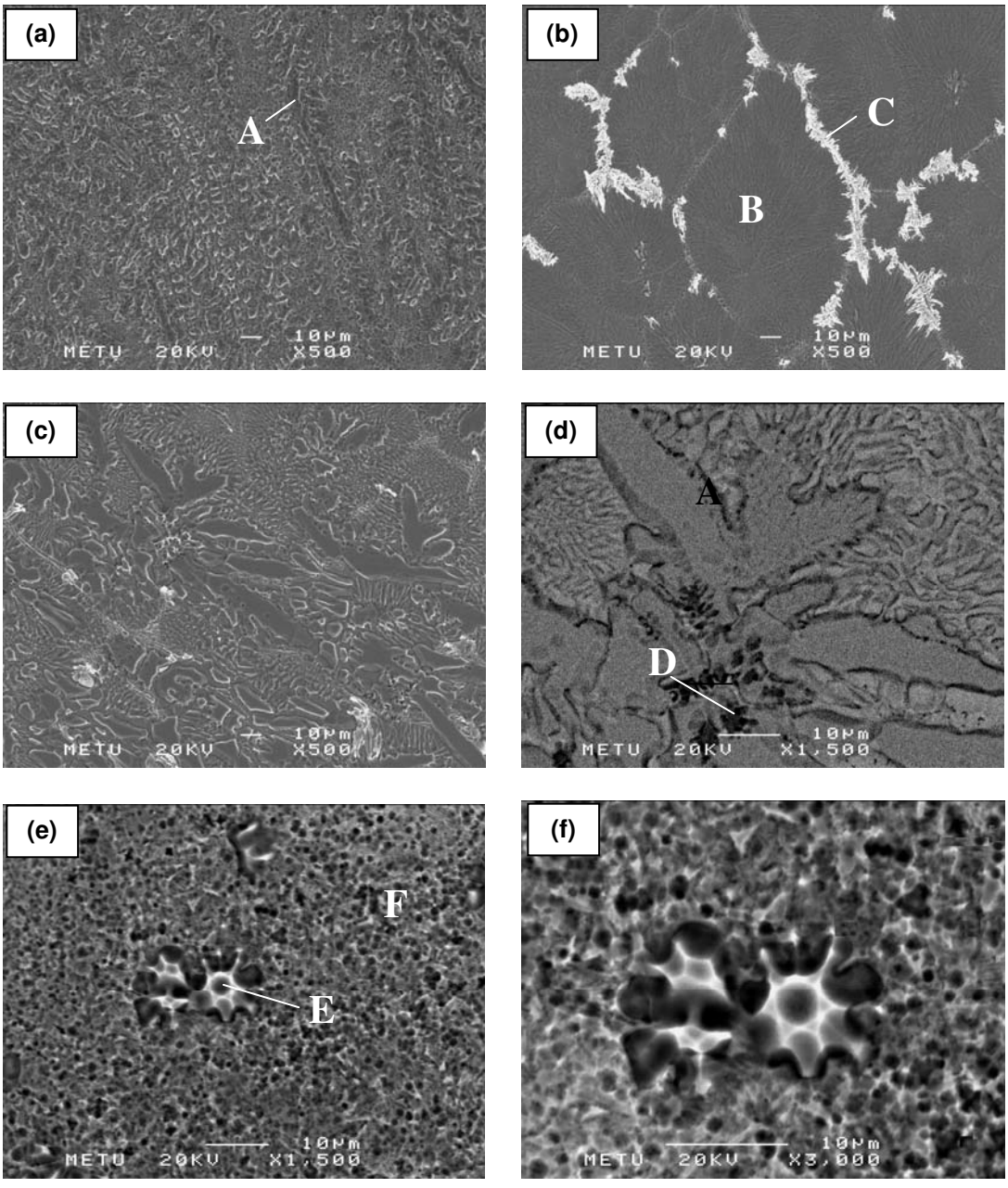

Figure 4.13 Microstructure of alloy A2 from (a) region 1, (b) region 2, (c) region 3, and (d) region 3 in back scattered electron mode. Microstructure of alloy C2 from region X at magnification of (e) 1500, and (f) 3000.

Table 4.18 EDS analysis for alloys A2 and C2.

A2	**at.% Ti**	**at.% Cu**	**at.% Mn**
General	61.28	33.44	5.28
A	67.21	31.33	1.46
B	63.35	31.57	5.08
C	32.26	65.24	2.50
D	96.97	3.03	0
C2	**at.% Ti**	**at.% Cu**	**at.% Mn**
General	63.11	32.60	4.29
E	96.75	3.00	0.25
F	60.97	33.14	5.88

In addition to the microstructral studies, thermal analyses of these alloys were also done to investigate the reactions that they undergo upon heating, Figure 4.14 and Table 4.19. Both of the alloys contained a deep peak which may indicate a first order reaction and a peak which may belong to melting at liquidus line. However the peak at T_1 temperature in alloy A2 was not observed in thermal behavior of alloy C2, indicating that with fast cooling conditions, this peak, which may belong to a second order transformation, was suppressed.

XRD analyses of alloy A2 and C2 revealed out that both of the alloys contained TiCu, Ti_2Cu, Cu_2Ti and Ti phases, Figure 4.15. The latter three phases were also confirmed with the SEM and EDS studies for alloy A2, however TiCu phase could not have been found to show a trail during the indicated analyses. But according to the XRD investigations, it is obvious that the alloy A2 contains TiCu phase, indicating that this phase may either come from the eutectic phase mixture or from a very fine microstructure that could not have been analyzed using SEM or EDS. However during the microstructral studies of alloy C2, only Ti phase could have been observed, meaning that other phases present are probably dispersed finely in the matrix from which separate analysis could not have been taken. Different from

diffraction pattern of alloy A2, alloy C2 was found to contain a peak belonging to O_2, which may indicate that the alloy was contaminated with air during the centrifugal casting operation.

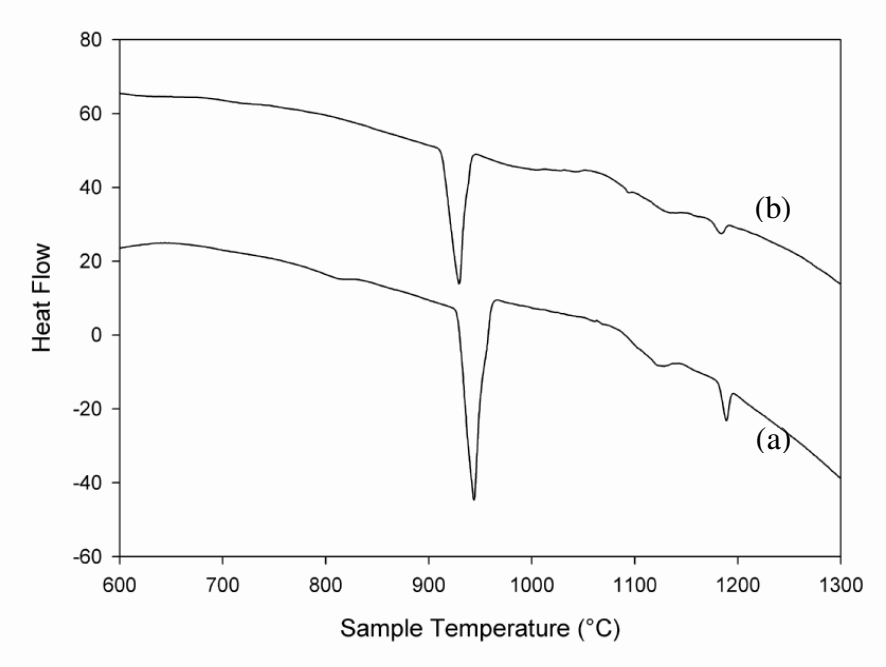

Figure 4.14 DSC heating curves for (a) alloy A2, and (b) alloy C2 obtained with a heating rate of 20°C/min.

Table 4.19 Thermal analysis data for alloys A2 and C2, where temperatures are in terms of °C, and enthalpy of mixing values are in terms of J/gr.

A2	T_1	T_2	T_3	T_4	$\Delta H^{M,1}$	$\Delta H^{M,2}$	$\Delta H^{M,3}$	$\Delta H^{M,4}$
	812	944.04	1122.44	1188.72	3.7009	158.1413	7.7405	10.7952
C2	T_1	T_2	$\Delta H^{M,1}$	$\Delta H^{M,2}$				
	929.50	1183.45	95.6732	4.8543				

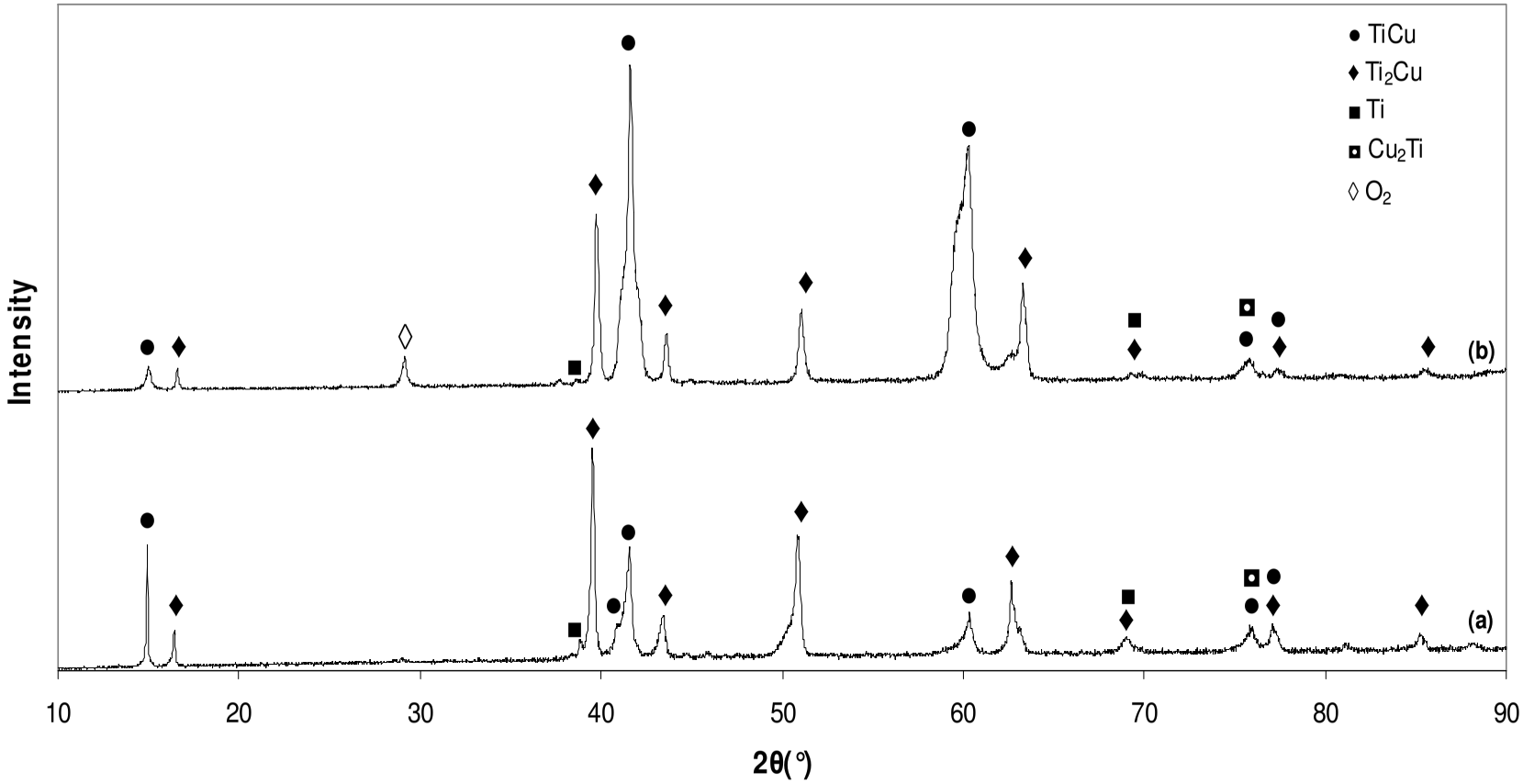

Figure 4.15 XRD pattern of (a) Alloy A2, (b) Alloy C2.

Afterwards, effects of Al were started to be investigated with producing alloys A3 and C3. However, during the casting operation to obtain alloy C3, some difficulties were encountered. The alloy was tried to be centrifugally cast at 1370°C, but still complete casting of the alloy into the Cu-mold could not have been achieved. SEM analyses for alloys A3 and C3 are given in Figure 4.16. As seen, the microstructure of the alloy changed a lot depending on the production method, in other words cooling rate. Alloy A3 was found to contain the same structure in all the investigated regions, Figure 4.16(a) and (b). The *A* grains were found to have a composition given in Table 4.20, with the possibility of being Ti_2Cu phase containing some Al dissolved in it. The thin phase between the grains, B, was analyzed to contain almost same amount of Ti and Cu, stating that this phase is most probably TiCu having some Al in it. Finally the black phase, C, was also analyzed and found to contain high amounts of Ti meaning that it can be either almost pure Ti or a Ti rich phase; exact decision could not have been made due to the very fine structure of this phase. When the microstructure of alloy C3 was analyzed, neither Ti_2Cu nor TiCu phases could have been observed, Figure 4.16(c) and (d). However Ti dendrites (D) were again present in the alloy. Moreover alloy C3 also contained *E* phase which is probably a complex intermetallic of Ti, Cu and Al elements, and *F* phase which acts like a matrix with having a composition close to the general composition of the ternary alloy, Table 4.20.

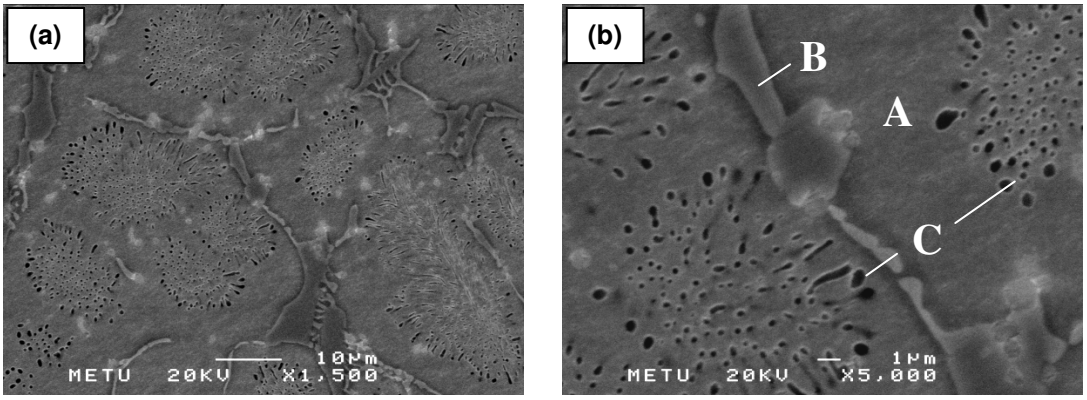

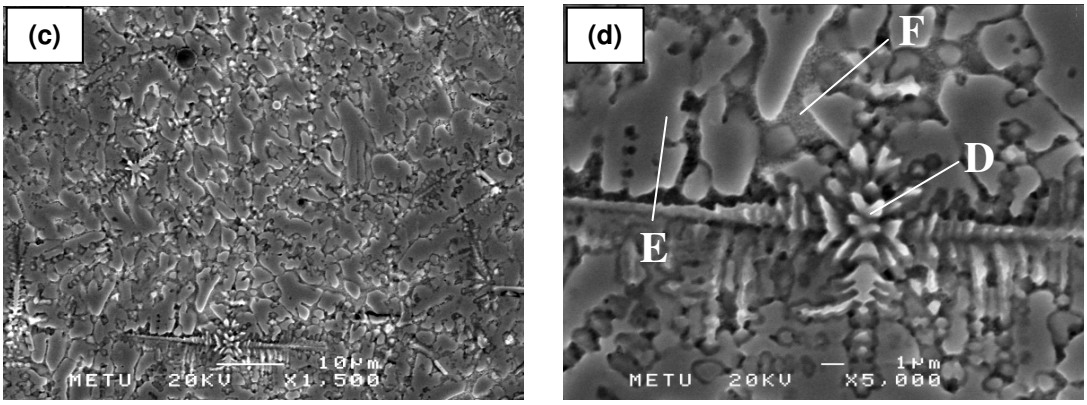

Figure 4.16 Microstructure of alloy A3 from region 1 at magnification of (a) 1500 and (b) 5000, alloy C3 from region X at magnification of (c) 1500 and (d) 5000.

Table 4.20 EDS analysis for alloys A3 and C3.

A3	**at.% Ti**	**at.% Cu**	**at.% Al**
General	59.65	35.35	5.00
A	63.63	32.85	3.52
B	47.24	47.82	4.94
C	73.10	22.13	4.78
C3	**at.% Ti**	**at.% Cu**	**at.% Al**
General	59.87	32.42	7.71
D	92.18	6.05	1.83
E	39.54	34.54	25.92
F	54.46	39.15	6.29

Thermal analyses of alloys A3 and C3 exhibited different behavior as seen in Figure 4.17. Alloy A3 was found to contain three reactions that are close to each other at the temperatures indicated in Table 4.21. However alloy C3 did not have any of these reactions at the stated temperatures. Instead, it showed a single peak at a higher temperature and another peak which may belong to a second order transition. Alloy A3 did not have any of these reactions seen in alloy C3, but exhibited a peak at temperature T_4, which may belong to the reaction at liquidus line.

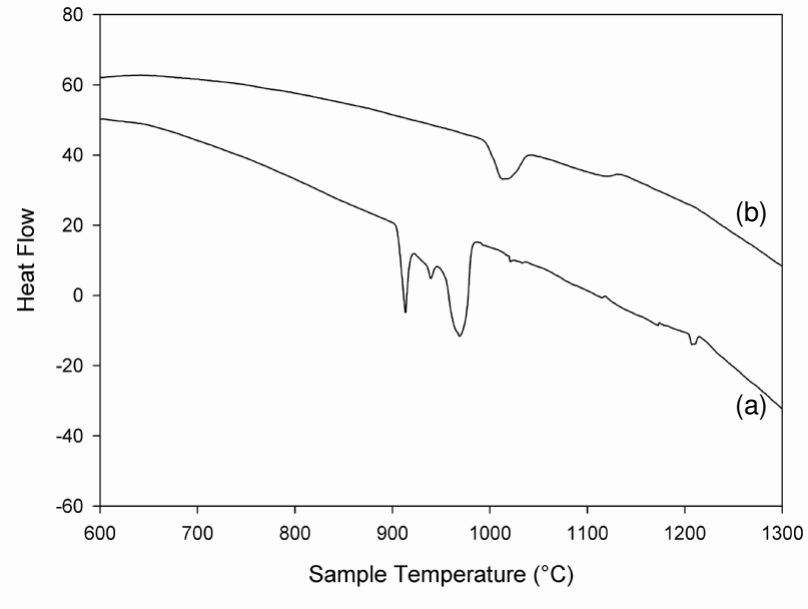

Figure 4.17 DSC heating curves for (a) alloy A3, and (b) alloy C3 obtained with a heating rate of 20°C/min.

Table 4.21 Thermal data for alloys A3 and C3, where temperatures are in terms of °C, and enthalpy of mixing values are in terms of J/gr.

A3	T_1	T_2	T_3	T_4	$\Delta H^{M,1}$	$\Delta H^{M,2}$	$\Delta H^{M,3}$	$\Delta H^{M,4}$
	913.35	939.15	969.12	1207.13	20.6103	2.1667	61.8516	1.5702
C3	T_1	T_2	$\Delta H^{M,1}$	$\Delta H^{M,2}$				
	1012.78	1115.90	45.6308	9.3447				

When alloys A3 and C3 were analyzed with XRD, they were both found to contain Ti_2Cu, TiCu and Ti phases. Existence of all these phases was also confirmed with SEM and EDS analyses for alloy A3. However, these were not the only phases observed in alloy C3 with using XRD; the alloy also contained Al_2Ti and $AlCu_2Ti$. There also existed peaks that could not have been identified. They also may belong to a complex intermetallic of Ti, Cu and Al. The presence of O_2 was also observed meaning that the alloy was again contaminated with air during the centrifugal casting operation.

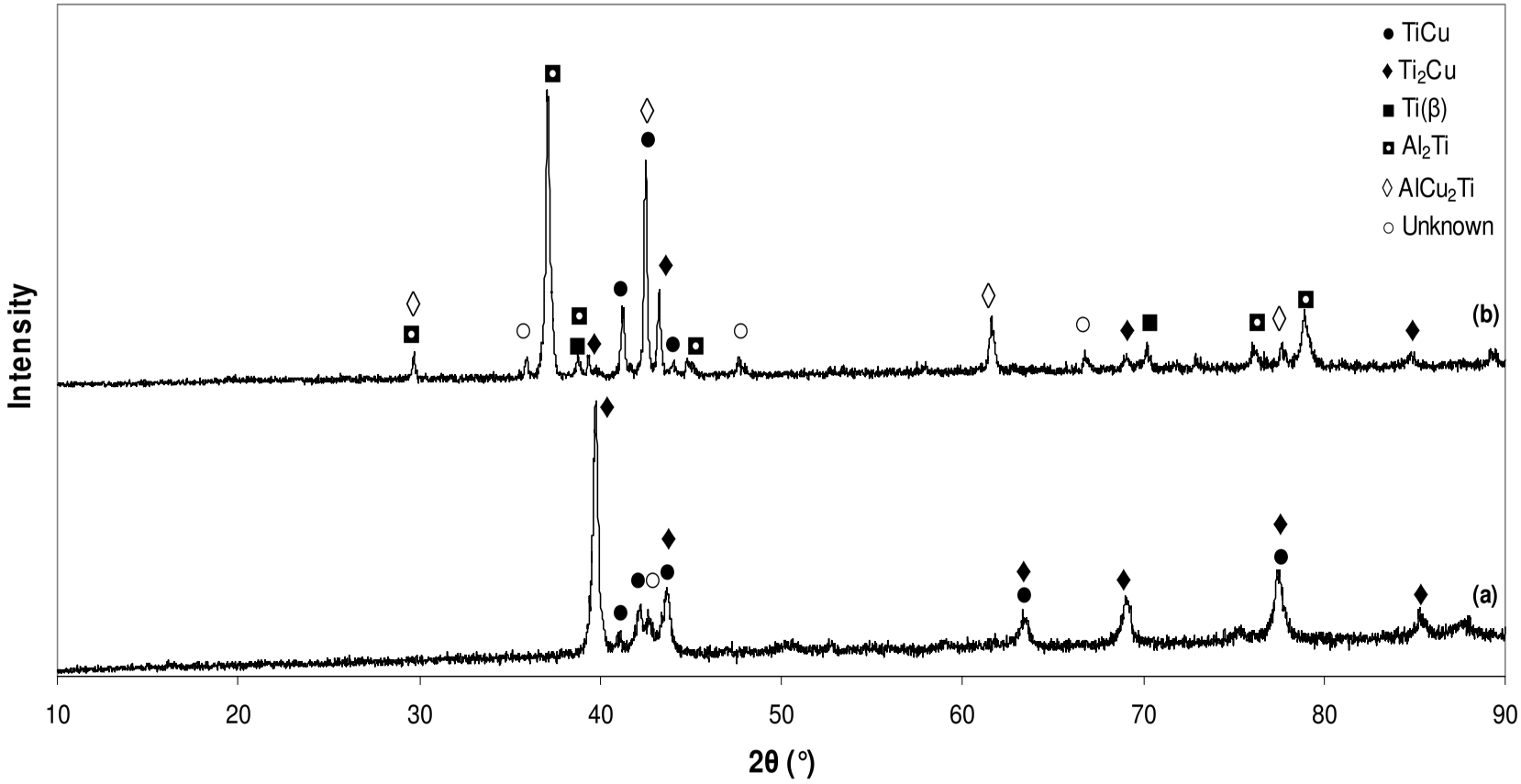

Figure 4.18 XRD pattern of (a) Alloy A3, (b) Alloy C3.

Later on, alloys A4 and C4 were produced and investigated. Centrifugal casting operation to obtain alloy C4 was performed at 1370°C, however complete casting of it could not have been achieved. The microstructure of alloy A4 was investigated to be same in all regions, containing three different structures, Figure 4.19(a) and (b). The phase *A* was found to contain almost equal amounts of Ti and Cu, Table 4.22, suggesting that it can be TiCu with some Ni dissolved in it. When phase *B* was analyzed, its composition was found to be close to Ti_2Cu containing some dissolved Ni, whereas phase *C* was found to have more Ni when compared to the other phases, suggesting that it may be a complex intermetallic of Ti, Cu and Ni. However alloy C4 did not reveal out a similar microstructure and did not contain the phases present in alloy A4, Figure 4.19(c) and (d). Moreover, as a striking fact, it was found to contain very high amounts of Al, Table 4.22. But this was not an expected result since the alloy A4 did not contain any Al in it. When the black particles (D) that were all over the alloy were analyzed with EDS, they were found to contain high amounts of Al and O, suggesting that they may be Al_2O_3 particles. The first idea that came into mind was that, these particles might have come from the polishing step which was done using Al_2O_3 particles. Hence the alloy C4 was metallographically prepared again from starting the grinding step. When the alloy was analyzed after grinding operation, it was again found to contain the same particles, meaning that they did not come from the polishing step. So the reason of the presence of these particles was attributed to contamination with Al_2O_3 crucible that was used during the centrifugal casting operation. Apart from the *D* particles, there also existed three different phases in the microstructure; *E* dendrites containing high amounts of Ti suggesting that they may be Ti dendrites, *F* phase containing slightly higher concentration of Cu, and *G* phase containing almost equal amounts of Ti, Cu and Al, Table 4.22.

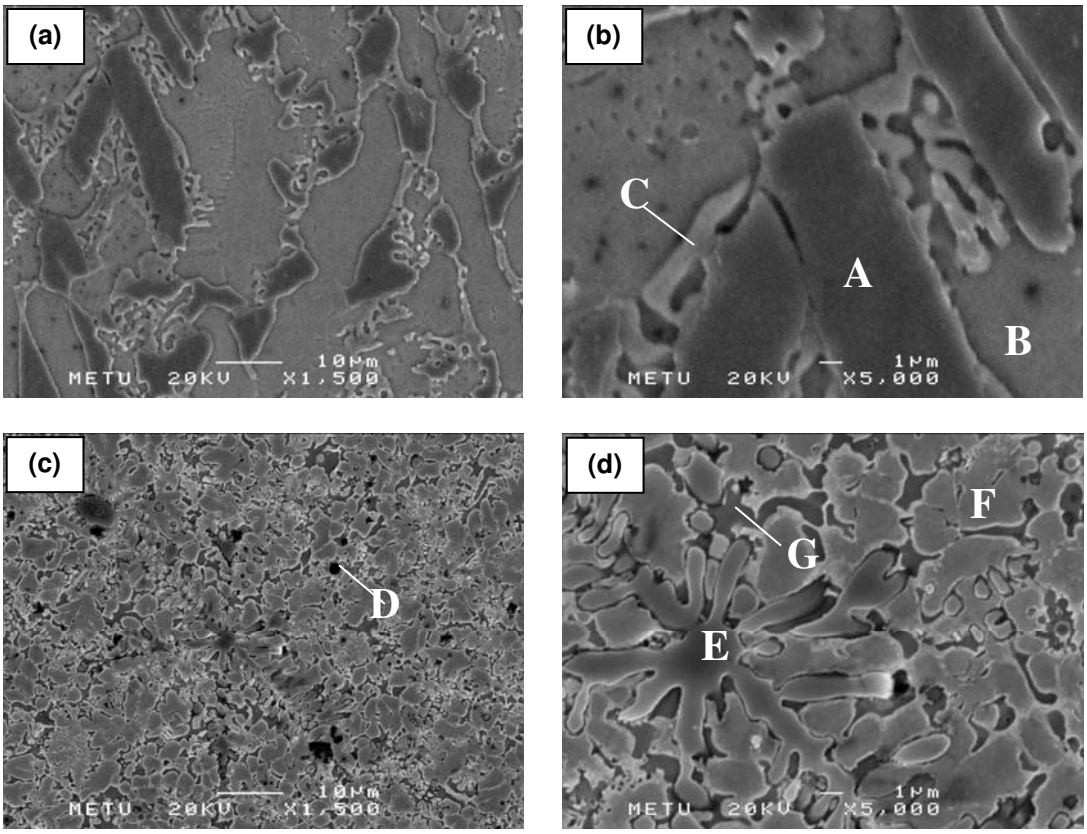

Figure 4.19 Microstructure of alloy A4 from region 1 at magnification of (a) 1500 and (b) 5000, alloy C4 from region X at magnification of (c) 1500 and (d) 5000.

Table 4.22 EDS analysis for alloys A4 and C4.

A4	**at.% Ti**	**at.% Cu**	**at.% Ni**		
General	60.37	34.44	5.20		
A	49.52	47.96	2.51		
B	68.52	28.04	3.44		
C	53.73	33.56	12.71		
C4	**at.% Ti**	**at.% Cu**	**at.% Ni**	**at.% Al**	**at.% O**
General	33.95	34.86	5.20	25.99	0
D	12.50	2.71	0.44	30.33	54.02
E	87.20	5.47	0	7.33	0
F	28.20	38.21	7.21	26.38	0
G	34.94	31.95	2.09	31.02	0

Thermal analyses for alloys A4 and C4 revealed out different behavior, Figure 4.20; DSC thermogram of alloy A4 was found to contain two peaks that are very close to each other at T_1 and T_2 temperatures, Table 4.23. However these peaks were not present for alloy C4, instead it only contained a one staged reaction at the indicated temperature. There also existed a reaction at temperature T_3 in alloy A4 that was not again present in alloy C4, which may belong to reaction at liquidus line.

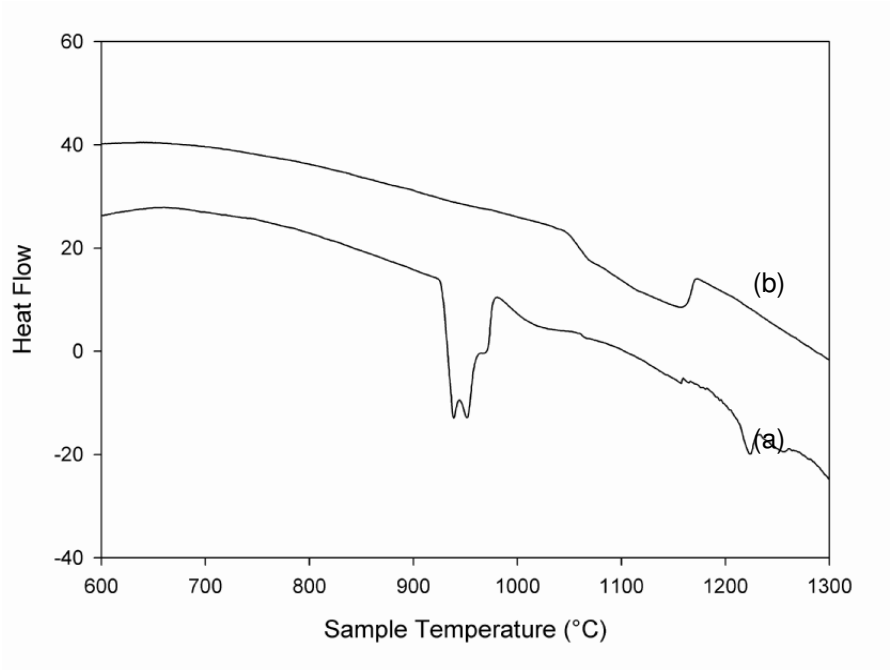

Figure 4.20 DSC heating curves for (a) alloy A4, and (b) alloy C4 obtained with a heating rate of 20°C/min.

Table 4.23 Thermal data for alloys A4 and C4, where temperatures are in terms of °C, and enthalpy of mixing values are in terms of J/gr.

A4	T_1	T_2	T_3	$\Delta H^{M,1}$	$\Delta H^{M,2}$	$\Delta H^{M,3}$
	937.86	952.36	1223.16	9.1010	6.4437	8.3224
C4	T_1	$\Delta H^{M,1}$				
	1146.71	104.7500				

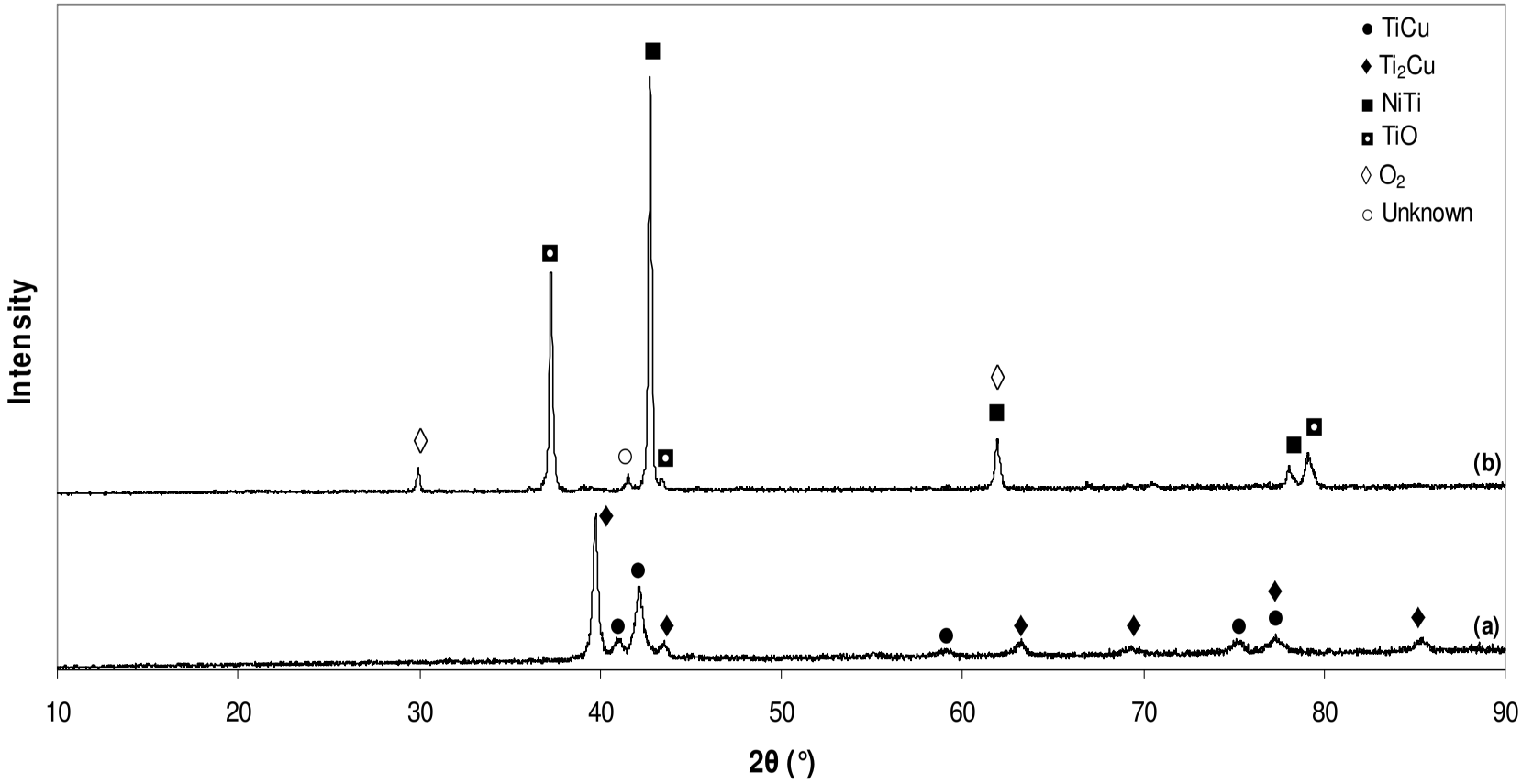

Figure 4.21 XRD pattern of (a) Alloy A4, (b) Alloy C4.

The XRD results for alloys A4 and C4 show that these two alloys contain different phases, Figure 4.21. Alloy A4 was analyzed to contain diffraction peaks of TiCu and Ti_2Cu, which were also confirmed with SEM and EDS studies. On the other hand, alloy C4 was found to contain neither of these phases; instead it was revealed out that this alloy has TiO, NiTi and O_2 in it. Moreover there also exists a peak that could not have been identified and may belong to a complex intermetallic of the elements present inside the structure. XRD results also confirmed that alloy C4 has undergone contamination with air during the centrifugal casting operation.

After experimentally investigating the effects of the ternary alloying elements one by one, multicomponent alloys containing different combinations of these elements were decided to be produced in order to analyze the effects of the elements when they were added together. Hence; multicomponent alloy systems stated in Table 4.17 were produced and characterized.

Alloy A5 was centrifugally cast at 1300°C, and alloy C5 was obtained to investigate the effects of Mn and Al addition. The changing cooling rate resulted in the occurrence of completely different microstructures in these alloys, Figure 4.22. Alloy A5 was found to contain different structures in different regions of the alloy. Region 1 contained a lamellar phase mixture and dendrites which started to occupy more place while getting closer to region 2. Region 2 was investigated to contain mainly two different dendrites and an interdendritic lamellar phase mixture, whereas region 3 exhibited a higher concentration of lamellar phase mixture in which two types of dendrites were scattered. When the matrices in each region were analyzed with EDS, they were all found to have a similar composition which is close to the composition of alloy A5, Table 4.24. The analyses of the two dendrites which are present in regions 2 and 3 suggested that they belong to Ti_2Cu (A) and Ti (C) phases. However SEM studies for alloy C4 showed that, the possible Ti_2Cu dendrites were not present in the structure, whereas the lamellar phase mixture (D) and Ti dendrites (F) still continued their existence. In addition to these indicated

structures, alloy C5 also contained another phase, E, which's composition is close to the composition of lamellar phase mixture.

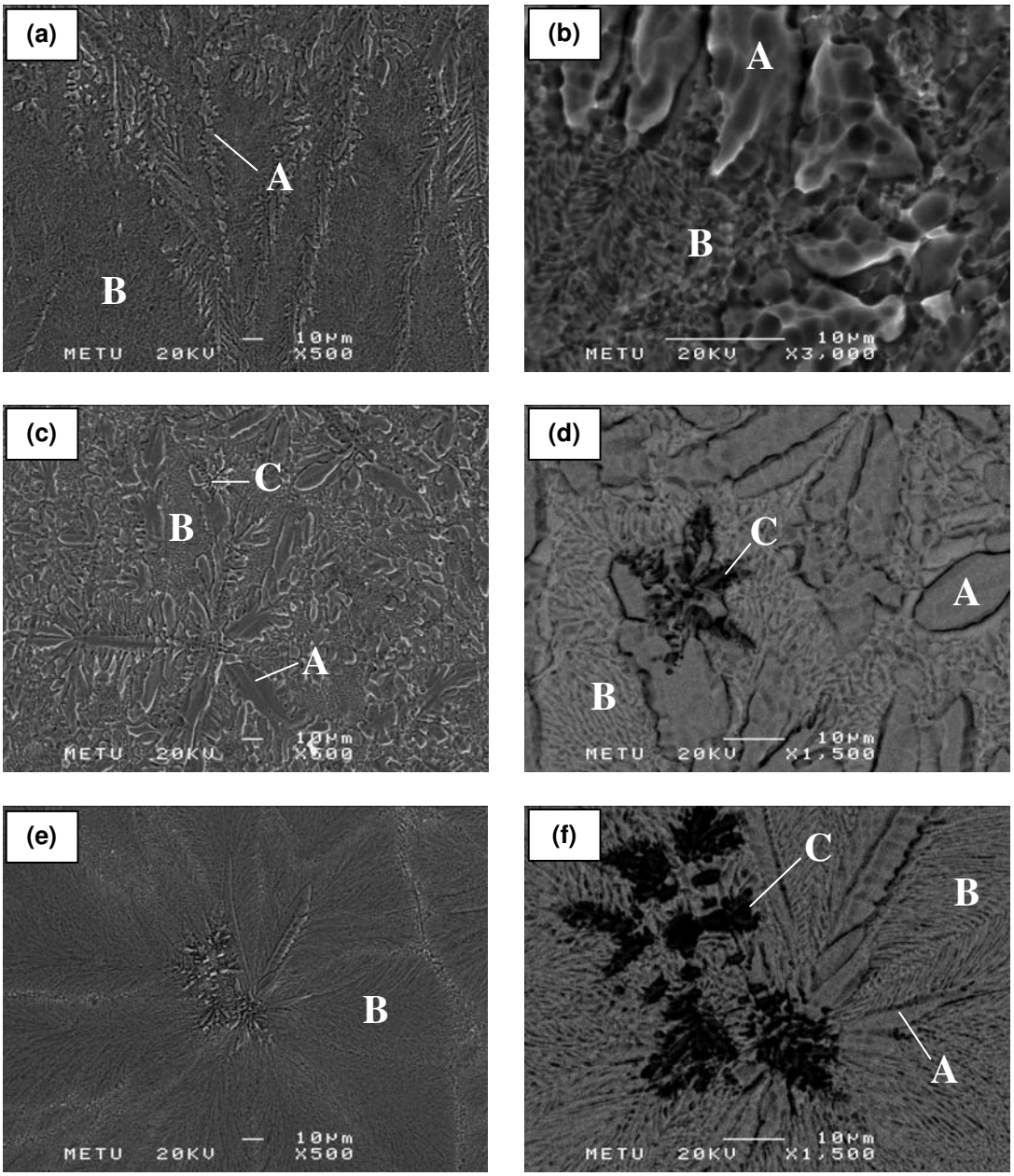

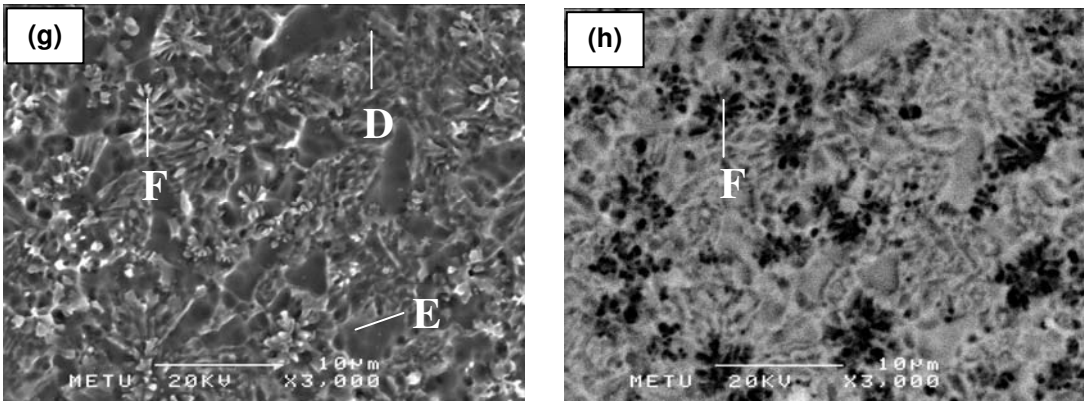

Figure 4.22 Microstructure of alloy A5 from (a) and (b) region 1, (c) region 2, (d) region 2 in back scattered electron mode, (e) region 3 and (f) region 3 in back scattered electron mode. Microstructure of alloy C5 from (g) region X and (h) region X in back scattered electron mode.

Table 4.24 EDS analyses for alloys A5 and C5.

A5	**at.% Ti**	**at.% Cu**	**at.% Mn**	**at.% Al**
General	62.84	31.93	4.42	0.81
A	68.61	29.89	1.51	0
B	59.92	32.96	5.70	1.41
C	86.84	11.12	2.04	0
C5	**at.% Ti**	**at.% Cu**	**at.% Mn**	**at.% Al**
General	61.55	31.06	4.93	2.46
D	56.71	37.53	2.88	2.88
E	53.67	35.62	8.39	2.31
F	91.55	6.05	1.62	0.79

Afterwards, alloys A5 and C5 were thermally analyzed to predict the reactions that will take place in the alloys upon heating. The results of this study are given in Figure 4.23 and Table 4.25. Both of the alloys revealed a deep eutectic like reaction peak at the almost same temperature; however they exhibited different low entropy peaks at higher temperatures.

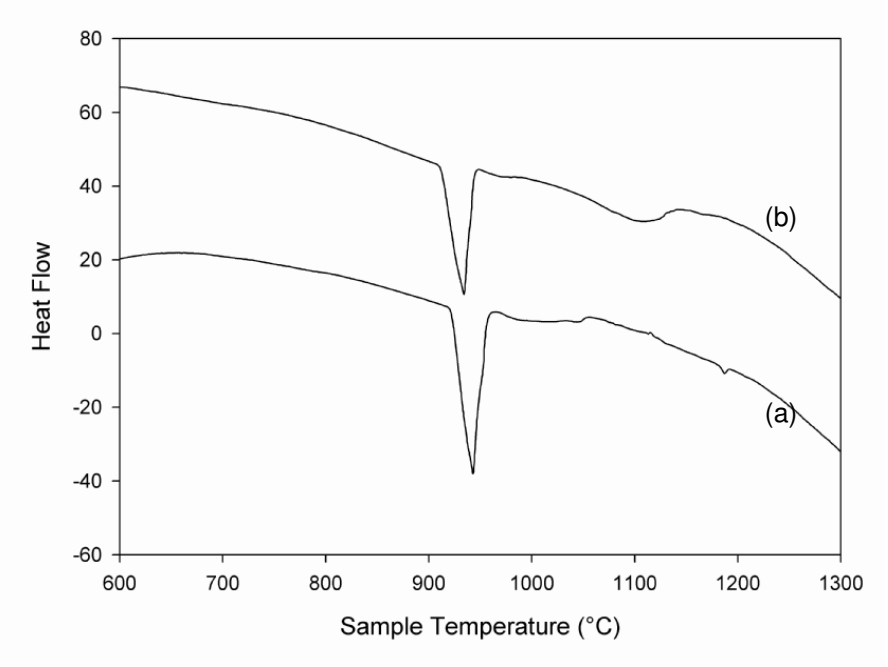

Figure 4.23 DSC heating curves for (a) alloy A5, and (b) alloy C5 obtained with a heating rate of 20°C/min.

Table 4.25 Thermal data for alloys A5 and C5, where temperatures are in terms of °C, and enthalpy of mixing values are in terms of J/gr.

A5	T_1	T_2	$\Delta H^{M,1}$	$\Delta H^{M,2}$
	942.92	1187.11	152.5845	1.5271
C5	T_1	T_2	$\Delta H^{M,1}$	$\Delta H^{M,2}$
	934.19	1102.20	114.2486	65.1178

When XRD studies for alloys A5 and C5 were compared, it was seen that they both contain same phases; Ti_2Cu, Ti and $Al_{80}Mn_{20}$, Figure 4.24. In addition to these phases, there also existed a peak which could not have been identified in the diffraction patterns of both alloys.

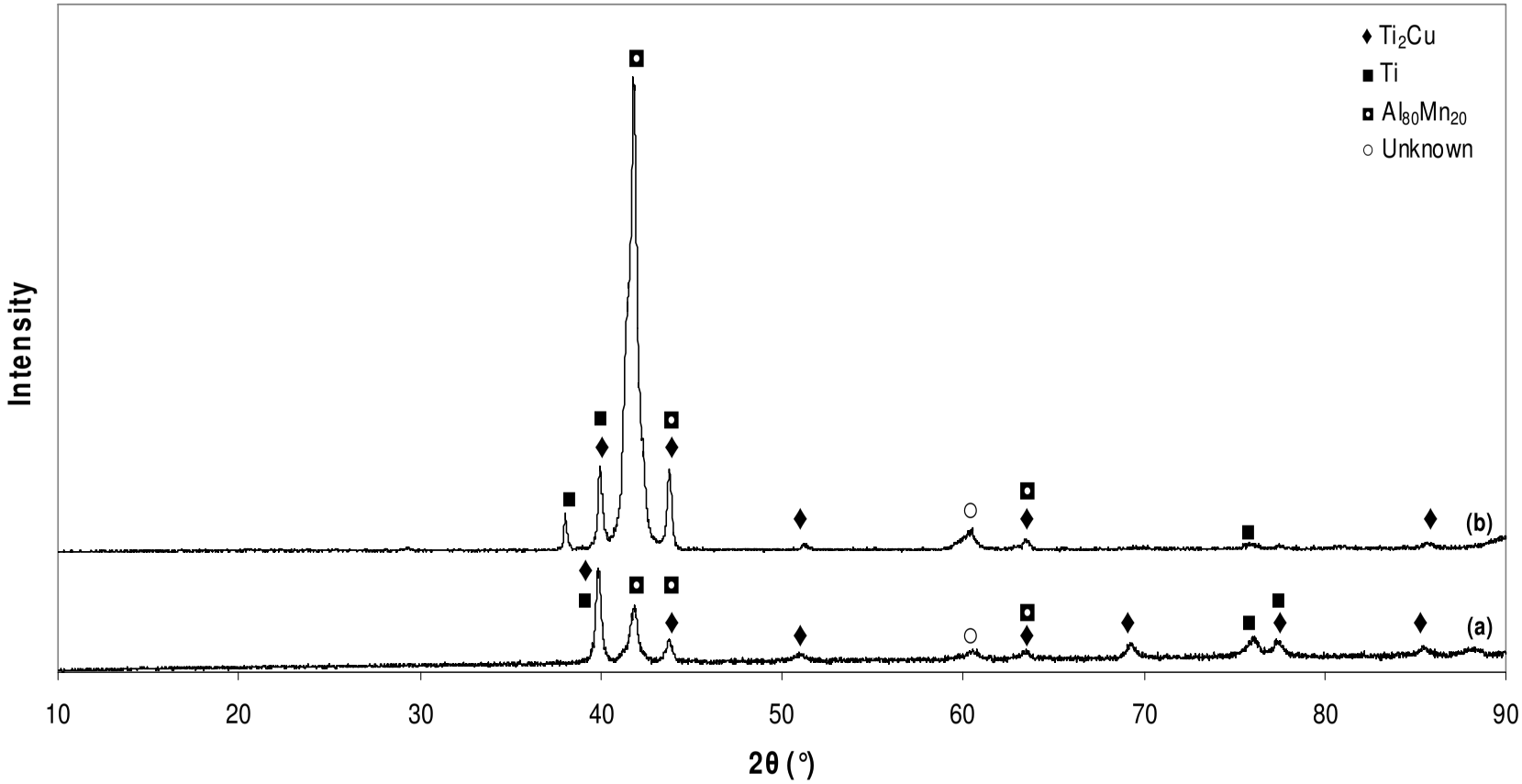

Figure 4.24 XRD pattern of (a) Alloy A5, (b) Alloy C5.

Alloys A6 and C6 have been prepared to investigate the effects of Mn and Ni additions. Casting operation was performed at 1370°C, where complete casting of the alloy could not have been achieved. When the microstructures of the alloys were studied, it was obvious that they contain very different structures. Region 1 and 2 of alloy A6 had the same microstructure, which included dendrites of *A*, dendrites of *B*, a white contrasted phase *C* and a lamellar phase mixture *D*, Figure 4.25(a) and (b). EDS results revealed out that, *A* dendrites may belong to Ti_2Cu containing some dissolved Mn, *B* dendrites may be a complex intermetallic of Ti, Cu, Mn and Ni elements, *C* phase can be a Cu rich phase, and *D* lamellar phase has a composition which is similar to the composition of the multicomponent alloy. On the other hand, upon going to region 3, all the other phases except the lamellar eutectic phase mixture were observed to disappear, Figure 4.25(c). However the EDS analyses for alloy C6 showed that there exits high amounts of Al in the alloy, suggesting that the alloy was contaminated with alumina crucible during the centrifugal casting operation, Table 4.26. The microstructure of this alloy was found to be composed of a matrix phase, F, which may be $AlCu_2Ti$ phase, and dendrites of *E* that were analyzed to contain very high amounts of Ti.

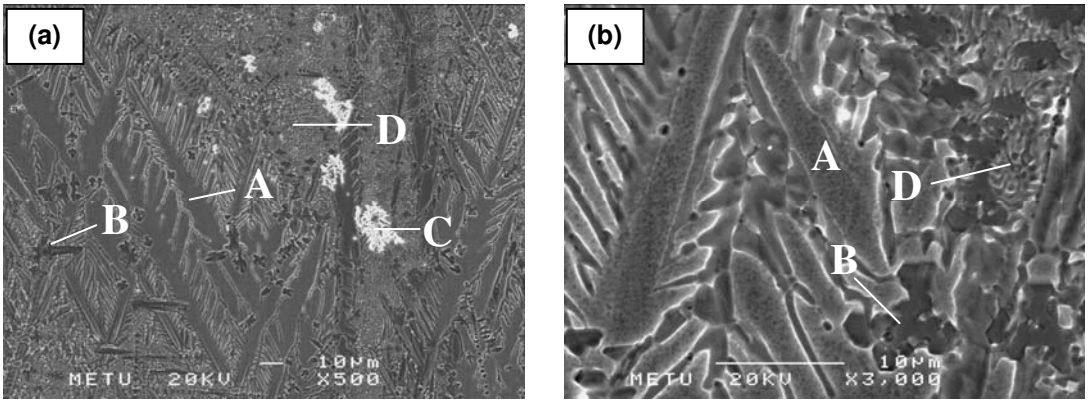

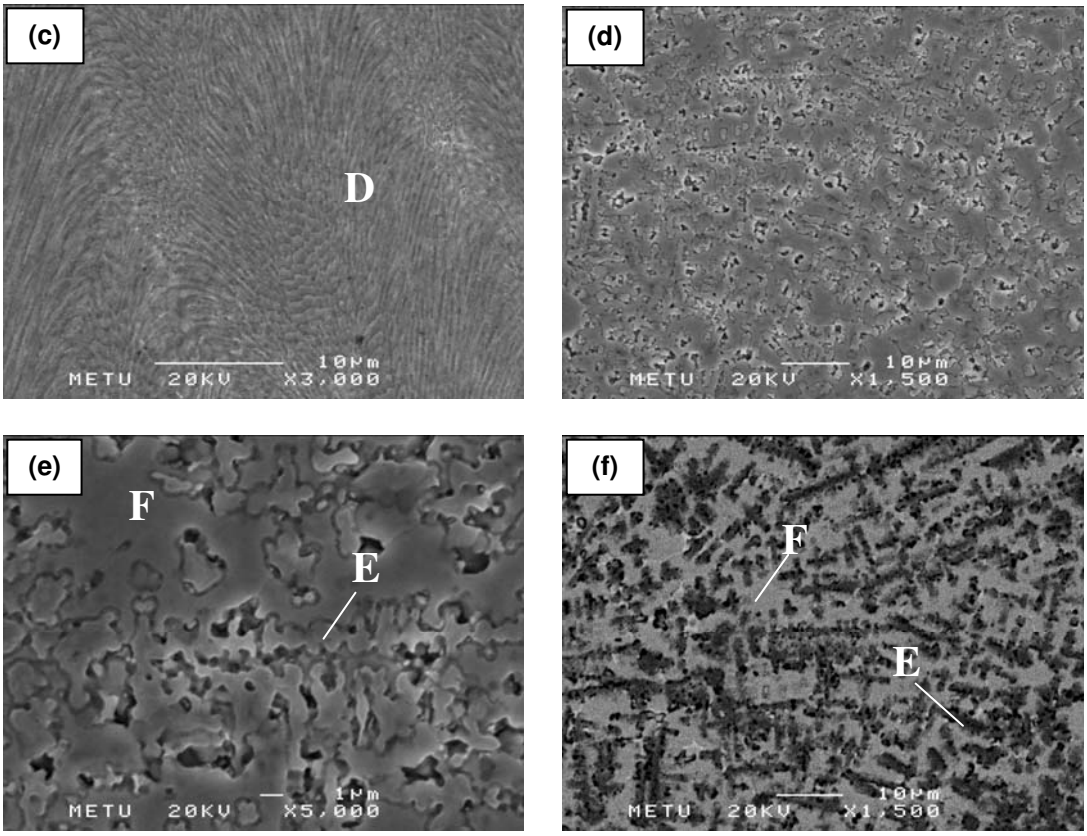

Figure 4.25 Microstructure of alloy A6 from (a) and (b) region 1, (c) region 3. Microstructure of alloy C6 from (d) and (e) region X, (f) region X in back scattered electron mode.

Table 4.26 EDS analyses for alloys A6 and C6.

A6	**at.% Ti**	**at.% Cu**	**at.% Mn**	**at.% Ni**	
General	59.68	34.86	4.51	0.95	
A	68.10	30.51	1.39	0	
B	66.30	27.46	4.60	1.49	
C	18.80	78.31	2.09	0.79	
D	57.71	34.90	6.61	1.22	
C6	**at.% Ti**	**at.% Cu**	**at.% Mn**	**at.% Ni**	**at.% Al**
General	54.04	28.65	4.76	0	12.55
E	85.68	9.29	1.69	0	3.34
F	27.39	45.20	4.67	1.59	21.16

Thermal analyses for alloys A6 and C6 were also different from each other. They both contained a peak having low enthalpy at almost the same temperature, but alloy A6 also contained a deep peak which had high enthalpy value at temperature T_2, whereas alloy C6 did not have such a peak.

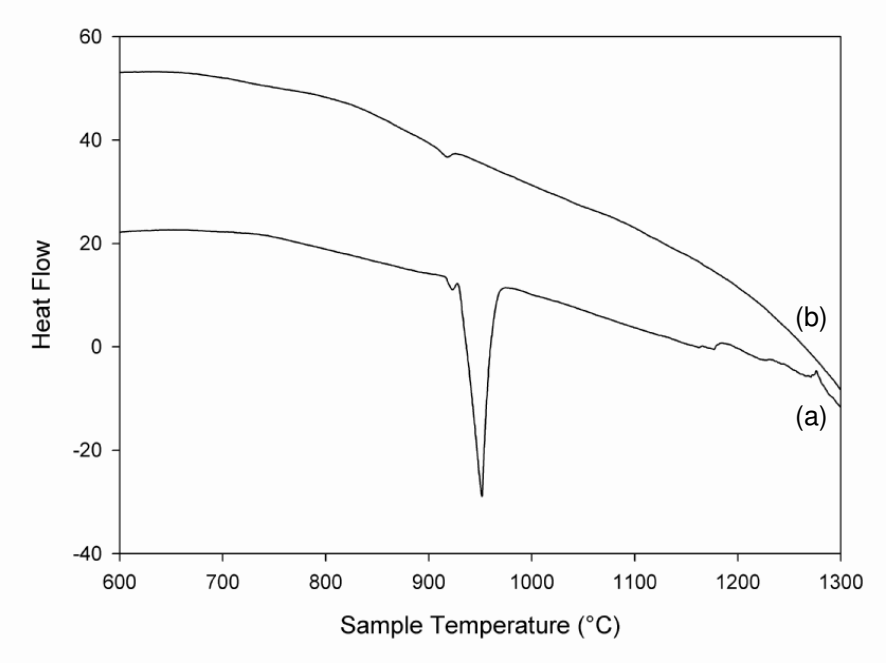

Figure 4.26 DSC heating curves for (a) alloy A6, and (b) alloy C6 obtained with a heating rate of 20°C/min.

Table 4.27 Thermal data for alloys A6 and C6, where temperatures are in terms of °C, and enthalpy of mixing values are in terms of J/gr.

A6	T_1	T_2	$\Delta H^{M,1}$	$\Delta H^{M,2}$
	922.68	951.52	1.6147	105.2218
C6	T_1	$\Delta H^{M,1}$		
	917.91	3.3421		

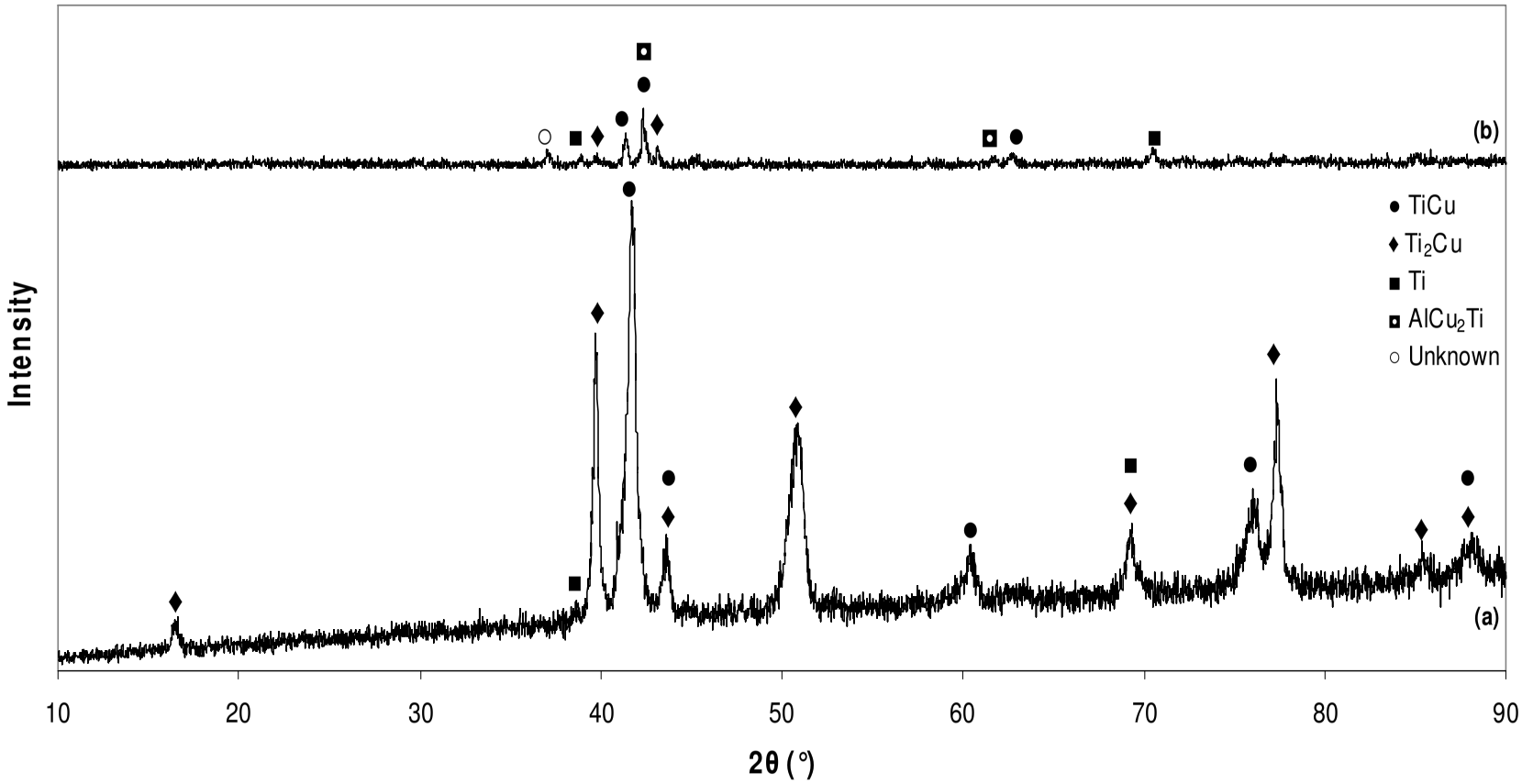

Figure 4.27 XRD pattern of (a) Alloy A6, (b) Alloy C6.

XRD analyses of the alloys A6 and C6 revealed out that both of the alloys contain TiCu, Ti_2Cu and Ti phases, Figure 4.27. In addition to these phases, alloy C6 was found to have peaks belonging to $AlCu_2Ti$ phase, which was also suggested to be present with the EDS analyses.

Finally, Mn, Al and Ni were decided to be added at the same time to the Ti-Cu binary system, and alloys A7 and C7 were produced. The casting operation of the alloy was done at 1370°C, which have also led to contamination problems. Hence; high amounts of Al concentration was observed in alloy C7, Table 4.28. When the microstructures of the alloys were compared, they were found to have different phases. Alloy A7 contained small dendrites of *A* and a white contrasted phase (B) in a lamellar phase mixture (C). On the other hand, microstructure of alloy C7 revealed neither of these phases. EDS analyses of each phase present in each alloy is given in Table 4.28.

Alloys A7 and C7 both contained one peak in their DSC thermogram, whereas the temperature and enthalpy values of these peaks were completely different from each other, Figure 4.29 and Table 4.29.

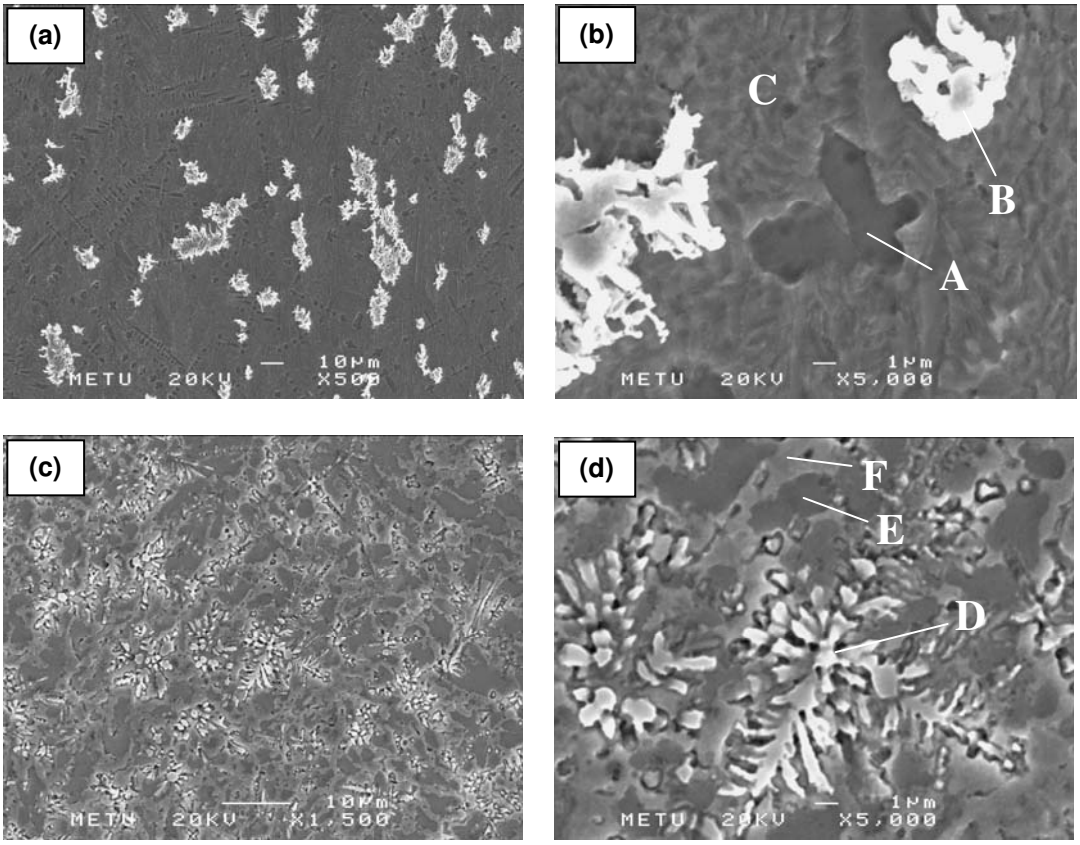

Figure 4.28 Microstructure of alloy A7 from (a) and (b) region 1. Microstructure of alloy C7 from (d) and (e) region X.

Table 4.28 EDS Analyses for alloys A7 and C7.

A7	**at.% Ti**	**at.% Cu**	**at.% Mn**	**at.% Al**	**at.% Ni**
General	58.41	34.75	4.76	1.00	1.08
A	67.96	24.52	5.64	0	1.87
B	29.45	69.19	1.39	0	0
C	62.13	31.90	4.65	0	1.32
C7	**at.% Ti**	**at.% Cu**	**at.% Mn**	**at.% Al**	**at.% Ni**
General	36.92	34.83	5.10	22.26	0.88
D	81.41	12.42	1.46	4.71	0
E	34.20	29.19	6.04	28.85	1.74
F	26.44	42.28	4.98	25.52	0.78

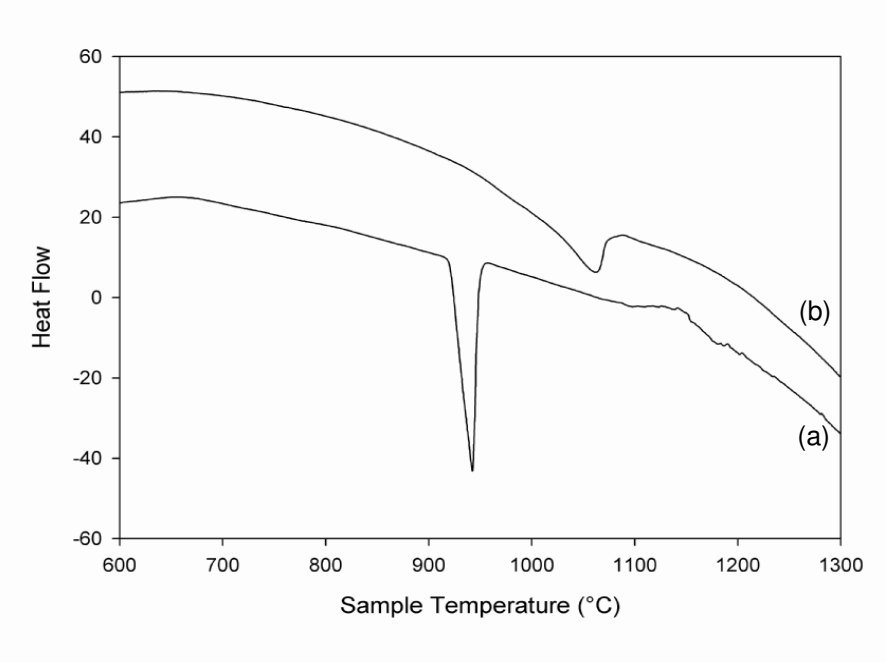

Figure 4.29 DSC heating curves for (a) alloy A7, and (b) alloy C7 obtained with a heating rate of 20°C/min.

Table 4.29 Thermal data for alloys A7 and C7, where temperatures are in terms of °C, and enthalpy of mixing values are in terms of J/gr.

A7	T_1	$\Delta H^{M,1}$
	942.43	136.2197
C7	T_1	$\Delta H^{M,1}$
	1060.93	56.9572

XRD results for the alloys A7 and C7 showed that, A7 alloy contains Ti_2Cu, whereas alloy C7 was found to contain only TiCu peaks, Figure 4.30. Also, both alloys had peaks that could not have been identified and that might belong to a complex intermetallic of the phases present.

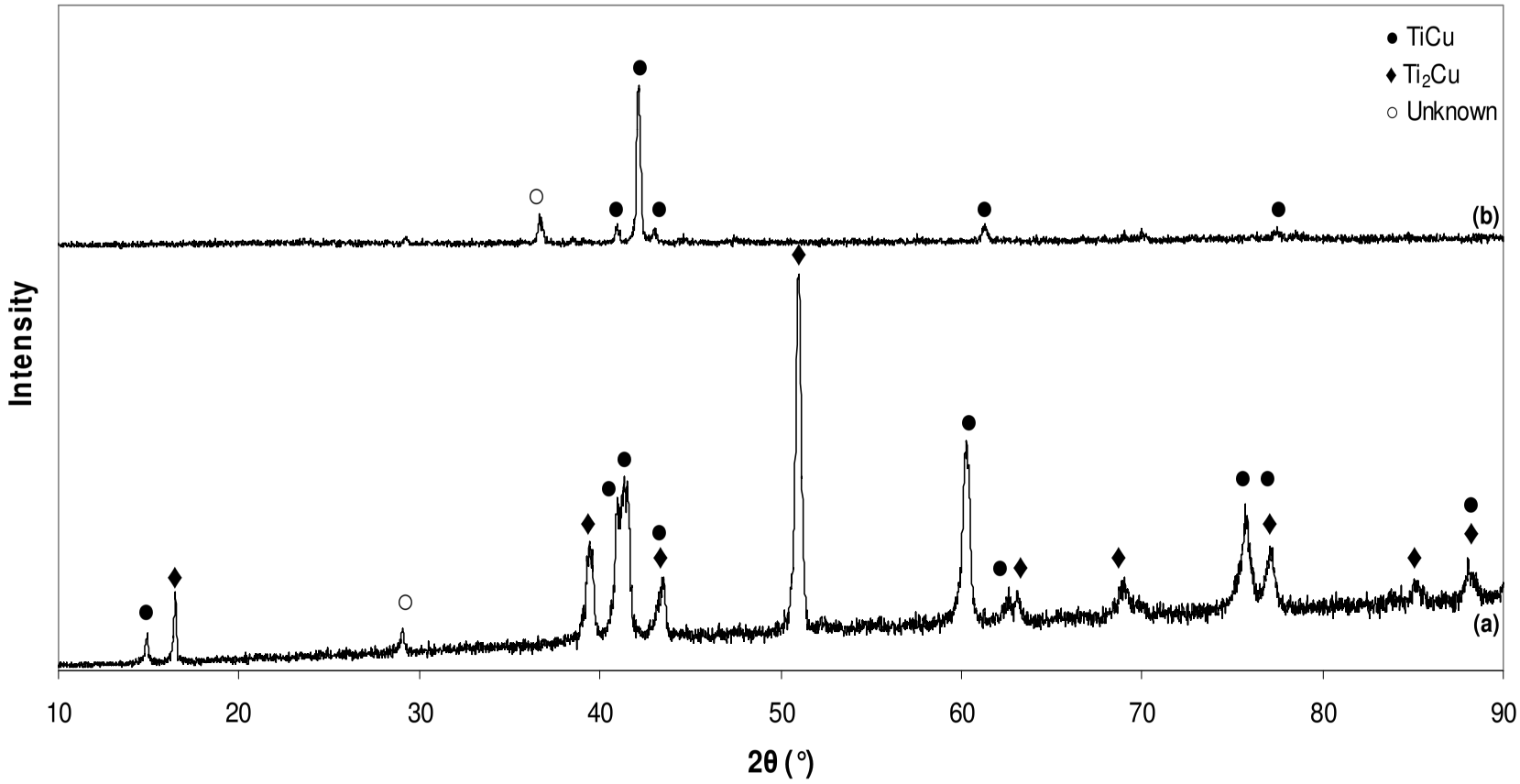

Figure 4.30 XRD pattern of (a) Alloy A7, (b) Alloy C7.

Figure 4.31 and 4.32 summarizes the XRD and DSC patterns of the centrifugal cast alloys that were studied in this thesis. There occurred significant changes with addition of alloying elements in both of the patterns. Upon presence of the selected alloying elements, peaks present in the XRD patterns started to be less intense. This difference is more pronounced in the trace of alloys C6 and C7. Eutectic and peritectic reactions are seen in DSC trace of alloy C1, whereas all the other alloys show different reaction peaks, so it can be said that alloying element additions significantly changed the thermal behavior of the alloy.

XRD, DSC and SEM analyses showed that minor additions of alloying elements into the $Ti_{65}Cu_{35}$ alloy had major effects on both thermal and microstructural properties. These indicated that the elements have important effects on the BGFA of the alloy. However, forming the composition of the multicomponent alloy is not a straightforward process. The amount of the alloying element that is to be added can take several values, and there is not an exact method to choose it. Hence; several alloys having different compositions should be tried to find the glass forming composition. But it is worth noting that the elements selected during this study showed positive effects on the BGFA. Making small alterations in the compositions would probably result in the synthesis of a bulk metallic glass.

Moreover, difficulties were encountered during the casting operations of some of the alloy systems studied. These difficulties may be attributed to the dependency of titanium alloys on casting conditions. It has been pointed out that the BGFA of Ti-based bulk metallic glasses appears to be strongly affected by the contamination of oxygen and other impurity elements either from the raw material or from the processing. Oxygen contamination and presence of certain impurities promote crystallization [49, 90]. It appears that the residual oxygen content of the alloy has a strong influence on the crystallization during solidification; hence the synthesis of the alloys proposed in this study can be possible with a better control of oxygen and impurities.

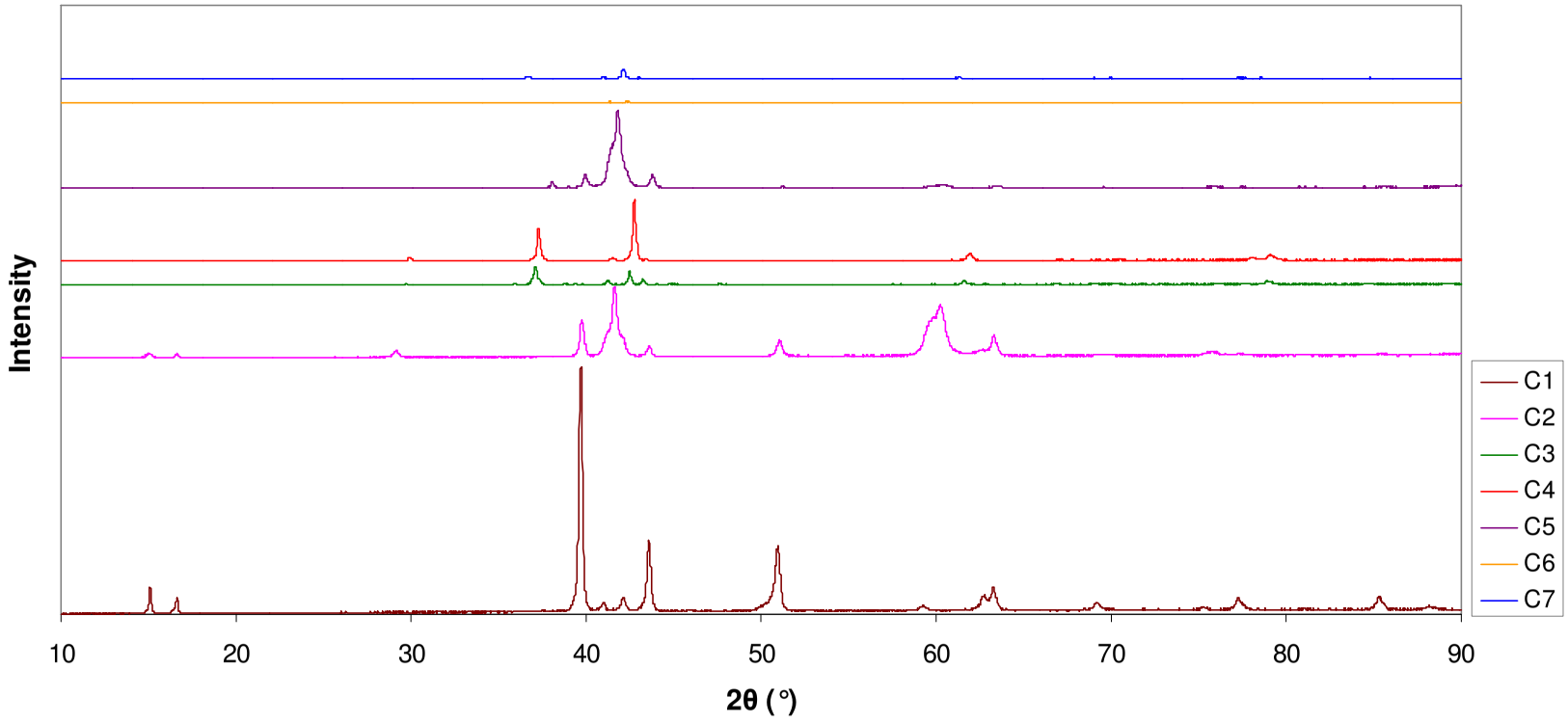

Figure 4.31 Comparison of XRD patterns of centrifugal cast alloys.

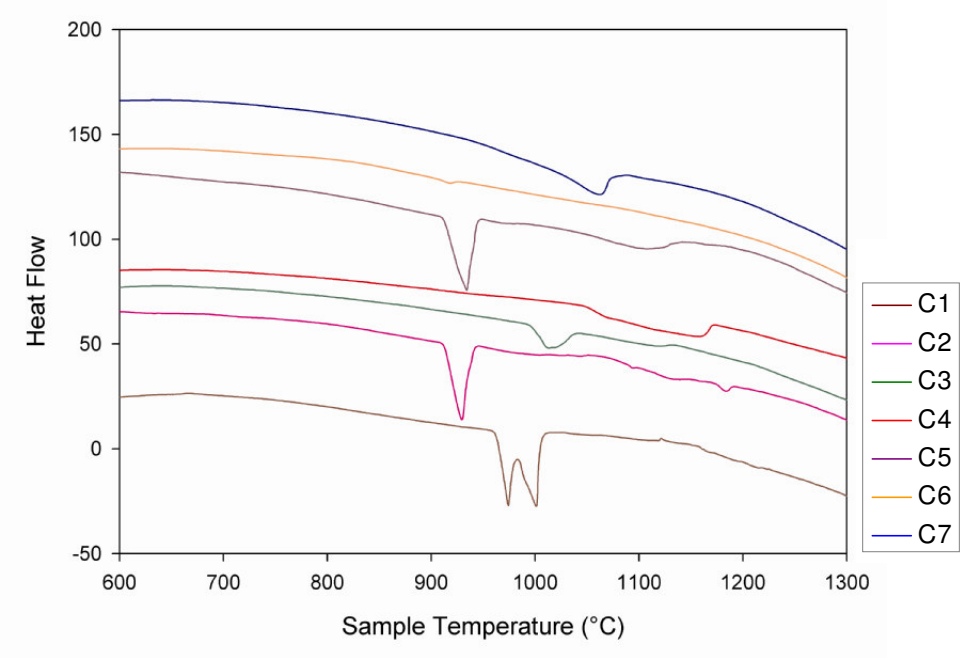

Figure 4.32 Comparison of DSC patterns of centrifugal cast alloys.

CHAPTER 5

CONCLUSIONS

In this thesis study, BGFA of Ti-Cu, Ti-Co and Ti-Zr systems were theoretically investigated. In addition to these theoretical studies, experimental studies were also performed for the predicted alloys systems which seem to exhibit higher BGFA. The crucial points of the theoretical and experimental studies can be summarized as follows:

i. According to the theoretical studies, $Ti_{65}Cu_{35}$ binary system has the most negative enthalpy of mixing and short range order parameter, highest $\Delta\eta/\eta_0$, and lowest critical cooling rate among the other systems that were investigated. As a result, $Ti_{65}Cu_{35}$ binary system exhibits highest BGFA; hence was selected for the experimental studies.

ii. For the production of the ternary systems, alloying element atoms were decided to be added in the place of titanium atoms, based on the fact that $Ti_{64}Cu_{35}X_1$ systems were found to have lower critical cooling rates and higher negative enthalpy of mixing values compared to $Ti_{65}Cu_{34}X_1$ alloys.

iii. The alloying elements of Ag, Au, Li, Cd, P, Si, V, Ga, Ge, Al, Hg, Sc and Zn were found to decrease the enthalpy of mixing upon addition to $Ti_{65}Cu_{35}$ binary system in the place of titanium atoms.

iv. Ag, Au, P, Li, Si, Cd, V, Y, Sc, Ge, Hg, Ga, Al, La, Zn, Mg, Mn, Co, Ni, Fe, In, Pt, Cr, Te, Be and Sn elements were found to decrease the critical

cooling rate of the $Ti_{65}Cu_{35}$ binary system when added in the place of titanium atoms.

v. Ternary alloying element additions into the $Ti_{65}Cu_{35}$ binary system were performed with considering the critical cooling rates and binary phase diagrams of the constituent elements. Under the light of these investigations, Mn, Al and Ni were chosen as the ternary alloying elements for the experimental investigations.

vi. Theoretical results show a good agreement with the experimental investigations present in literature.

vii. Microstructure of all the multicomponent alloys became very fine after the centrifugal casting operation, indicating that the alloying elements added affected the BGFA in a positively manner.

viii. Minor additions of alloying elements resulted in major changes in the properties of the alloys. In addition to the microstructural analysis, these changes were also detected with XRD and DSC analyses.

ix. Upon addition of alloying elements, intensities of the peaks present in the XRD pattern of binary alloy decreased. This positive effect is more significant for alloys C6: $Ti_{59}Cu_{35}Mn_5Ni_1$ and C7: $Ti_{58}Cu_{35}Mn_5Al_1Ni_1$.

x. The proposed alloys have positive effects on the BGFA of the $Ti_{65}Cu_{35}$ binary alloy. However, to achieve a bulk glass forming alloy, small changes can be performed for the compositions, and this can be the concept of another study.

REFERENCES

1. T. R. Anantharaman, *"Metallic Glasses, Production, Properties and Applications"*. 1984, Switzerland: Trans. Tech. Publications.
2. A. Inoue, *"Bulk Amorphous Alloys, Preparation and Fundamental Characteristics"*, ed. Materials Science Found. 4. 1998, Switzerland: Trans. Tech. Publications Ltd.
3. A. Inoue and A. Takeuchi, Mater. Trans., 2002. **43**(8): p. 1892.
4. A. Inoue, Acta Mater., 2000. **48**: p. 279.
5. M. X. Xia, et al., Mater. Sci. Eng., 2005. **A 390**: p. 372.
6. A. Peker and W. L. Johnson, Appl. Phys. Lett., 1993. **63**: p. 2342.
7. A. Inoue, et al., Mater. Trans. JIM, 1991. **32**: p. 609.
8. W. H. Wang, C. Dong, and C. H. Shek, Mater. Sci. Eng., 2004. **R 44**: p. 45.
9. J. K. Lee, et al., Mater. Trans. JIM, 2001. **42**: p. 592.
10. Y. C. Kim, et al., Appl. Phys. Lett., 2003. **83**: p. 3093.
11. D. H. Xu, et al., Acta Mater., 2004. **52**: p. 2621.
12. M. V. Akdeniz and J. V. Wood, J. Mater. Sci., 1996. **31**: p. 545.
13. M. V. Akdeniz and A. O. Mekhrabov, J. Nanosci. Nanotechnol., 2008. **8**: p. 894.
14. H. Men, et al., Mater. Trans., 2005. **JIM 46**: p. 2218.
15. M. Ishimaru, et al., Phil. Mag. Lett., 2005. **85 (3)**: p. 125.
16. X. F. Wu et al., J. Alloys Comp., 2008. **452**: p. 268.
17. S. J. Pang, et al., Intermetallics, 2007. **15**: p. 683.
18. A. H. Cai, et al., Mater. Sci. Eng, 2007. **A 457**: p. 6.
19. J. G. Lee, et al., Intermetallics, 2006. **14**: p. 987.
20. M. V. Akdeniz, A. O. Mekhrabov, and M. K. Pehlivanoğlu, J. Alloys Comp., 2005. **386**: p. 185.
21. W. Klement, R. H. Willens, and P. Duwez, Nature, 1960. **187**: p. 869.
22. M. H. Cohen and D. Turnbull, Nature, 1961. **189**: p. 131.
23. P. Duwez, R. H. Willens, and R. C. Crewdson, J. Appl. Phys., 1965. **36**: p. 2267.

24. P. Duwez and S. C. H. Lin, J. Appl. Phys., 1967. **38**: p. 4096.
25. R. C. Ruhl, et al., Acta Metall., 1967. **15**: p. 1963.
26. B. G. Bagley and F. J. DiSalvo, *Amorphous Magnetism*, ed. H.O.H.a.A.M.d. eds. Vol. 143. 1973, New York: Plenum.
27. H. S. Chen, Acta Metall., 1974. **22**: p. 1505.
28. W. L. Johnson, S. J. Poon, and P. Duwez, Phys. Rev., 1975. **B11**: p. 150.
29. A. Inoue, T. Zhang, and T. Masumoto, Mater. Trans. JIM, 1989. **30**: p. 965.
30. T. Zhang, A. Inoue, and T. Masumoto, Mater. Trans. JIM, 1991. **32**: p. 1005.
31. A. Inoue, N. Nishiyama, and H. Kimura, Mater. Trans. JIM, 1997. **38**: p. 179.
32. W. L. Johnson, MRS Bull., 1999. **24 (10)**: p. 42.
33. L. E. Tanner and R. Ray, Scripta Met., 1977. **11**: p. 783.
34. D. E. Polk, A. Calka, and B. C. Giessen, Acta Metall., 1978. **26**: p. 1097.
35. A. Inoue, et al., J. Phys., 1980. **41**: p. 758.
36. K. Amiya, et al., Mater. Sci. Eng., 1994. **A 179-180**: p. 692.
37. A. Peker and W. L. Johnson. 1994: US Patent 5, 288, 344.
38. X. H. Lin and W. L. Johnson, J. Appl. Phys., 1995. **78**: p. 6514.
39. T. Zhang, A. Inoue, and T. Masumoto, Mater. Sci. Eng., 1994. **A 181-182**: p. 1423.
40. A. Inoue, et al., Mater. Lett., 1994. **19**: p. 131.
41. T. Zhang and A. Inoue, Mater. Trans. JIM, 1998. **39**: p. 1001.
42. T. Zhang and A. Inoue, Mater. Trans. JIM, 1999. **40**: p. 301.
43. Y. C. Kim, W. T. Kim, and D. H. Kim, Mater. Trans. JIM, 2002. **43**: p. 1243.
44. C. L. Ma, et al., Mater. Trans., 2004. **45**: p. 1802.
45. T. Zhang, A. Inoue, and T. Masumoto, Mater. Sci. Eng., 1994. **A 181-182**: p. 131.
46. T. Zhang, A. Inoue, and T. Masumoto, Mater. Trans. JIM, 1995. **36**: p. 1411.
47. Y. C. Kim, et al., Mater. Sci. Forum, 2001. **360-362**: p. 67.

48. T. Zhang and A. Inoue, Mater. Sci. Eng., 2001. **A 304-306**: p. 771.
49. Y. C. Kim, W. T. Kim, and D. H. Kim, Mater. Sci. Eng., 2004. **A 375-377**: p. 127.
50. Y. C. Kim, et al., J. Non-Cryst. Solids, 2003. **325**: p. 242.
51. C. L. Ma, et al., Mater. Trans. JIM, 2004. **45**: p. 3223.
52. M. X. Xia, et al., J. Non-Cryst. Solids, 2005. **351**: p. 3747.
53. G. J. Hao, et al., Mater. Lett., 2006. **60**: p. 1256.
54. P. P. Choi, et al., Mater. Lett., 2007. **61**: p. 4591.
55. Y. J. Huang, et al., J. Alloys Compd., 2007. **427**: p. 171.
56. N. Mattern, J. Non-Cryst. Solids, 2007. **353**: p. 1723.
57. A. Inoue, T. Zhang, and T. Masumoto, J. Non-Cryst. Solids, 1993. **156-158**: p. 473.
58. Y. Li, et al., Scripta Met., 1997. **36**: p. 783.
59. Z. P. Lu and C. T. Liu, Acta Mater., 2002. **50**: p. 3501.
60. K. Mondal and B. S. Murty, J. Non-Cryst. Solids, 2005. **351**: p. 1366.
61. J. H. Kim, et al., J. Non-Cryst. Solids, 2005. **351**: p. 1433.
62. D. B. Miracle and O. N. Senkov, Mater. Sci. Eng, 2003. **A 347**: p. 50.
63. H. Warlimont, Mater. Sci. Eng, 2001. **A 304-306**: p. 61.
64. A. Takeuchi and A. Inoue, Mater. Sci. Eng, 2001. **A 304-306**: p. 446.
65. R. N. Singh and F. Sommer, Rep. Prog. Phys., 1997. **60**: p. 57.
66. F. Sommer, R. N. Singh, and V. Witusiewicz, J. Alloys Comp., 2001. **325**: p. 118.
67. L. Battezzati and A. L. Greer, Acta Metall., 1989. **37**: p. 1791.
68. O. Akinlade, R. N. Singh, and F. Sommer, J. Alloys Comp., 1998. **267**: p. 195.
69. L. I. Yastrebov and A. A. Katsnelson, "Foundations of One Electron Theory of Solids", English Translation, Mir Publishers, 1987.
70. J. M. Ziman, "Principles of the theory of Solids", Cambridge University Press., Cambridge, 1969.
71. V. Heine, M. L. Cohen, and D. Weaine, Solid State Phys., 1970. **24 E.** by H. Ehrenreich et al., Academic Press, New York.

72. A. O. Mekhrabov and M. V. Akdeniz, Metall. Mater. Trans., 2003. **34A**: p. 721.
73. A. O. Mekhrabov and M. V. Akdeniz, Chem. Eng. Comm., 2003. **190**: p. 898.
74. A. O. Mekhrabov and M. V. Akdeniz, Acta Mater., 1999. **47,**: p. 2067.
75. A. O. Mekhrabov and M. V. Akdeniz, Acta Mater., 1998. **46**: p. 1185.
76. A. O. Mekhrabov, M. V. Akdeniz, and M. M. Arer, Acta Mater., 1997. **45**: p. 1077.
77. O. N. Senkov and D. B. Miracle, Mater. Res. Bull., 2001. **36**: p. 2183.
78. A. O. E. Animalu and V. Heine, Phil. Mag., 1965. **12**: p. 1249.
79. A. O. E. Animalu, Phys. Rev., 1973. **B 8**: p. 3542.
80. A. O. E. Animalu, Phys. Rev., 1973. **B 8**: p. 3555.
81. J. Hubbard, Proc. Roy. Soc. (London), 1957. **A 240**: p. 359.
82. J. Hubbard, Proc. Roy. Soc. (London), 1957. **A 243**: p. 336.
83. L. J. Sham, Proc. Roy. Soc. (London), 1965. **A 283**: p. 33.
84. L. T. To and Z. H. Stachurski, J. Non-Cryst. Solids, 2004. **333**: p. 161.
85. A. Inoue and A. Takeuchi, Mater. Sci. Eng, 2004. **A 375-377**: p. 16.
86. D. V. Louzguine and A. Inoue, J. Mater. Res., 1999. **14**: p. 4426.
87. L. C. Zhang and J. Xu, J. Non-Cryst. Solids, 2004. **347**: p. 166.
88. W. Kurz and D. J. Fisher, Fundamentals of Solidification, Trans. Tech. Publications, 1992.
89. H. Tan, et al., Acta Mater., 2003. **51**: p. 4551.
90. M. V. Akdeniz and A. O. Mekhrabov, J. Nanosci. Nanotechnol., 2007. **10**: p. 1.

APPENDIX A

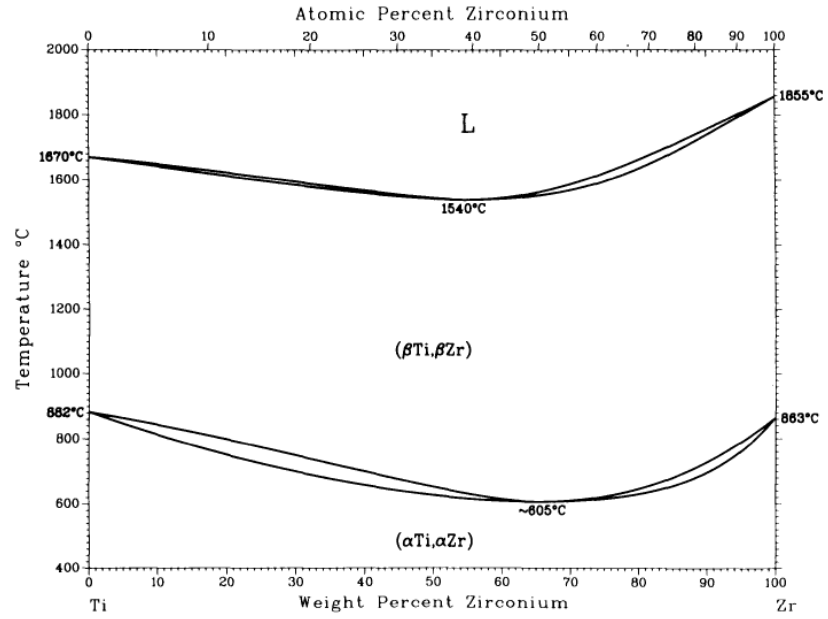

Figure A. 1 Equilibrium binary phase diagram of Ti-Zr.

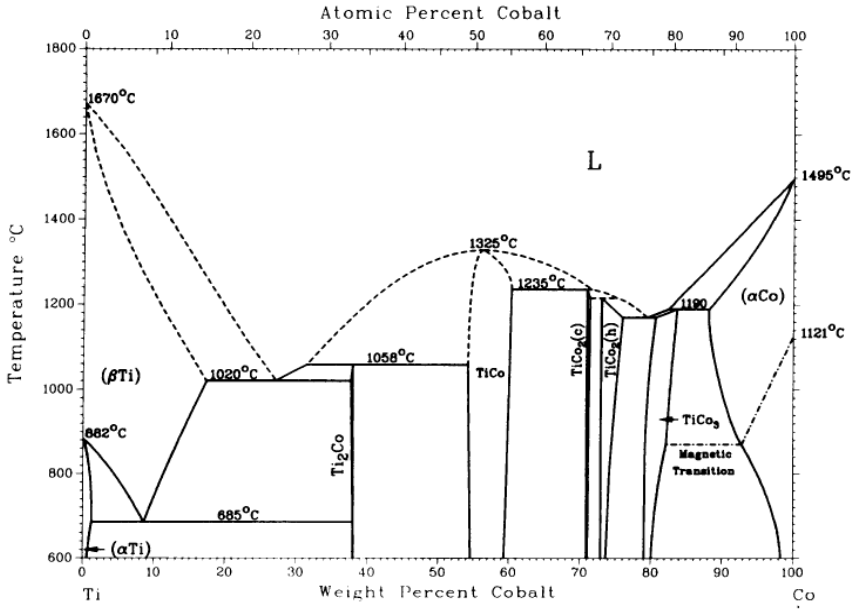

Figure A. 2 Equilibrium binary phase diagram of Ti-Co.

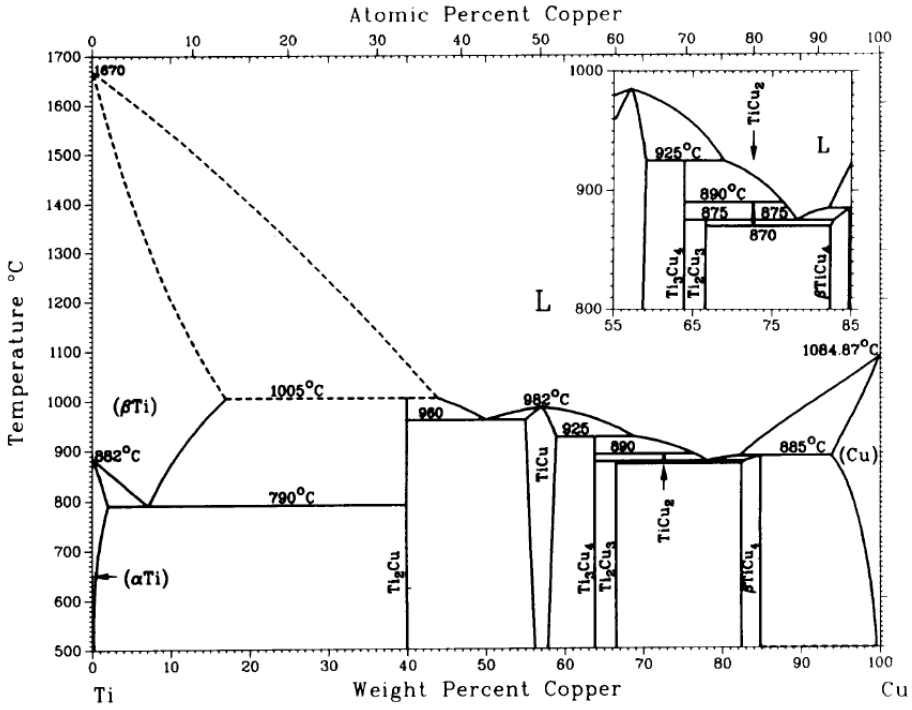

Figure A. 3 Equilibrium binary phase diagram of Ti-Cu.

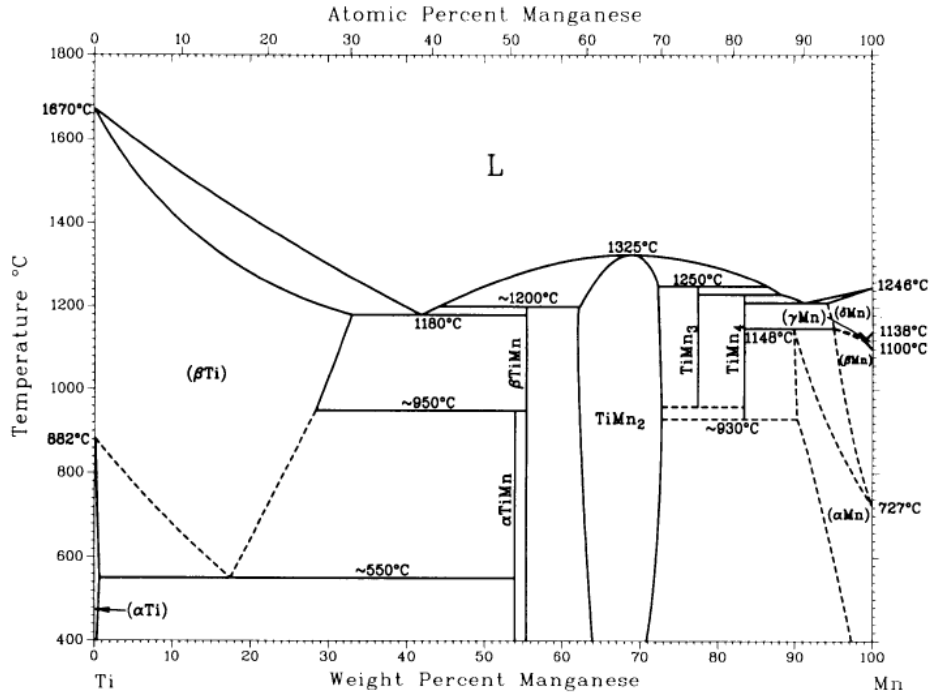

Figure A. 4 Equilibrium binary phase diagram of Ti-Mn.

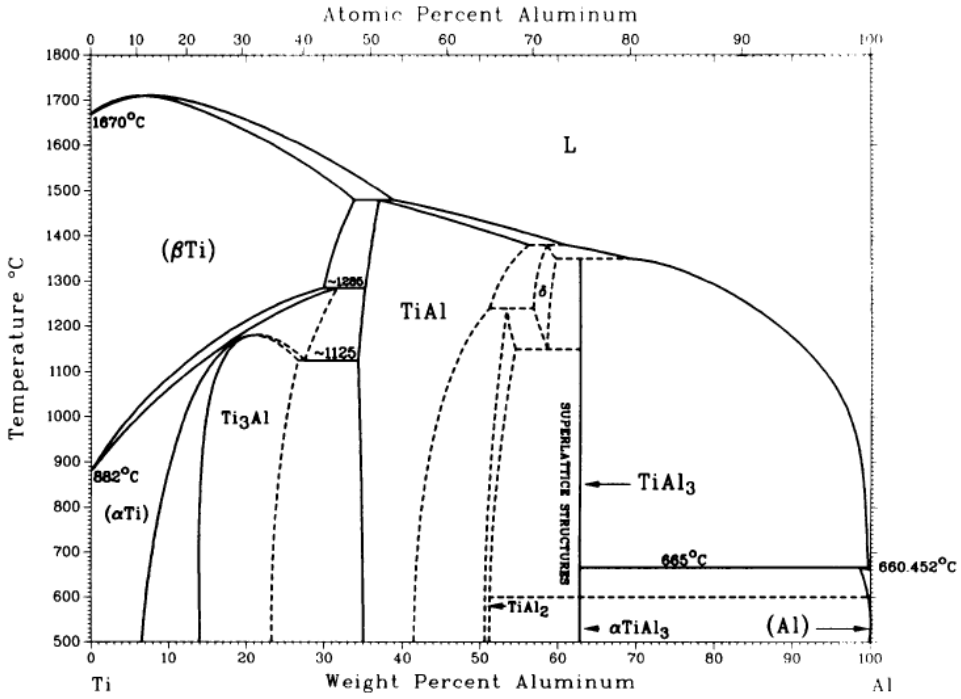

Figure A. 5 Equilibrium binary phase diagram of Ti-Al.

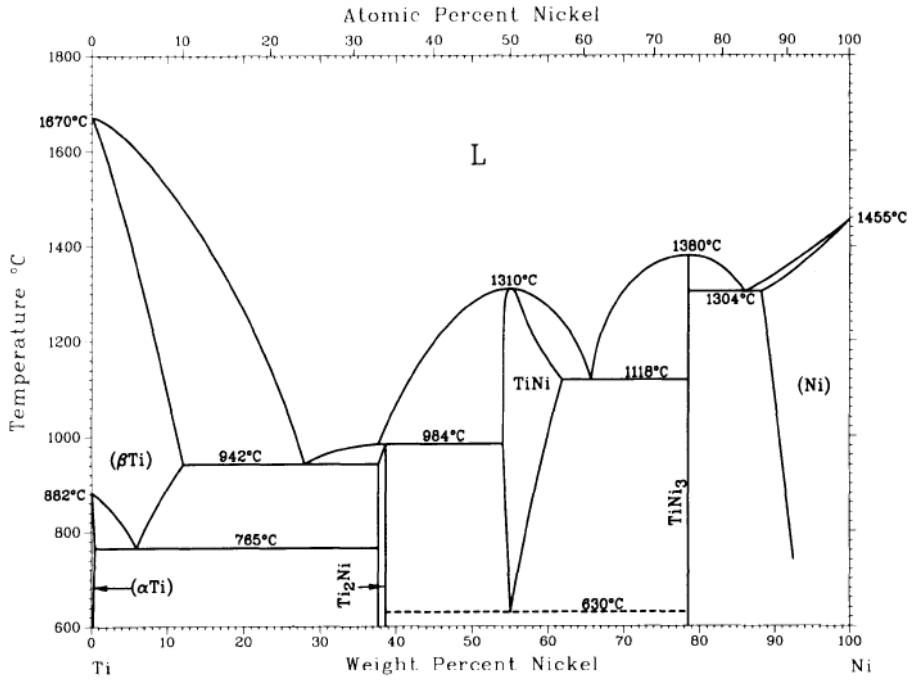

Figure A. 6 Equilibrium binary phase diagram of Ti-Ni.

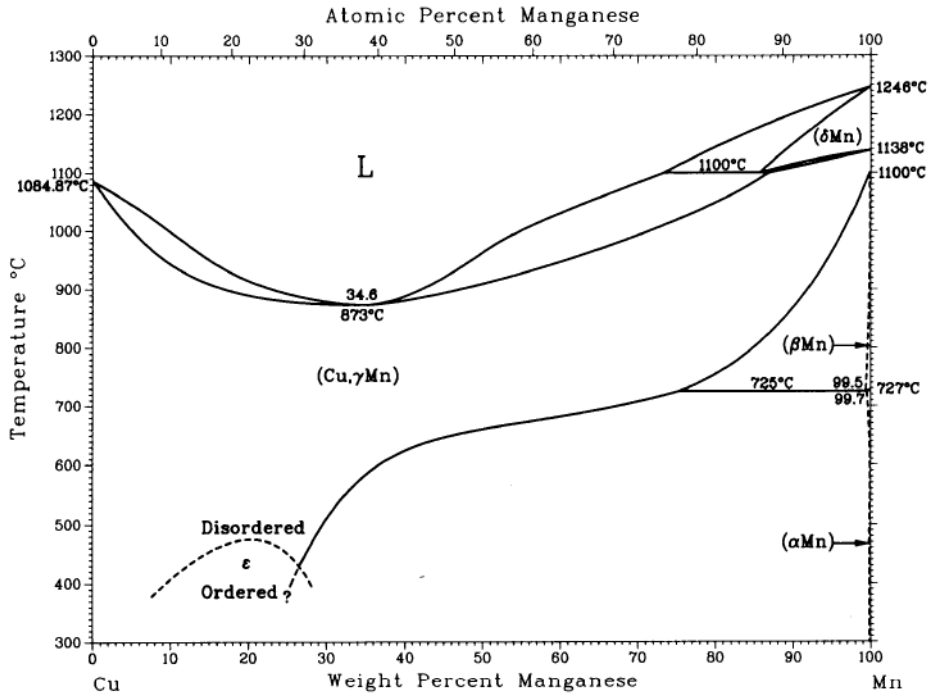

Figure A. 7 Equilibrium binary phase diagram of Cu-Mn.

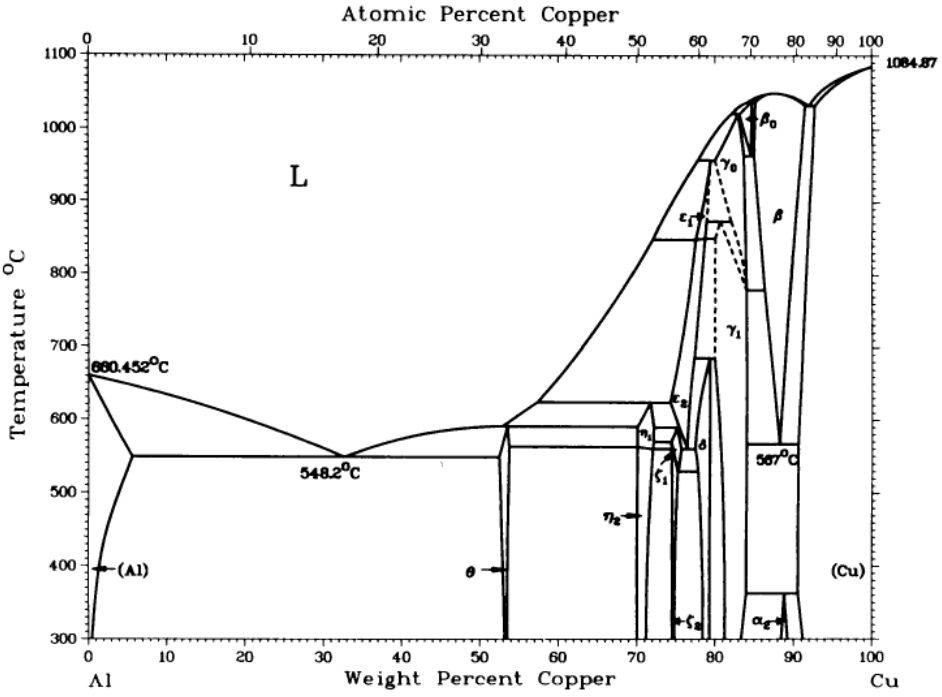

Figure A. 8 Equilibrium binary phase diagram of Cu-Al.

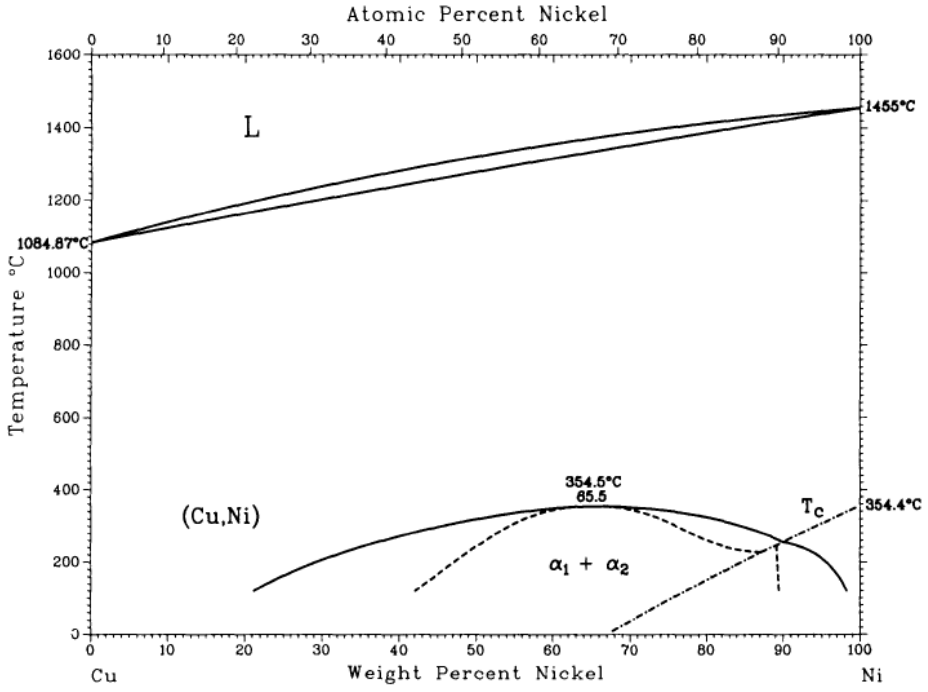

Figure A. 9 Equilibrium binary phase diagram of Cu-Ni.

APPENDIX B

Table B. 1 Ordering energy and interchange energy values for $Ti_{60}Zr_{39}X_1$ alloy (in atomic unit of energy).

$Ti_{60}Zr_{39}X_1$						
X	W_{Ti-Zr} **a.u** (10^{-3})	W_{Ti-X} **a.u** (10^{-3})	W_{Zr-X} **a.u** (10^{-3})	ω_{Ti-Zr} **a.u** (10^{-2})	ω_{Ti-X} **a.u** (10^{-2})	ω_{Zr-X} **a.u** (10^{-2})
None	3.6214	-	-	-2.1728	-	-
Ag	3.6004	-0.5469	-9.4340	-2.1602	0.3282	5.6604
Au	3.5994	2.4727	-11.1927	-2.1596	-1.4836	6.7156
Zn	3.6174	-1.3791	4.5404	-2.1704	0.8275	-2.7242
Cd	3.6024	-2.1096	2.4041	-2.1615	1.2658	-1.4425
Cu	3.6124	-1.9724	-0.5515	-2.1675	1.1834	0.3309
Hg	3.5984	-0.2016	-0.2568	-2.1590	0.1209	0.1541
Sc	3.6084	0.5105	4.5305	-2.1650	-0.3063	-2.7183
Y	3.5914	1.1809	0.0264	-2.1548	-0.7085	-0.0158
La	3.5804	4.4125	-1.3543	-2.1482	-2.6475	0.8126
Hf	3.6234	5.6654	-0.4150	-2.1740	-3.3992	0.2490
V	3.6513	0.3014	5.9231	-2.1908	-0.1809	-3.5539
Nb	3.6424	1.4687	-0.4400	-2.1854	-0.8812	0.2640
Cr	3.6344	0.9027	9.3225	-2.1806	-0.5416	-5.5935
Mo	3.6554	7.1568	-0.7044	-2.1932	-4.2941	0.4226
W	3.6573	6.1897	-0.9213	-2.1944	-3.7138	0.5528
Mn	3.6224	-0.6775	3.8077	-2.1734	0.4065	-2.2846
Re	3.6693	2.6998	-2.4040	-2.2016	-1.6199	1.4424
Fe	3.6334	0.5836	4.6937	-2.1800	-0.3502	-2.8162
Ru	3.6404	3.5796	0.0000	-2.1842	-2.1478	0.0000
Os	3.6394	5.6033	-0.4487	-2.1836	-3.3620	0.2692
Co	3.6254	-0.7393	6.4285	-2.1752	0.4436	-3.8571
Ir	3.6394	5.5984	-0.4477	-2.1836	-3.3590	0.2686
Ni	3.6263	-0.7532	6.4363	-2.1758	0.4519	-3.8618
Pd	3.6184	6.5128	17.4537	-2.1710	-3.9077	-10.4722
Pt	3.6174	-0.1913	0.4126	-2.1704	0.1148	-0.2476
Li	3.5954	-4.6667	5.4790	-2.1572	2.8000	-3.2874
Be	3.6334	-1.3705	12.0934	-2.1800	0.8223	-7.2560
Mg	3.6024	-4.7899	10.7239	-2.1614	2.8739	-6.4344
Al	3.6264	-2.3785	8.8055	-2.1758	1.4271	-5.2833
Ga	3.6204	-0.7658	3.3950	-2.1722	0.4595	-2.0370
In	3.6054	2.8570	-5.9294	-2.1632	-1.7142	3.5577
Si	3.6314	-1.2067	7.6213	-2.1788	0.7240	-4.5728
Ge	3.6263	-0.1744	3.8771	-2.1758	0.1046	-2.3263
Sn	3.6154	1.9041	0.1728	-2.1692	-1.1425	-0.1037
Pb	3.6084	6.4287	-11.2329	-2.1650	-3.8572	6.7398
Sb	3.6204	4.3976	-4.1874	-2.1722	-2.6386	2.5125
Te	3.6244	1.3442	-1.9771	-2.1746	-0.8065	1.1863
B	3.6454	2.2147	7.0732	-2.1872	-1.3288	-4.2439

Table B. 2 Ordering energy and interchange energy values for $Ti_{60}Zr_{39}X_1$ alloy (in SI units).

$Ti_{60}Zr_{39}X_1$						
X	W_{Ti-Zr} J/mol (10^3)	W_{Ti-X} J/mol (10^3)	W_{Zr-X} J/mol (10^3)	ω_{Ti-Zr} J/mol (10^4)	ω_{Ti-X} J/mol (10^4)	ω_{Zr-X} J/mol (10^4)
None	9.5043	-	-	-5.7026	-	-
Ag	9.4492	-1.4354	-24.7594	-5.6695	0.8613	14.8556
Au	9.4465	6.4896	-29.3751	-5.6679	-3.8938	17.6251
Zn	9.4938	-3.6195	11.9162	-5.6963	2.1717	-7.1497
Cd	9.4546	-5.5366	6.3095	-5.6727	3.3220	-3.7857
Cu	9.4808	-5.1764	-1.4475	-5.6885	3.1059	0.8685
Hg	9.4439	-0.5290	-0.6741	-5.6663	0.3174	0.4044
Sc	9.4702	1.3398	11.8904	-5.6821	-0.8039	-7.1342
Y	9.4255	3.0992	0.0692	-5.6553	-1.8595	-0.0415
La	9.3967	11.5806	-3.5542	-5.6380	-6.9484	2.1325
Hf	9.5095	14.8686	-1.0892	-5.7057	-8.9212	0.6535
V	9.5828	0.7911	15.5451	-5.7497	-0.4746	-9.3271
Nb	9.5594	3.8547	-1.1549	-5.7356	-2.3128	0.6929
Cr	9.5384	2.3692	24.4668	-5.7230	-1.4215	-14.6801
Mo	9.5935	18.7829	-1.8487	-5.7561	-11.2698	1.1092
W	9.5986	16.2448	-2.4178	-5.7592	-9.7469	1.4507
Mn	9.5069	-1.7780	9.9932	-5.7041	1.0668	-5.9959
Re	9.6301	7.0856	-6.3093	-5.7780	-4.2514	3.7856
Fe	9.5358	1.5318	12.3185	-5.7215	-0.9191	-7.3911
Ru	9.5541	9.3947	0.0000	-5.7325	-5.6368	0.0000
Os	9.5515	14.7058	-1.1777	-5.7309	-8.8235	0.7066
Co	9.5148	-1.9403	16.8716	-5.7089	1.1642	-10.1230
Ir	9.5515	14.6928	-1.1751	-5.7309	-8.8157	0.7051
Ni	9.5172	-1.9767	16.8919	-5.7103	1.1860	-10.1352
Pd	9.4964	17.0928	45.8071	-5.6978	-10.2557	-27.4843
Pt	9.4938	-0.5021	1.0830	-5.6963	0.3013	-0.6498
Li	9.4360	-12.2477	14.3795	-5.6616	7.3486	-8.6277
Be	9.5358	-3.5968	31.7390	-5.7215	2.1581	-19.0434
Mg	9.4544	-12.5710	28.1448	-5.6726	7.5426	-16.8869
Al	9.5174	-6.2422	23.1100	-5.7104	3.7453	-13.8660
Ga	9.5017	-2.0099	8.9100	-5.7010	1.2060	-5.3460
In	9.4623	7.4982	-15.5617	-5.6774	-4.4989	9.3370
Si	9.5305	-3.1671	20.0020	-5.7183	1.9002	-12.0012
Ge	9.5172	-0.4577	10.1755	-5.7103	0.2746	-6.1053
Sn	9.4885	4.9974	0.4534	-5.6931	-2.9984	-0.2721
Pb	9.4702	16.8720	-29.4807	-5.6821	-10.1232	17.6884
Sb	9.5017	11.5415	-10.9898	-5.7010	-6.9249	6.5939
Te	9.5121	3.5277	-5.1889	-5.7073	-2.1166	3.1134
B	9.5673	5.8125	18.5636	-5.7404	-3.4875	-11.1381

Table B. 3 Ordering energy and interchange energy values for $Ti_{59}Zr_{40}X_1$ alloy (in atomic unit of energy).

$Ti_{59}Zr_{40}X_1$						
X	W_{Ti-Zr} **a.u** (10^{-3})	W_{Ti-X} **a.u** (10^{-3})	W_{Zr-X} **a.u** (10^{-3})	ω_{Ti-Zr} **a.u** (10^{-2})	ω_{Ti-X} **a.u** (10^{-2})	ω_{Zr-X} **a.u** (10^{-2})
None	3.6214	-	-	-2.1728	-	-
Ag	3.5874	-0.5696	-9.4724	-2.1525	0.3418	5.6834
Au	3.5864	2.4546	-11.1803	-2.1519	-1.4728	6.7082
Zn	3.6044	-1.3811	4.5236	-2.1627	0.8287	-2.7141
Cd	3.5904	-2.1136	2.3991	-2.1543	1.2682	-1.4395
Cu	3.6004	-1.9823	-0.5894	-2.1603	1.1894	0.3536
Hg	3.5854	-0.2084	-0.2294	-2.1513	0.1250	0.1377
Sc	3.5964	0.5126	4.4970	-2.1578	-0.3075	-2.6982
Y	3.5784	1.1669	0.0254	-2.1471	-0.7001	-0.0153
La	3.5674	4.3988	-1.3543	-2.1405	-2.6393	0.8126
Hf	3.6114	5.6545	-0.4141	-2.1668	-3.3927	0.2484
V	3.6394	0.2965	5.8766	-2.1836	-0.1779	-3.5260
Nb	3.6313	1.4496	-0.4430	-2.1788	-0.8698	0.2658
Cr	3.6224	0.9129	9.2955	-2.1734	-0.5478	-5.5773
Mo	3.6443	7.1302	-0.7063	-2.1866	-4.2781	0.4238
W	3.6454	6.1719	-0.9243	-2.1872	-3.7031	0.5546
Mn	3.6104	-0.6755	3.7781	-2.1662	0.4053	-2.2669
Re	3.6583	2.6670	-2.4149	-2.1950	-1.6002	1.4490
Fe	3.6214	0.5847	4.6592	-2.1728	-0.3508	-2.7955
Ru	3.6293	3.5686	0.0000	-2.1776	-2.1412	0.0000
Os	3.6283	5.5935	-0.4478	-2.1770	-3.3561	0.2687
Co	3.6134	-0.7372	6.4001	-2.1680	0.4423	-3.8400
Ir	3.6283	5.5877	-0.4468	-2.1770	-3.3526	0.2681
Ni	3.6144	-0.7502	6.4068	-2.1686	0.4501	-3.8441
Pd	3.6054	6.5625	17.4163	-2.1633	-3.9375	-10.4498
Pt	3.6054	-0.1981	0.4430	-2.1632	0.1188	-0.2658
Li	3.5824	-4.6778	5.4449	-2.1494	2.8067	-3.2670
Be	3.6223	-1.3615	12.0791	-2.1734	0.8169	-7.2475
Mg	3.5894	-4.7582	10.7299	-2.1537	2.8549	-6.4379
Al	3.6144	-2.3666	8.7971	-2.1686	1.4200	-5.2783
Ga	3.6084	-0.7698	3.3979	-2.1650	0.4619	-2.0387
In	3.5924	2.8502	-5.9359	-2.1555	-1.7101	3.5615
Si	3.6194	-1.2059	7.6137	-2.1716	0.7235	-4.5682
Ge	3.6144	-0.1735	3.8653	-2.1686	0.1041	-2.3192
Sn	3.6034	1.9061	0.1569	-2.1620	-1.1437	-0.0941
Pb	3.5954	6.4259	-11.2498	-2.1573	-3.8556	6.7499
Sb	3.6084	4.3987	-4.1927	-2.1650	-2.6392	2.5156
Te	3.6124	1.3402	-1.9842	-2.1674	-0.8041	1.1905
B	3.6343	2.2297	7.1184	-2.1806	-1.3378	-4.2711

Table B. 4 Ordering energy and interchange energy values for $Ti_{59}Zr_{40}X_1$ alloy (in SI units).

$Ti_{59}Zr_{40}X_1$						
X	W_{Ti-Zr} J/mol (10^3)	W_{Ti-X} J/mol (10^3)	W_{Zr-X} J/mol (10^3)	ω_{Ti-Zr} J/mol (10^4)	ω_{Ti-X} J/mol (10^4)	ω_{Zr-X} J/mol (10^4)
None	9.5043	-	-	-5.7026	-	-
Ag	9.4152	-1.4949	-24.8601	-5.6491	0.8970	14.9161
Au	9.4126	6.4421	-29.3425	-5.6476	-3.8653	17.6055
Zn	9.4598	-3.6248	11.8721	-5.6759	2.1749	-7.1232
Cd	9.4231	-5.5471	6.2964	-5.6539	3.3283	-3.7778
Cu	9.4493	-5.2025	-1.5468	-5.6696	3.1215	0.9281
Hg	9.4100	-0.5469	-0.6021	-5.6460	0.3281	0.3613
Sc	9.4387	1.3453	11.8023	-5.6632	-0.8072	-7.0814
Y	9.3916	3.0624	0.0667	-5.6350	-1.8375	-0.0400
La	9.3627	11.5445	-3.5544	-5.6176	-6.9267	2.1326
Hf	9.4780	14.8403	-1.0867	-5.6868	-8.9042	0.6520
V	9.5515	0.7781	15.4231	-5.7309	-0.4669	-9.2539
Nb	9.5304	3.8045	-1.1627	-5.7182	-2.2827	0.6976
Cr	9.5069	2.3960	24.3960	-5.7041	-1.4376	-14.6376
Mo	9.5645	18.7131	-1.8537	-5.7387	-11.2279	1.1122
W	9.5673	16.1981	-2.4257	-5.7404	-9.7188	1.4554
Mn	9.4754	-1.7727	9.9156	-5.6852	1.0636	-5.9494
Re	9.6012	6.9995	-6.3380	-5.7607	-4.1997	3.8028
Fe	9.5043	1.5346	12.2280	-5.7026	-0.9207	-7.3368
Ru	9.5251	9.3659	0.0000	-5.7151	-5.6195	0.0000
Os	9.5225	14.6800	-1.1753	-5.7135	-8.8080	0.7052
Co	9.4833	-1.9348	16.7969	-5.6900	1.1609	-10.0781
Ir	9.5225	14.6648	-1.1726	-5.7135	-8.7989	0.7036
Ni	9.4859	-1.9689	16.8146	-5.6915	1.1813	-10.0887
Pd	9.4625	17.2232	45.7087	-5.6775	-10.3339	-27.4252
Pt	9.4623	-0.5198	1.1626	-5.6774	0.3119	-0.6976
Li	9.4019	-12.2768	14.2901	-5.6412	7.3661	-8.5741
Be	9.5067	-3.5732	31.7015	-5.7040	2.1439	-19.0209
Mg	9.4205	-12.4877	28.1605	-5.6523	7.4926	-16.8963
Al	9.4859	-6.2112	23.0879	-5.6915	3.7267	-13.8528
Ga	9.4702	-2.0204	8.9177	-5.6821	1.2123	-5.3506
In	9.4283	7.4803	-15.5786	-5.6570	-4.4882	9.3472
Si	9.4990	-3.1648	19.9821	-5.6994	1.8989	-11.9892
Ge	9.4859	-0.4552	10.1445	-5.6915	0.2731	-6.0867
Sn	9.4570	5.0026	0.4118	-5.6742	-3.0016	-0.2471
Pb	9.4362	16.8648	-29.5249	-5.6617	-10.1189	17.7149
Sb	9.4702	11.5444	-11.0036	-5.6821	-6.9267	6.6022
Te	9.4807	3.5174	-5.2075	-5.6884	-2.1104	3.1245
B	9.5382	5.8518	18.6822	-5.7229	-3.5111	-11.2093

Table B. 5 Ordering energy and interchange energy values for $Ti_{50}Zr_{49}X_1$ alloy (in atomic unit of energy).

$Ti_{50}Zr_{49}X_1$						
X	W_{Ti-Zr} **a.u** (10^{-3})	W_{Ti-C} **a.u** (10^{-3})	W_{Zr-C} **a.u** (10^{-3})	ω_{Ti-Zr} **a.u** (10^{-2})	ω_{Ti-C} **a.u** (10^{-2})	ω_{Zr-C} **a.u** (10^{-2})
None	3.4960	-	-	-2.0976		
Ag	4.1330	-0.7760	-9.8040	-2.4798	0.4656	5.8824
Au	3.4700	2.2550	-11.0510	-2.0820	-1.3530	6.6306
Zn	3.4900	-1.4050	4.3710	-2.0940	0.8430	-2.6226
Cd	3.4740	-2.1500	2.3400	-2.0844	1.2900	-1.4040
Cu	3.4850	-2.0770	-0.9290	-2.0910	1.2462	0.5574
Hg	3.4690	-0.2830	0.0220	-2.0814	0.1698	-0.0132
Sc	3.4800	0.5260	4.1780	-2.0880	-0.3156	-2.5068
Y	3.4610	1.0310	0.0190	-2.0766	-0.6186	-0.0114
La	3.4490	4.2610	-1.3490	-2.0694	-2.5566	0.8094
Hf	3.4980	5.5460	-0.4070	-2.0988	-3.3276	0.2442
V	3.5290	0.2450	5.4370	-2.1174	-0.1470	-3.2622
Nb	3.5190	1.2790	-0.0466	-2.1114	-0.7674	0.0280
Cr	3.5100	0.9960	9.0120	-2.1060	-0.5976	-5.4072
Mo	3.5350	6.8730	-0.7250	-2.1210	-4.1238	0.4350
W	3.5360	6.0010	-0.9530	-2.1216	-3.6006	0.5718
Mn	3.4960	-0.6650	3.5040	-2.0976	0.3990	-2.1024
Re	3.5500	2.3680	-2.5160	-2.1300	-1.4208	1.5096
Fe	3.5080	0.5970	4.3370	-2.1048	-0.3582	-2.6022
Ru	3.5170	3.4610	0.0000	-2.1102	-2.0766	0.0000
Os	3.5160	5.4920	-0.4410	-2.1096	-3.2952	0.2646
Co	3.4990	-0.7180	6.1190	-2.0994	0.4308	-3.6714
Ir	3.5160	5.4870	-0.4400	-2.1096	-3.2922	0.2640
Ni	3.5000	-0.7320	6.1250	-2.1000	0.4392	-3.6750
Pd	3.4910	6.9690	16.9930	-2.0946	-4.1814	-10.1958
Pt	3.4900	-0.2620	0.7150	-2.0940	0.1572	-0.4290
Li	3.4650	-4.7580	5.5120	-2.0790	2.8548	-3.3072
Be	3.5080	-1.2850	11.9160	-2.1048	0.7710	-7.1496
Mg	3.4730	-4.4770	10.7380	-2.0838	2.6862	-6.4428
Al	3.5010	-2.2600	8.6990	-2.1006	1.3560	-5.2194
Ga	3.4940	-0.8060	3.4140	-2.0964	0.4836	-2.0484
In	3.4780	2.7820	-5.9840	-2.0868	-1.6692	3.5904
Si	3.5060	-1.2000	7.5370	-2.1036	0.7200	-4.5222
Ge	3.5000	-0.1680	3.7580	-2.1000	0.1008	-2.2548
Sn	3.4880	1.9300	0.0180	-2.0928	-1.1580	-0.0108
Pb	3.4800	6.3920	-11.3780	-2.0880	-3.8352	6.8268
Sb	3.4940	4.3970	-4.2280	-2.0964	-2.6382	2.5368
Te	3.4990	1.3030	-2.0540	-2.0994	-0.7818	1.2324
B	3.5220	2.3560	7.5200	-2.1132	-1.4136	-4.5120

Table B. 6 Ordering energy and interchange energy values for $Ti_{50}Zr_{49}X_1$ alloy (in SI units).

$Ti_{50}Zr_{49}X_1$						
X	W_{Ti-Zr} J/mol (10^3)	W_{Ti-C} J/mol (10^3)	W_{Zr-C} J/mol (10^3)	ω_{Ti-Zr} J/mol (10^4)	ω_{Ti-C} J/mol (10^4)	ω_{Zr-C} J/mol (10^4)
None	9.1752	-	-	-5.5051	-	-
Ag	10.8470	-2.0366	-25.7305	-6.5082	1.2220	15.4383
Au	9.1070	5.9182	-29.0032	-5.4642	-3.5509	17.4019
Zn	9.1595	-3.6874	11.4716	-5.4957	2.2124	-6.8830
Cd	9.1175	-5.6426	6.1413	-5.4705	3.3856	-3.6848
Cu	9.1463	-5.4511	-2.4381	-5.4878	3.2706	1.4629
Hg	9.1043	-0.7427	0.0577	-5.4626	0.4456	-0.0346
Sc	9.1332	1.3805	10.9651	-5.4799	-0.8283	-6.5791
Y	9.0833	2.7058	0.0499	-5.4500	-1.6235	-0.0299
La	9.0519	11.1829	-3.5404	-5.4311	-6.7098	2.1243
Hf	9.1805	14.5554	-1.0682	-5.5083	-8.7332	0.6409
V	9.2618	0.6430	14.2693	-5.5571	-0.3858	-8.5616
Nb	9.2356	3.3567	-0.1223	-5.5413	-2.0140	0.0734
Cr	9.2119	2.6140	23.6519	-5.5272	-1.5684	-14.1911
Mo	9.2776	18.0381	-1.9028	-5.5665	-10.8229	1.1417
W	9.2802	15.7495	-2.5011	-5.5681	-9.4497	1.5007
Mn	9.1752	-1.7453	9.1962	-5.5051	1.0472	-5.5177
Re	9.3169	6.2148	-6.6032	-5.5902	-3.7289	3.9619
Fe	9.2067	1.5668	11.3824	-5.5240	-0.9401	-6.8294
Ru	9.2303	9.0833	0.0000	-5.5382	-5.4500	0.0000
Os	9.2277	14.4137	-1.1574	-5.5366	-8.6482	0.6944
Co	9.1831	-1.8844	16.0592	-5.5098	1.1306	-9.6355
Ir	9.2277	14.4006	-1.1548	-5.5366	-8.6403	0.6929
Ni	9.1857	-1.9211	16.0750	-5.5114	1.1527	-9.6450
Pd	9.1621	18.2900	44.5979	-5.4972	-10.9740	-26.7587
Pt	9.1595	-0.6876	1.8765	-5.4957	0.4126	-1.1259
Li	9.0938	-12.4873	14.4662	-5.4563	7.4924	-8.6797
Be	9.2067	-3.3725	31.2734	-5.5240	2.0235	-18.7640
Mg	9.1148	-11.7498	28.1817	-5.4689	7.0499	-16.9090
Al	9.1883	-5.9313	22.8304	-5.5130	3.5588	-13.6982
Ga	9.1700	-2.1153	8.9600	-5.5020	1.2692	-5.3760
In	9.1280	7.3013	-15.7049	-5.4768	-4.3808	9.4230
Si	9.2014	-3.1494	19.7808	-5.5209	1.8896	-11.8685
Ge	9.1857	-0.4409	9.8628	-5.5114	0.2645	-5.9177
Sn	9.1542	5.0653	0.0472	-5.4925	-3.0392	-0.0283
Pb	9.1332	16.7757	-29.8614	-5.4799	-10.0654	17.9168
Sb	9.1700	11.5399	-11.0963	-5.5020	-6.9239	6.6578
Te	9.1831	3.4197	-5.3907	-5.5098	-2.0518	3.2344
B	9.2434	6.1833	19.7361	-5.5461	-3.7100	-11.8417

Table B. 7 Ordering energy and interchange energy values for $Ti_{49}Zr_{50}X_1$ alloy (in terms of atomic unit of energy).

$Ti_{49}Zr_{50}X_1$						
X	W_{Ti-Zr} a.u (10^{-3})	W_{Ti-X} a.u (10^{-3})	W_{Zr-X} a.u (10^{-3})	ω_{Ti-Zr} a.u (10^{-2})	ω_{Ti-X} a.u (10^{-2})	ω_{Zr-X} a.u (10^{-2})
None	3.4960	-	-	-2.0976	-	-
Ag	3.4574	-0.7996	-9.8397	-2.0744	0.4797	5.9038
Au	3.4564	2.2278	-11.0344	-2.0738	-1.3367	6.6206
Zn	3.4764	-1.4080	4.3529	-2.0858	0.8448	-2.6118
Cd	3.4613	-2.1537	16.3343	-2.0768	1.2922	-9.8006
Cu	3.4714	-2.0881	-0.9665	-2.0828	1.2528	0.5799
Hg	3.4554	-0.2923	0.0508	-2.0732	0.1754	-0.0305
Sc	3.4673	0.5272	4.1409	-2.0804	-0.3163	-2.4846
Y	3.4483	1.0153	0.0193	-2.0690	-0.6092	-0.0116
La	3.4363	4.2457	-1.3483	-2.0618	-2.5474	0.8090
Hf	3.4853	5.5327	-0.4064	-2.0912	-3.3196	0.2438
V	3.5164	0.2386	5.3867	-2.1098	-0.1432	-3.2320
Nb	3.5064	1.2603	-0.4690	-2.1038	-0.7562	0.2814
Cr	3.4964	1.0037	8.9761	-2.0979	-0.6022	-5.3857
Mo	3.5224	6.8420	-0.7267	-2.1134	-4.1052	0.4360
W	3.5234	5.9814	-0.9570	-2.1140	-3.5888	0.5742
Mn	3.4834	-0.6639	3.4719	-2.0900	0.3984	-2.0832
Re	3.5384	2.3345	-2.5270	-2.1230	-1.4007	1.5162
Fe	3.4954	0.5984	4.3003	-2.0972	-0.3590	-2.5802
Ru	3.5044	3.4487	0.0000	-2.1026	-2.0692	0.0000
Os	3.5034	5.4806	-0.4402	-2.1020	-3.2884	0.2641
Co	3.4864	-0.7156	6.0852	-2.0918	0.4294	-3.6511
Ir	3.5034	5.4738	-0.4401	-2.1020	-3.2843	0.2641
Ni	3.4873	-0.7295	6.0850	-2.0924	0.4377	-3.6510
Pd	3.4774	7.0095	16.9359	-2.0864	-4.2057	-10.1615
Pt	3.4774	-0.2701	0.7449	-2.0864	0.1620	-0.4470
Li	3.4513	-4.7680	5.5139	-2.0708	2.8608	-3.3084
Be	3.4954	-1.2767	11.8950	-2.0972	0.7660	-7.1370
Mg	3.4594	-4.4467	10.7342	-2.0756	2.6680	-6.4405
Al	3.4874	-2.2485	8.6856	-2.0924	1.3491	-5.2114
Ga	3.4804	-0.8098	3.4146	-2.0882	0.4859	-2.0488
In	3.4634	2.7745	-5.9882	-2.0780	-1.6647	3.5929
Si	3.4934	-1.1987	7.5259	-2.0960	0.7192	-4.5155
Ge	3.4874	-0.1666	3.7455	-2.0924	0.1000	-2.2473
Sn	3.4754	1.9321	0.0024	-2.0852	-1.1593	-0.0014
Pb	3.4673	6.3873	-11.3896	-2.0804	-3.8324	6.8337
Sb	3.4813	4.3964	-4.2308	-2.0888	-2.6378	2.5385
Te	3.4863	1.2987	-2.0609	-2.0918	-0.7792	1.2365
B	3.5094	2.3688	7.5649	-2.1056	-1.4213	-4.5389

Table B. 8 Ordering energy and interchange energy values for $Ti_{49}Zr_{50}X_1$ alloy (in SI units).

$Ti_{49}Zr_{50}X_1$						
X	W_{Ti-Zr} J/mol (10^3)	W_{Ti-X} J/mol (10^3)	W_{Zr-X} J/mol (10^3)	ω_{Ti-Zr} J/mol (10^4)	ω_{Ti-X} J/mol (10^4)	ω_{Zr-X} J/mol (10^4)
None	9.1752	-	-	-5.5051	-	-
Ag	9.0739	-2.0985	-25.8243	-5.4443	1.2591	15.4946
Au	9.0712	5.8469	-28.9595	-5.4427	-3.5082	17.3757
Zn	9.1237	-3.6953	11.4242	-5.4742	2.2172	-6.8545
Cd	9.0842	-5.6525	42.8693	-5.4505	3.3915	-25.7216
Cu	9.1106	-5.4801	-2.5367	-5.4664	3.2881	1.5220
Hg	9.0686	-0.7670	0.1332	-5.4412	0.4602	-0.0799
Sc	9.0999	1.3835	10.8678	-5.4600	-0.8301	-6.5207
Y	9.0501	2.6645	0.0506	-5.4300	-1.5987	-0.0304
La	9.0184	11.1427	-3.5386	-5.4110	-6.6856	2.1231
Hf	9.1472	14.5204	-1.0666	-5.4883	-8.7123	0.6399
V	9.2287	0.6263	14.1373	-5.5372	-0.3758	-8.4824
Nb	9.2025	3.3077	-1.2308	-5.5215	-1.9846	0.7385
Cr	9.1764	2.6343	23.5576	-5.5058	-1.5806	-14.1346
Mo	9.2445	17.9567	-1.9072	-5.5467	-10.7740	1.1443
W	9.2471	15.6981	-2.5116	-5.5482	-9.4188	1.5070
Mn	9.1421	-1.7425	9.1120	-5.4853	1.0455	-5.4672
Re	9.2864	6.1268	-6.6322	-5.5719	-3.6761	3.9793
Fe	9.1736	1.5704	11.2860	-5.5042	-0.9422	-6.7716
Ru	9.1972	9.0511	0.0000	-5.5183	-5.4307	0.0000
Os	9.1946	14.3838	-1.1553	-5.5168	-8.6303	0.6932
Co	9.1500	-1.8781	15.9706	-5.4900	1.1269	-9.5824
Ir	9.1946	14.3659	-1.1551	-5.5168	-8.6196	0.6931
Ni	9.1524	-1.9147	15.9701	-5.4915	1.1488	-9.5820
Pd	9.1263	18.3964	44.4480	-5.4758	-11.0379	-26.6688
Pt	9.1263	-0.7088	1.9551	-5.4758	0.4253	-1.1730
Li	9.0579	-12.5135	14.4712	-5.4348	7.5081	-8.6827
Be	9.1736	-3.3508	31.2183	-5.5042	2.0105	-18.7310
Mg	9.0791	-11.6702	28.1717	-5.4475	7.0021	-16.9030
Al	9.1526	-5.9010	22.7953	-5.4916	3.5406	-13.6772
Ga	9.1342	-2.1254	8.9617	-5.4805	1.2752	-5.3770
In	9.0896	7.2815	-15.7159	-5.4538	-4.3689	9.4296
Si	9.1683	-3.1460	19.7515	-5.5010	1.8876	-11.8509
Ge	9.1526	-0.4374	9.8301	-5.4916	0.2624	-5.8981
Sn	9.1211	5.0708	0.0062	-5.4727	-3.0425	-0.0037
Pb	9.0999	16.7634	-29.8918	-5.4600	-10.0581	17.9351
Sb	9.1367	11.5382	-11.1036	-5.4820	-6.9229	6.6622
Te	9.1498	3.4085	-5.4088	-5.4899	-2.0451	3.2453
B	9.2103	6.2170	19.8540	-5.5262	-3.7302	-11.9124

Table B. 9 Ordering energy and interchange energy values for $Ti_{40}Zr_{59}X_1$ alloy (in atomic unit of energy).

$Ti_{40}Zr_{59}X_1$						
X	W_{Ti-Zr} **a.u** (10^{-3})	W_{Ti-X} **a.u** (10^{-3})	W_{Zr-X} **a.u** (10^{-3})	ω_{Ti-Zr} **a.u** (10^{-2})	ω_{Ti-X} **a.u** (10^{-2})	ω_{Zr-X} **a.u** (10^{-2})
None	3.3591	-	-	-2.0154	-	-
Ag	3.3311	-1.0159	-10.1340	-1.9986	0.6096	6.0804
Au	3.3301	1.9570	0.0122	-1.9980	-1.1742	-0.0073
Zn	3.3521	-1.4319	4.1849	-2.0112	0.8592	-2.5109
Cd	3.3351	-2.1898	2.2599	-2.0010	1.3139	-1.3559
Cu	3.3461	-2.1850	-1.3081	-2.0076	1.3110	0.7849
Hg	3.3300	-0.3814	0.3107	-1.9980	0.2288	-0.1864
Sc	3.3420	0.5357	3.7990	-2.0052	-0.3214	-2.2794
Y	3.3219	0.8723	0.0133	-1.9932	-0.5234	-0.0080
La	3.3089	4.0881	-1.3401	-1.9854	-2.4528	0.8041
Hf	3.3611	5.4034	-0.3987	-2.0167	-3.2420	0.2392
V	3.3952	0.1815	4.9156	-2.0371	-0.1089	-2.9493
Nb	3.3842	1.0899	-0.4910	-2.0305	-0.6539	0.2946
Cr	3.3732	1.0644	8.6170	-2.0239	-0.6387	-5.1702
Mo	3.4013	6.5549	-0.7492	-2.0408	-3.9329	0.4495
W	3.4032	5.7915	-0.9869	-2.0419	-3.4749	0.5921
Mn	3.3591	-0.6566	3.1750	-2.0154	0.3940	-1.9050
Re	3.4193	2.0236	-2.6283	-2.0516	-1.2141	1.5770
Fe	3.3721	0.6059	3.9525	-2.0233	-0.3636	-2.3715
Ru	3.3821	3.3305	0.0000	-2.0293	-1.9983	0.0000
Os	3.3802	5.3583	-0.4325	-2.0281	-3.2150	0.2595
Co	3.3621	-0.7030	5.7694	-2.0173	0.4218	-3.4616
Ir	3.3802	5.3515	-0.4325	-2.0281	-3.2109	0.2595
Ni	3.3631	-0.7179	5.7751	-2.0178	0.4307	-3.4651
Pd	3.3531	7.3358	16.3481	-2.0118	-4.4015	-9.8088
Pt	3.3521	-0.3503	1.0246	-2.0113	0.2102	-0.6147
Li	3.3249	-4.8625	5.5267	-1.9950	2.9175	-3.3160
Be	3.3721	-1.2069	11.6786	-2.0233	0.7242	-7.0072
Mg	3.3340	-4.1768	10.6611	-2.0004	2.5061	-6.3967
Al	3.3641	-2.1419	8.5453	-2.0184	1.2852	-5.1272
Ga	3.3561	-0.8449	3.4202	-2.0137	0.5069	-2.0521
In	3.3381	2.6935	-6.0121	-2.0028	-1.6161	3.6073
Si	3.3701	-1.1885	7.4214	-2.0221	0.7131	-4.4529
Ge	3.3641	-0.1598	3.6255	-2.0184	0.0959	-2.1753
Sn	3.3511	1.9531	-0.1384	-2.0106	-1.1718	0.0830
Pb	3.3421	6.3394	-11.4695	-2.0052	-3.8036	6.8817
Sb	3.3571	4.3817	-4.2525	-2.0142	-2.6290	2.5515
Te	3.3631	1.2561	-2.1295	-2.0178	-0.7537	1.2777
B	3.3871	2.4820	7.9643	-2.0323	-1.4892	-4.7786

Table B. 10 Ordering energy and interchange energy values for $Ti_{40}Zr_{59}X_1$ alloy (in SI units).

$Ti_{40}Zr_{59}X_1$						
X	W_{Ti-Zr} J/mol (10^3)	W_{Ti-X} J/mol (10^3)	W_{Zr-X} J/mol (10^3)	ω_{Ti-Zr} J/mol (10^4)	ω_{Ti-X} J/mol (10^4)	ω_{Zr-X} J/mol (10^4)
None	8.8158	-	-	-5.2895	-	-
Ag	8.7423	-2.6663	-26.5964	-5.2454	1.5998	15.9579
Au	8.7397	5.1360	0.0321	-5.2438	-3.0816	-0.0193
Zn	8.7974	-3.7581	10.9832	-5.2785	2.2549	-6.5899
Cd	8.7528	-5.7471	5.9310	-5.2517	3.4483	-3.5586
Cu	8.7817	-5.7346	-3.4332	-5.2690	3.4408	2.0599
Hg	8.7395	-1.0009	0.8154	-5.2437	0.6006	-0.4892
Sc	8.7710	1.4060	9.9705	-5.2626	-0.8436	-5.9823
Y	8.7184	2.2894	0.0349	-5.2310	-1.3736	-0.0209
La	8.6843	10.7291	-3.5171	-5.2106	-6.4374	2.1103
Hf	8.8212	14.1810	-1.0464	-5.2927	-8.5086	0.6278
V	8.9106	0.4763	12.9009	-5.3464	-0.2858	-7.7405
Nb	8.8818	2.8604	-1.2885	-5.3291	-1.7163	0.7731
Cr	8.8529	2.7936	22.6153	-5.3117	-1.6761	-13.5692
Mo	8.9265	17.2032	-1.9662	-5.3559	-10.3219	1.1797
W	8.9316	15.1997	-2.5900	-5.3590	-9.1198	1.5540
Mn	8.8158	-1.7233	8.3327	-5.2895	1.0340	-4.9996
Re	8.9738	5.3109	-6.8980	-5.3843	-3.1865	4.1388
Fe	8.8501	1.5903	10.3734	-5.3101	-0.9542	-6.2240
Ru	8.8763	8.7409	0.0000	-5.3258	-5.2445	0.0000
Os	8.8713	14.0628	-1.1351	-5.3228	-8.4377	0.6811
Co	8.8239	-1.8449	15.1416	-5.2943	1.1070	-9.0850
Ir	8.8713	14.0449	-1.1350	-5.3228	-8.4269	0.6810
Ni	8.8263	-1.8841	15.1567	-5.2958	1.1305	-9.0940
Pd	8.8001	19.2527	42.9053	-5.2800	-11.5516	-25.7432
Pt	8.7976	-0.9192	2.6890	-5.2786	0.5515	-1.6134
Li	8.7262	-12.7614	14.5047	-5.2357	7.6569	-8.7028
Be	8.8501	-3.1676	30.6504	-5.3101	1.9006	-18.3903
Mg	8.7500	-10.9620	27.9800	-5.2500	6.5772	-16.7880
Al	8.8289	-5.6215	22.4269	-5.2974	3.3729	-13.4561
Ga	8.8081	-2.2174	8.9762	-5.2849	1.3305	-5.3857
In	8.7607	7.0689	-15.7787	-5.2564	-4.2414	9.4672
Si	8.8449	-3.1192	19.4775	-5.3069	1.8715	-11.6865
Ge	8.8289	-0.4195	9.5149	-5.2974	0.2517	-5.7090
Sn	8.7948	5.1258	-0.3632	-5.2769	-3.0755	0.2179
Pb	8.7712	16.6376	-30.1017	-5.2627	-9.9826	18.0610
Sb	8.8106	11.4997	-11.1608	-5.2863	-6.8998	6.6965
Te	8.8263	3.2967	-5.5888	-5.2958	-1.9780	3.3533
B	8.8895	6.5141	20.9022	-5.3337	-3.9084	-12.5413

Table B. 11 Ordering energy and interchange energy values for $Ti_{39}Zr_{60}X_1$ alloy (in atomic unit of energy).

$Ti_{39}Zr_{60}X_1$						
X	W_{Ti-Zr} **a.u** (10^{-3})	W_{Ti-X} **a.u** (10^{-3})	W_{Zr-X} **a.u** (10^{-3})	ω_{Ti-Zr} **a.u** (10^{-2})	ω_{Ti-X} **a.u** (10^{-2})	ω_{Zr-X} **a.u** (10^{-2})
None	3.3591	-	-	-2.0154	-	-
Ag	3.3170	-1.0406	-10.1643	-1.9902	0.6244	6.0986
Au	3.3160	1.9229	-10.8700	-1.9896	-1.1537	6.5220
Zn	3.3371	-1.4339	4.1660	-2.0022	0.8604	-2.4996
Cd	3.3210	-2.1938	2.2519	-1.9926	1.3163	-1.3511
Cu	3.3320	-2.1960	-1.3460	-1.9992	1.3176	0.8076
Hg	3.3150	-0.3922	0.3402	-1.9890	0.2353	-0.2041
Sc	3.3279	0.5368	3.7604	-1.9968	-0.3221	-2.2562
Y	3.3079	0.8563	0.0123	-1.9847	-0.5138	-0.0074
La	3.2949	4.0693	-1.3392	-1.9769	-2.4416	0.8035
Hf	3.3471	5.3885	-0.3977	-2.0082	-3.2331	0.2386
V	3.3811	0.1746	4.8620	-2.0287	-0.1048	-2.9172
Nb	3.3702	1.0707	-0.4939	-2.0221	-0.6424	0.2963
Cr	3.3591	1.0705	8.5729	-2.0155	-0.6423	-5.1438
Mo	3.3882	6.5212	-0.7520	-2.0329	-3.9127	0.4512
W	3.3892	5.7695	-0.9899	-2.0335	-3.4617	0.5939
Mn	3.3441	-0.6565	3.1404	-2.0064	0.3939	-1.8842
Re	3.4052	1.9886	-2.6393	-2.0431	-1.1932	1.5836
Fe	3.3581	0.6060	3.9138	-2.0149	-0.3636	-2.3483
Ru	3.3681	3.3174	0.0000	-2.0209	-1.9905	0.0000
Os	3.3661	5.3435	-0.4325	-2.0197	-3.2061	0.2595
Co	3.3481	-0.7019	5.7328	-2.0088	0.4211	-3.4397
Ir	3.3661	5.3376	-0.4315	-2.0197	-3.2026	0.2589
Ni	3.3481	-0.7168	5.7306	-2.0088	0.4301	-3.4384
Pd	3.3390	7.3675	16.2743	-2.0034	-4.4205	-9.7646
Pt	3.3381	-0.3601	1.0560	-2.0028	0.2160	-0.6336
Li	3.3099	-4.8726	5.5276	-1.9860	2.9235	-3.3166
Be	3.3571	-1.1999	11.6513	-2.0143	0.7200	-6.9908
Mg	3.3190	-4.1479	10.6490	-1.9914	2.4888	-6.3894
Al	3.3500	-2.1301	8.5277	-2.0100	1.2780	-5.1166
Ga	3.3421	-0.8489	3.4211	-2.0052	0.5093	-2.0526
In	3.3240	2.6836	-6.0136	-1.9944	-1.6102	3.6081
Si	3.3561	-1.1866	7.4078	-2.0136	0.7120	-4.4447
Ge	3.3491	-0.1589	3.6106	-2.0094	0.0953	-2.1663
Sn	3.3370	1.9551	-0.1544	-2.0022	-1.1730	0.0926
Pb	3.3280	6.3336	-11.4763	-1.9968	-3.8001	6.8858
Sb	3.3431	4.3789	-4.2539	-2.0058	-2.6273	2.5523
Te	3.3490	1.2512	-2.1375	-2.0094	-0.7507	1.2825
B	3.3731	2.4940	8.0085	-2.0239	-1.4964	-4.8051

Table B. 12 Ordering energy and interchange energy values for $Ti_{39}Zr_{60}X_1$ alloy (in SI units).

$Ti_{39}Zr_{60}X_1$						
X	W_{Ti-Zr} J/mol (10^3)	W_{Ti-X} J/mol (10^3)	W_{Zr-X} J/mol (10^3)	ω_{Ti-Zr} J/mol (10^4)	ω_{Ti-X} J/mol (10^4)	ω_{Zr-X} J/mol (10^4)
None	8.8158	-	-	-5.2895	-	-
Ag	8.7054	-2.7311	-26.6762	-5.2232	1.6386	16.0057
Au	8.7028	5.0466	-28.5281	-5.2217	-3.0279	17.1168
Zn	8.7581	-3.7633	10.9335	-5.2548	2.2580	-6.5601
Cd	8.7159	-5.7576	5.9100	-5.2295	3.4546	-3.5460
Cu	8.7448	-5.7633	-3.5326	-5.2469	3.4580	2.1195
Hg	8.7002	-1.0293	0.8927	-5.2201	0.6176	-0.5356
Sc	8.7341	1.4088	9.8690	-5.2405	-0.8453	-5.9214
Y	8.6815	2.2474	0.0323	-5.2089	-1.3484	-0.0194
La	8.6473	10.6799	-3.5147	-5.1884	-6.4079	2.1088
Hf	8.7843	14.1420	-1.0438	-5.2706	-8.4852	0.6263
V	8.8737	0.4583	12.7602	-5.3242	-0.2750	-7.6561
Nb	8.8450	2.8101	-1.2962	-5.3070	-1.6860	0.7777
Cr	8.8160	2.8096	22.4995	-5.2896	-1.6858	-13.4997
Mo	8.8923	17.1149	-1.9737	-5.3354	-10.2689	1.1842
W	8.8949	15.1421	-2.5979	-5.3369	-9.0853	1.5587
Mn	8.7764	-1.7229	8.2418	-5.2659	1.0338	-4.9451
Re	8.9369	5.2192	-6.9267	-5.3621	-3.1315	4.1560
Fe	8.8134	1.5904	10.2717	-5.2880	-0.9543	-6.1630
Ru	8.8396	8.7066	0.0000	-5.3038	-5.2240	0.0000
Os	8.8344	14.0239	-1.1350	-5.3006	-8.4143	0.6810
Co	8.7869	-1.8421	15.0457	-5.2722	1.1053	-9.0274
Ir	8.8344	14.0085	-1.1325	-5.3006	-8.4051	0.6795
Ni	8.7869	-1.8813	15.0399	-5.2722	1.1288	-9.0239
Pd	8.7632	19.3359	42.7116	-5.2579	-11.6016	-25.6269
Pt	8.7607	-0.9450	2.7714	-5.2564	0.5670	-1.6629
Li	8.6869	-12.7880	14.5071	-5.2121	7.6728	-8.7043
Be	8.8107	-3.1492	30.5786	-5.2864	1.8895	-18.3472
Mg	8.7107	-10.8862	27.9481	-5.2264	6.5317	-16.7688
Al	8.7920	-5.5903	22.3808	-5.2752	3.3542	-13.4285
Ga	8.7712	-2.2279	8.9785	-5.2627	1.3368	-5.3871
In	8.7238	7.0432	-15.7826	-5.2343	-4.2259	9.4695
Si	8.8079	-3.1142	19.4416	-5.2848	1.8685	-11.6650
Ge	8.7896	-0.4170	9.4759	-5.2737	0.2502	-5.6855
Sn	8.7579	5.1310	-0.4052	-5.2547	-3.0786	0.2431
Pb	8.7343	16.6224	-30.1193	-5.2406	-9.9734	18.0716
Sb	8.7738	11.4924	-11.1642	-5.2643	-6.8954	6.6985
Te	8.7894	3.2837	-5.6100	-5.2736	-1.9702	3.3660
B	8.8527	6.5455	21.0183	-5.3116	-3.9273	-12.6110

Table B. 13 Ordering energy and interchange energy values for $Ti_{68}Co_{31}X_1$ alloy (in atomic unit of energy).

$Ti_{68}Co_{31}X_1$						
X	**W_{Ti-Co} a.u (10^{-3})**	**W_{Ti-X} a.u (10^{-3})**	**W_{Co-X} a.u (10^{-3})**	**ω_{Ti-Co} a.u (10^{-2})**	**ω_{Ti-X} a.u (10^{-2})**	**ω_{Co-X} a.u (10^{-2})**
None	0.3482	-	-	-0.2089	-	-
Ag	0.3204	-8.8528	0.8697	-0.1922	5.3117	-0.5218
Au	0.3204	-7.8234	8.0441	-0.1922	4.6940	-4.8265
Zn	0.3588	-1.2065	0.6130	-0.2153	0.7239	-0.3678
Cd	0.3214	-3.3861	0.1918	-0.1928	2.0317	-0.1151
Cu	0.3343	-4.1094	-0.5318	-0.2006	2.4656	0.3191
Hg	0.3167	-2.7988	6.6461	-0.1900	1.6793	-3.9877
Sc	0.3251	1.1306	0.2954	-0.1951	-0.6784	-0.1773
Y	0.3048	5.0986	7.7077	-0.1829	-3.0592	-4.6246
La	0.2929	7.7282	12.8403	-0.1757	-4.6369	-7.7042
Hf	0.3442	14.9040	18.1065	-0.2065	-8.9424	-10.8639
V	0.3767	-0.5189	-4.8673	-0.2260	0.3114	2.9204
Nb	0.3665	12.7488	12.3314	-0.2199	-7.6493	-7.3988
Cr	0.3581	2.2825	0.3006	-0.2149	-1.3695	-0.1804
Mo	0.3832	22.6138	24.4005	-0.2299	-13.5683	-14.6403
W	0.3832	24.6120	25.2043	-0.2299	-14.7672	-15.1226
Mn	0.3455	-0.0330	0.4944	-0.2073	0.0198	-0.2966
Re	0.3978	17.0625	16.1942	-0.2387	-10.2375	-9.7165
Fe	0.3581	1.1767	0.1712	-0.2149	-0.7060	-0.1027
Ru	0.3655	14.4179	16.0209	-0.2193	-8.6508	-9.6126
Os	0.3645	14.7230	17.9671	-0.2187	-8.8338	-10.7803
Zr	0.3415	14.7247	16.2406	-0.2049	-8.8348	-9.7444
Ir	0.3638	14.6872	17.9426	-0.2183	-8.8123	-10.7656
Ni	0.3489	0.3302	0.0000	-0.2094	-0.1981	0.0000
Pd	0.3390	17.0184	10.0499	-0.2034	-10.2110	-6.0299
Pt	0.3387	-2.0460	7.4790	-0.2032	1.2276	-4.4874
Li	0.3102	-4.3926	-0.4716	-0.1861	2.6356	0.2829
Be	0.3571	2.7098	0.2020	-0.2143	-1.6259	-0.1212
Mg	0.3187	2.8769	-1.6432	-0.1912	-1.7262	0.9859
Al	0.3472	0.2562	-3.2624	-0.2083	-0.1537	1.9575
Ga	0.3397	-1.7542	1.1992	-0.2038	1.0525	-0.7195
In	0.3224	2.0799	10.0083	-0.1934	-1.2480	-6.0050
Si	0.3509	-1.3963	-3.7317	-0.2106	0.8378	2.2390
Ge	0.3445	0.2581	-0.1462	-0.2067	-0.1549	0.0877
Sn	0.3326	6.2202	6.8083	-0.1995	-3.7321	-4.0850
Pb	0.3241	10.5824	19.4103	-0.1945	-6.3495	-11.6462
Sb	0.3363	11.4515	14.9037	-0.2018	-6.8709	-8.9422
Te	0.3397	7.4043	7.1579	-0.2038	-4.4426	-4.2947
B	0.3703	11.4582	17.9834	-0.2222	-6.8749	-10.7901

Table B. 14 Ordering energy and interchange energy values for $Ti_{68}Co_{31}X_1$ alloy (in SI units).

$Ti_{68}Co_{31}X_1$						
X	W_{Ti-Co} J/mol (10^3)	W_{Ti-X} J/mol (10^3)	W_{Co-X} J/mol (10^3)	ω_{Ti-Co} J/mol (10^4)	ω_{Ti-X} J/mol (10^4)	ω_{Co-X} J/mol (10^4)
None	0.9138			-0.5483		
Ag	0.8409	-23.2341	2.2824	-0.5045	13.9404	-1.3694
Au	0.8409	-20.5323	21.1117	-0.5045	12.3194	-12.6670
Zn	0.9416	-3.1663	1.6089	-0.5650	1.8998	-0.9653
Cd	0.8435	-8.8869	0.5033	-0.5061	5.3321	-0.3020
Cu	0.8774	-10.7850	-1.3956	-0.5264	6.4710	0.8373
Hg	0.8311	-7.3454	17.4426	-0.4987	4.4073	-10.4656
Sc	0.8533	2.9672	0.7753	-0.5120	-1.7803	-0.4652
Y	0.7999	13.3812	20.2287	-0.4799	-8.0287	-12.1372
La	0.7687	20.2827	33.6992	-0.4612	-12.1696	-20.2195
Hf	0.9033	39.1154	47.5201	-0.5420	-23.4693	-28.5121
V	0.9887	-1.3619	-12.7740	-0.5932	0.8172	7.6644
Nb	0.9620	33.4591	32.3635	-0.5772	-20.0755	-19.4181
Cr	0.9398	5.9905	0.7889	-0.5639	-3.5943	-0.4733
Mo	1.0056	59.3496	64.0388	-0.6034	-35.6097	-38.4233
W	1.0056	64.5939	66.1485	-0.6034	-38.7563	-39.6891
Mn	0.9067	-0.0866	1.2976	-0.5440	0.0520	-0.7785
Re	1.0440	44.7803	42.5014	-0.6264	-26.8682	-25.5009
Fe	0.9398	3.0882	0.4492	-0.5639	-1.8529	-0.2695
Ru	0.9594	37.8396	42.0467	-0.5756	-22.7038	-25.2280
Os	0.9567	38.6402	47.1545	-0.5740	-23.1841	-28.2927
Zr	0.8962	38.6447	42.6233	-0.5377	-23.1868	-25.5740
Ir	0.9548	38.5463	47.0902	-0.5729	-23.1278	-28.2541
Ni	0.9157	0.8666	0.0000	-0.5494	-0.5200	0.0000
Pd	0.8898	44.6645	26.3758	-0.5339	-26.7987	-15.8255
Pt	0.8890	-5.3697	19.6286	-0.5334	3.2218	-11.7772
Li	0.8142	-11.5283	-1.2376	-0.4885	6.9170	0.7426
Be	0.9372	7.1118	0.5301	-0.5623	-4.2671	-0.3181
Mg	0.8364	7.5505	-4.3127	-0.5018	-4.5303	2.5876
Al	0.9112	0.6724	-8.5623	-0.5467	-0.4034	5.1374
Ga	0.8917	-4.6038	3.1472	-0.5350	2.7623	-1.8883
In	0.8461	5.4588	26.2667	-0.5077	-3.2753	-15.7600
Si	0.9210	-3.6646	-9.7939	-0.5526	2.1987	5.8763
Ge	0.9041	0.6773	-0.3836	-0.5424	-0.4064	0.2302
Sn	0.8728	16.3247	17.8684	-0.5237	-9.7948	-10.7210
Pb	0.8507	27.7735	50.9421	-0.5104	-16.6641	-30.5653
Sb	0.8826	30.0542	39.1146	-0.5296	-18.0325	-23.4687
Te	0.8917	19.4324	18.7858	-0.5350	-11.6594	-11.2715
B	0.9718	30.0719	47.1973	-0.5831	-18.0432	-28.3184

Table B. 15 Ordering energy and interchange energy values for $Ti_{67}Co_{32}X_1$ alloy (in atomic unit of energy).

$Ti_{67}Co_{32}X_1$						
X	W_{Ti-Co} **a.u** (10^{-3})	W_{Ti-X} **a.u** (10^{-3})	W_{Co-X} **a.u** (10^{-3})	ω_{Ti-Co} **a.u** (10^{-2})	ω_{Ti-X} **a.u** (10^{-2})	ω_{Co-X} **a.u** (10^{-2})
None	0.3482	-	-	-0.2089		
Ag	0.3130	-8.8840	0.8538	-0.1878	5.3304	-0.5123
Au	0.3130	-7.8842	7.9830	-0.1878	4.7305	-4.7898
Zn	0.3306	-1.2105	0.6110	-0.1983	0.7263	-0.3666
Cd	0.3140	-3.3871	0.1858	-0.1884	2.0323	-0.1115
Cu	0.3269	-4.1278	-0.5378	-0.1961	2.4767	0.3227
Hg	0.3092	-2.8128	6.6210	-0.1855	1.6877	-3.9726
Sc	0.3177	1.1259	0.2952	-0.1906	-0.6755	-0.1771
Y	0.2973	5.0988	7.6754	-0.1784	-3.0593	-4.6052
La	0.2852	7.7085	12.7949	-0.1711	-4.6251	-7.6770
Hf	0.3370	14.8938	18.0613	-0.2022	-8.9363	-10.8368
V	0.3693	-0.5269	-4.8750	-0.2216	0.3162	2.9250
Nb	0.3591	12.7629	12.2925	-0.2155	-7.6577	-7.3755
Cr	0.3509	2.2737	0.2956	-0.2106	-1.3642	-0.1774
Mo	0.3764	22.5892	24.3196	-0.2259	-13.5535	-14.5918
W	0.3764	24.6042	25.1429	-0.2259	-14.7625	-15.0857
Mn	0.3380	-0.0394	0.4944	-0.2028	0.0237	-0.2966
Re	0.3903	17.0478	16.1177	-0.2342	-10.2287	-9.6706
Fe	0.3509	1.1720	0.1704	-0.2106	-0.7032	-0.1023
Ru	0.3584	14.4241	15.9859	-0.2150	-8.6545	-9.5916
Os	0.3574	14.7137	17.9230	-0.2144	-8.8282	-10.7538
Zr	0.3343	14.7316	16.2054	-0.2006	-8.8389	-9.7232
Ir	0.3571	14.6776	17.8992	-0.2143	-8.8066	-10.7395
Ni	0.3417	0.3230	0.0000	-0.2050	-0.1938	0.0000
Pd	0.3316	16.9803	10.0311	-0.1989	-10.1882	-6.0187
Pt	0.3306	-2.0590	7.4560	-0.1983	1.2354	-4.4736
Li	0.3028	-4.3949	-0.4806	-0.1817	2.6369	0.2883
Be	0.3499	2.7096	0.2013	-0.2100	-1.6258	-0.1208
Mg	0.3110	2.9018	-1.6295	-0.1866	-1.7411	0.9777
Al	0.3397	0.2719	-3.2610	-0.2038	-0.1632	1.9566
Ga	0.3323	-1.7544	1.1847	-0.1994	1.0527	-0.7108
In	0.3150	2.0635	9.9870	-0.1890	-1.2381	-5.9922
Si	0.3435	-1.3896	-3.7445	-0.2061	0.8337	2.2467
Ge	0.3370	0.2601	-0.1569	-0.2022	-0.1561	0.0941
Sn	0.3251	6.2214	6.7959	-0.1951	-3.7329	-4.0775
Pb	0.3167	10.5643	19.3955	-0.1900	-6.3386	-11.6373
Sb	0.3289	11.4400	14.8744	-0.1973	-6.8640	-8.9246
Te	0.3326	7.3983	7.1213	-0.1995	-4.4390	-4.2728
B	0.3635	11.4610	17.9809	-0.2181	-6.8766	-10.7886

Table B. 16 Ordering energy and interchange energy values for $Ti_{67}Co_{32}X_1$ alloy (in SI units).

$Ti_{67}Co_{32}X_1$						
X	W_{Ti-Co} J/mol (10^3)	W_{Ti-X} J/mol (10^3)	W_{Co-X} J/mol (10^3)	ω_{Ti-Co} J/mol (10^4)	ω_{Ti-X} J/mol (10^4)	ω_{Co-X} J/mol (10^4)
None	0.9138			-0.5483		
Ag	0.8214	-23.3159	2.2407	-0.4928	13.9895	-1.3444
Au	0.8214	-20.6919	20.9513	-0.4928	12.4151	-12.5708
Zn	0.8676	-3.1768	1.6037	-0.5206	1.9061	-0.9622
Cd	0.8240	-8.8895	0.4875	-0.4944	5.3337	-0.2925
Cu	0.8578	-10.8334	-1.4113	-0.5147	6.5001	0.8468
Hg	0.8116	-7.3822	17.3768	-0.4869	4.4293	-10.4261
Sc	0.8337	2.9548	0.7746	-0.5002	-1.7729	-0.4648
Y	0.7804	13.3817	20.1440	-0.4682	-8.0290	-12.0864
La	0.7484	20.2309	33.5801	-0.4490	-12.1385	-20.1481
Hf	0.8845	39.0885	47.4016	-0.5307	-23.4531	-28.4410
V	0.9691	-1.3829	-12.7943	-0.5815	0.8298	7.6766
Nb	0.9424	33.4961	32.2616	-0.5655	-20.0976	-19.3570
Cr	0.9210	5.9672	0.7758	-0.5526	-3.5803	-0.4655
Mo	0.9880	59.2851	63.8265	-0.5928	-35.5711	-38.2959
W	0.9880	64.5734	65.9872	-0.5928	-38.7440	-39.5923
Mn	0.8871	-0.1035	1.2976	-0.5323	0.0621	-0.7785
Re	1.0244	44.7418	42.3008	-0.6147	-26.8451	-25.3805
Fe	0.9210	3.0758	0.4473	-0.5526	-1.8455	-0.2684
Ru	0.9405	37.8558	41.9548	-0.5643	-22.7135	-25.1729
Os	0.9379	38.6159	47.0386	-0.5627	-23.1695	-28.2232
Zr	0.8774	38.6628	42.5308	-0.5264	-23.1977	-25.5185
Ir	0.9372	38.5212	46.9762	-0.5623	-23.1127	-28.1857
Ni	0.8969	0.8478	0.0000	-0.5381	-0.5087	0.0000
Pd	0.8702	44.5646	26.3265	-0.5221	-26.7388	-15.7959
Pt	0.8676	-5.4038	19.5680	-0.5206	3.2423	-11.7408
Li	0.7947	-11.5343	-1.2612	-0.4768	6.9206	0.7567
Be	0.9184	7.1113	0.5282	-0.5510	-4.2668	-0.3169
Mg	0.8161	7.6157	-4.2767	-0.4897	-4.5694	2.5660
Al	0.8917	0.7137	-8.5585	-0.5350	-0.4282	5.1351
Ga	0.8721	-4.6045	3.1093	-0.5233	2.7627	-1.8656
In	0.8266	5.4156	26.2107	-0.4960	-3.2494	-15.7264
Si	0.9014	-3.6469	-9.8273	-0.5409	2.1881	5.8964
Ge	0.8845	0.6826	-0.4118	-0.5307	-0.4096	0.2471
Sn	0.8533	16.3281	17.8357	-0.5120	-9.7968	-10.7014
Pb	0.8311	27.7258	50.9033	-0.4987	-16.6355	-30.5420
Sb	0.8631	30.0242	39.0376	-0.5178	-18.0145	-23.4225
Te	0.8728	19.4166	18.6897	-0.5237	-11.6500	-11.2138
B	0.9541	30.0794	47.1907	-0.5725	-18.0476	-28.3144

APPENDIX C

Table C. 1 ΔH^M, S^σ, ΔS^{ideal}, ΔS^M, $\Delta\eta/\eta_0$ and critical cooling rate for $Ti_{60}Zr_{39}X_1$ alloy (in SI units).

$Ti_{60}Zr_{39}X_1$						
X	**ΔH^M J/mol (10^4)**	**S^σ J/mol.K**	**ΔS^{ideal} J/mol.K**	**ΔS^M J/mol.K**	**$\Delta\eta/\eta_0$**	**R_c K/s (10^5)**
None	-1.3686	0.3871	5.5927	5.9799	0.9084	4.5131
Ag	-1.2636	0.3867	5.9813	6.3680	0.8387	5.0038
Au	-1.2809	0.3870	5.9813	6.3683	0.8502	4.7158
Zn	-1.3478	0.3945	5.9813	6.3758	0.8946	3.8702
Cd	-1.3223	0.3836	5.9813	6.3650	0.8776	4.2036
Cu	-1.3091	0.4254	5.9813	6.4067	0.8689	4.2329
Hg	-1.3224	0.3821	5.9813	6.3634	0.8778	4.1788
Sc	-1.3623	0.3935	5.9813	6.3748	0.9042	3.7142
Y	-1.3347	0.4498	5.9813	6.4311	0.8859	3.8292
La	-1.3527	0.4955	5.9813	6.4768	0.8978	3.4723
Hf	-1.3861	0.3844	5.9813	6.3657	0.9200	3.4492
V	-1.3847	0.4134	5.9813	6.3947	0.9191	3.4108
Nb	-1.3533	0.3887	5.9813	6.3701	0.8983	3.8173
Cr	-1.4050	0.4356	5.9813	6.4169	0.9325	3.1469
Mo	-1.4102	0.4012	5.9813	6.3825	0.9360	3.1811
W	-1.4005	0.4002	5.9813	6.3815	0.9296	3.2569
Mn	-1.3518	0.4042	5.9813	6.3856	0.8972	3.7948
Re	-1.3628	0.3984	5.9813	6.3798	0.9046	3.6525
Fe	-1.3732	0.4385	5.9813	6.4198	0.9114	3.4530
Ru	-1.3752	0.4072	5.9813	6.3885	0.9128	3.5144
Os	-1.3912	0.4037	5.9813	6.3850	0.9234	3.3370
Co	-1.3684	0.4349	5.9813	6.4162	0.9082	3.5135
Ir	-1.3912	0.4025	5.9813	6.3838	0.9234	3.3404
Ni	-1.3686	0.4367	5.9813	6.4181	0.9084	3.5050
Pd	-1.5020	0.3983	5.9813	6.3797	0.9970	2.4176
Pt	-1.3337	0.3959	5.9813	6.3773	0.8852	3.9934
Li	-1.3144	0.3820	5.9813	6.3633	0.8724	4.3458
Be	-1.4001	0.4878	5.9813	6.4691	0.9293	3.0609
Mg	-1.3480	0.3870	5.9813	6.3683	0.8947	3.9053
Al	-1.3678	0.3884	5.9813	6.3697	0.9079	3.6738
Ga	-1.3476	0.3949	5.9813	6.3763	0.8945	3.8688
In	-1.3191	0.3974	5.9813	6.3787	0.8755	4.1924
Si	-1.3735	0.4758	5.9813	6.4571	0.9116	3.3462
Ge	-1.3584	0.4390	5.9813	6.4203	0.9016	3.6039
Sn	-1.3512	0.3897	5.9813	6.3710	0.8969	3.8303
Pb	-1.3214	0.4262	5.9813	6.4075	0.8770	4.0322
Sb	-1.3499	0.3820	5.9813	6.3633	0.8960	3.8713
Te	-1.3361	0.3859	5.9813	6.3672	0.8868	4.0200
B	-1.4076	0.6709	5.9813	6.6522	0.9343	2.5506

Table C. 2 ΔH^M, S^σ, ΔS^{ideal}, ΔS^M, $\Delta\eta/\eta_0$ and critical cooling rate for $Ti_{59}Zr_{40}X_1$ alloy (in SI units).

$Ti_{59}Zr_{40}X_1$						
X	**ΔH^M J/mol (10^4)**	**S^σ J/mol.K**	**ΔS^{ideal} J/mol.K**	**ΔS^M J/mol.K**	**$\Delta\eta/\eta_0$**	**R_c K/s (10^5)**
None	-1.3686	0.3871	5.5927	5.9799	0.9084	4.5131
Ag	-1.2682	0.3890	6.0154	6.4043	0.8418	4.8175
Au	-1.2852	0.3893	6.0154	6.4047	0.8530	4.5458
Zn	-1.3552	0.3968	6.0154	6.4122	0.8995	3.6955
Cd	-1.3298	0.3856	6.0154	6.4010	0.8826	4.0136
Cu	-1.3159	0.4279	6.0154	6.4432	0.8734	4.0484
Hg	-1.3291	0.3842	6.0154	6.3996	0.8822	4.0004
Sc	-1.3696	0.3953	6.0154	6.4107	0.9091	3.5487
Y	-1.3409	0.4510	6.0154	6.4664	0.8900	3.6733
La	-1.3581	0.4964	6.0154	6.5118	0.9014	3.3395
Hf	-1.3920	0.3863	6.0154	6.4017	0.9239	3.3096
V	-1.3923	0.4159	6.0154	6.4313	0.9241	3.2543
Nb	-1.3602	0.3910	6.0154	6.4064	0.9028	3.6510
Cr	-1.4132	0.4381	6.0154	6.4535	0.9380	2.9967
Mo	-1.4161	0.4036	6.0154	6.4190	0.9399	3.0510
W	-1.4062	0.4026	6.0154	6.4180	0.9334	3.1250
Mn	-1.3592	0.4067	6.0154	6.4220	0.9022	3.6222
Re	-1.3691	0.4008	6.0154	6.4162	0.9087	3.4993
Fe	-1.3806	0.4411	6.0154	6.4564	0.9164	3.2962
Ru	-1.3819	0.4097	6.0154	6.4250	0.9172	3.3627
Os	-1.3975	0.4061	6.0154	6.4215	0.9276	3.1968
Co	-1.3763	0.4374	6.0154	6.4528	0.9135	3.3489
Ir	-1.3975	0.4049	6.0154	6.4202	0.9276	3.2001
Ni	-1.3766	0.4393	6.0154	6.4547	0.9137	3.3405
Pd	-1.5106	0.4007	6.0154	6.4161	1.0026	2.3005
Pt	-1.3408	0.3983	6.0154	6.4137	0.8900	3.8160
Li	-1.3221	0.3841	6.0154	6.3995	0.8776	4.1457
Be	-1.4096	0.4904	6.0154	6.5058	0.9356	2.9040
Mg	-1.3573	0.3889	6.0154	6.4043	0.9009	3.7089
Al	-1.3766	0.3907	6.0154	6.4060	0.9137	3.4934
Ga	-1.3552	0.3973	6.0154	6.4127	0.8995	3.6921
In	-1.3241	0.3991	6.0154	6.4145	0.8789	4.0337
Si	-1.3818	0.4784	6.0154	6.4938	0.9172	3.1854
Ge	-1.3659	0.4415	6.0154	6.4569	0.9066	3.4389
Sn	-1.3578	0.3916	6.0154	6.4069	0.9012	3.6682
Pb	-1.3250	0.4276	6.0154	6.4430	0.8795	3.8973
Sb	-1.3554	0.3841	6.0154	6.3995	0.8997	3.7178
Te	-1.3424	0.3881	6.0154	6.4035	0.8910	3.8511
B	-1.4162	0.6735	6.0154	6.6889	0.9400	2.4263

Table C. 3 ΔH^M, S^σ, ΔS^{ideal}, ΔS^M, $\Delta\eta/\eta_0$ and critical cooling rate for $Ti_{50}Zr_{49}X_1$ alloy (in SI units).

$Ti_{50}Zr_{49}X_1$						
X	**ΔH^M J/mol (10^4)**	**S^σ J/mol.K**	**ΔS^{ideal} J/mol.K**	**ΔS^M J/mol.K**	**$\Delta\eta/\eta_0$**	**R_c K/s (10^5)**
None	-1.3763	0.3916	5.7601	6.1516	0.9011	3.8489
Ag	-1.5128	0.3947	6.1674	6.5621	0.9904	2.0300
Au	-1.2712	0.3950	6.1674	6.5624	0.8323	4.1704
Zn	-1.3691	0.4033	6.1674	6.5707	0.8964	3.1131
Cd	-1.3414	0.3889	6.1674	6.5563	0.8782	3.4154
Cu	-1.3210	0.4357	6.1674	6.6031	0.8649	3.4967
Hg	-1.3363	0.3888	6.1674	6.5562	0.8749	3.4472
Sc	-1.3790	0.3969	6.1674	6.5643	0.9028	3.0438
Y	-1.3435	0.4477	6.1674	6.6151	0.8796	3.2271
La	-1.3538	0.4902	6.1674	6.6576	0.8863	3.0029
Hf	-1.3901	0.3894	6.1674	6.5569	0.9101	2.9351
V	-1.4054	0.4233	6.1674	6.5907	0.9201	2.7451
Nb	-1.3673	0.3970	6.1674	6.5644	0.8952	3.1409
Cr	-1.4315	0.4462	6.1674	6.6136	0.9372	2.4864
Mo	-1.4123	0.4105	6.1674	6.5779	0.9247	2.7102
W	-1.4041	0.4094	6.1674	6.5768	0.9193	2.7634
Mn	-1.3706	0.4137	6.1674	6.5811	0.8973	3.0734
Re	-1.3688	0.4075	6.1674	6.5749	0.8962	3.0773
Fe	-1.3915	0.4492	6.1674	6.6166	0.9111	2.7959
Ru	-1.3841	0.4168	6.1674	6.5842	0.9062	2.9327
Os	-1.3963	0.4131	6.1674	6.5805	0.9142	2.8184
Co	-1.3915	0.4454	6.1674	6.6128	0.9110	2.8052
Ir	-1.3963	0.4118	6.1674	6.5792	0.9142	2.8214
Ni	-1.3918	0.4474	6.1674	6.6148	0.9112	2.7978
Pd	-1.5328	0.4074	6.1674	6.5748	1.0036	1.8898
Pt	-1.3499	0.4049	6.1674	6.5723	0.8838	3.2633
Li	-1.3419	0.3884	6.1674	6.5558	0.8785	3.4382
Be	-1.4352	0.4992	6.1674	6.6666	0.9397	2.3537
Mg	-1.3875	0.3914	6.1674	6.5588	0.9084	2.9855
Al	-1.4000	0.3966	6.1674	6.5640	0.9166	2.8615
Ga	-1.3680	0.4038	6.1674	6.5712	0.8956	3.1212
In	-1.3175	0.4002	6.1674	6.5676	0.8626	3.6324
Si	-1.4013	0.4871	6.1674	6.6545	0.9175	2.6306
Ge	-1.3780	0.4496	6.1674	6.6171	0.9022	2.9078
Sn	-1.3610	0.3937	6.1674	6.5611	0.8911	3.2048
Pb	-1.3051	0.4260	6.1674	6.5934	0.8545	3.6615
Sb	-1.3500	0.3882	6.1674	6.5556	0.8839	3.3282
Te	-1.3443	0.3937	6.1674	6.5611	0.8802	3.3675
B	-1.4354	0.6822	6.1674	6.8496	0.9398	2.0006

Table C. 4 ΔH^M, S^σ, ΔS^{ideal}, ΔS^M, $\Delta\eta/\eta_0$ and critical cooling rate for $Ti_{49}Zr_{50}X_1$ alloy (in SI units).

$Ti_{49}Zr_{50}X_1$						
X	**ΔH^M J/mol (10^4)**	**S^σ J/mol.K**	**ΔS^{ideal} J/mol.K**	**ΔS^M J/mol.K**	**$\Delta\eta/\eta_0$**	**R_c K/s (10^5)**
None	-1.3763	0.3916	5.7601	6.1516	0.9011	3.8489
Ag	-1.2502	0.3937	6.1674	6.5611	0.8185	4.4620
Au	-1.2638	0.3941	6.1674	6.5615	0.8274	4.2552
Zn	-1.3646	0.4024	6.1674	6.5698	0.8934	3.1482
Cd	-1.4474	0.3877	6.1674	6.5551	0.9476	2.4780
Cu	-1.3155	0.4350	6.1674	6.6024	0.8613	3.5458
Hg	-1.3312	0.3877	6.1674	6.5551	0.8716	3.4926
Sc	-1.3744	0.3955	6.1674	6.5629	0.8998	3.0804
Y	-1.3383	0.4458	6.1674	6.6132	0.8762	3.2731
La	-1.3478	0.4880	6.1674	6.6554	0.8825	3.0534
Hf	-1.3841	0.3882	6.1674	6.5556	0.9062	2.9820
V	-1.4009	0.4226	6.1674	6.5900	0.9172	2.7757
Nb	-1.3588	0.3961	6.1674	6.5635	0.8896	3.2154
Cr	-1.4273	0.4455	6.1674	6.6129	0.9345	2.5116
Mo	-1.4060	0.4097	6.1674	6.5771	0.9205	2.7556
W	-1.3979	0.4086	6.1674	6.5760	0.9153	2.8085
Mn	-1.3661	0.4129	6.1674	6.5803	0.8944	3.1074
Re	-1.3632	0.4067	6.1674	6.5741	0.8925	3.1223
Fe	-1.3870	0.4485	6.1674	6.6159	0.9081	2.8274
Ru	-1.3786	0.4160	6.1674	6.5834	0.9026	2.9746
Os	-1.3904	0.4123	6.1674	6.5797	0.9103	2.8620
Co	-1.3874	0.4447	6.1674	6.6121	0.9084	2.8324
Ir	-1.3904	0.4110	6.1674	6.5784	0.9103	2.8653
Ni	-1.3877	0.4467	6.1674	6.6141	0.9085	2.8255
Pd	-1.5290	0.4066	6.1674	6.5740	1.0011	1.9071
Pt	-1.3454	0.4040	6.1674	6.5714	0.8808	3.3006
Li	-1.3381	0.3873	6.1674	6.5547	0.8761	3.4693
Be	-1.4323	0.4986	6.1674	6.6660	0.9378	2.3681
Mg	-1.3848	0.3901	6.1674	6.5576	0.9067	3.0034
Al	-1.3965	0.3956	6.1674	6.5630	0.9143	2.8855
Ga	-1.3634	0.4029	6.1674	6.5703	0.8926	3.1574
In	-1.3104	0.3988	6.1674	6.5662	0.8580	3.7042
Si	-1.3978	0.4865	6.1674	6.6539	0.9151	2.6522
Ge	-1.3736	0.4490	6.1674	6.6164	0.8993	2.9386
Sn	-1.3557	0.3923	6.1674	6.5597	0.8876	3.2499
Pb	-1.2973	0.4243	6.1674	6.5917	0.8494	3.7429
Sb	-1.3437	0.3871	6.1674	6.5545	0.8797	3.3845
Te	-1.3388	0.3927	6.1674	6.5601	0.8765	3.4162
B	-1.4318	0.6816	6.1674	6.8490	0.9374	2.0172

Table C. 5 ΔH^M, S^σ, ΔS^{ideal}, ΔS^M, $\Delta\eta/\eta_0$ and critical cooling rate for $Ti_{40}Zr_{59}X_1$ alloy (in SI units).

$Ti_{40}Zr_{59}X_1$						
X	**ΔH^M J/mol (10^4)**	**S^σ J/mol.K**	**ΔS^{ideal} J/mol.K**	**ΔS^M J/mol.K**	**$\Delta\eta/\eta_0$**	**R_c K/s (10^5)**
None	-1.2695	0.3653	5.5927	5.9580	0.8070	5.5554
Ag	-1.1374	0.3716	6.0154	6.3870	0.7230	6.4537
Au	-1.2500	0.3720	6.0154	6.3874	0.7946	4.5698
Zn	-1.2756	0.3810	6.0154	6.3964	0.8109	4.2340
Cd	-1.2466	0.3635	6.0154	6.3788	0.7925	4.6792
Cu	-1.2176	0.4148	6.0154	6.4302	0.7740	4.8891
Hg	-1.2380	0.3645	6.0154	6.3799	0.7870	4.7689
Sc	-1.2806	0.3696	6.0154	6.3850	0.8141	4.2194
Y	-1.2401	0.4154	6.0154	6.4308	0.7883	4.5576
La	-1.2430	0.4550	6.0154	6.4704	0.7902	4.3442
Hf	-1.2794	0.3638	6.0154	6.3791	0.8133	4.2194
V	-1.3086	0.4021	6.0154	6.4174	0.8318	3.7650
Nb	-1.2600	0.3742	6.0154	6.3896	0.8010	4.4570
Cr	-1.3403	0.4255	6.0154	6.4409	0.8520	3.3491
Mo	-1.2983	0.3887	6.0154	6.4040	0.8253	3.9184
W	-1.2920	0.3875	6.0154	6.4029	0.8213	3.9739
Mn	-1.2737	0.3920	6.0154	6.4074	0.8097	4.2187
Re	-1.2590	0.3855	6.0154	6.4009	0.8003	4.3961
Fe	-1.2937	0.4286	6.0154	6.4440	0.8224	3.8415
Ru	-1.2779	0.3953	6.0154	6.4107	0.8123	4.1406
Os	-1.2859	0.3914	6.0154	6.4068	0.8174	4.0318
Co	-1.2986	0.4248	6.0154	6.4402	0.8255	3.7975
Ir	-1.2859	0.3901	6.0154	6.4054	0.8174	4.0367
Ni	-1.2989	0.4268	6.0154	6.4421	0.8257	3.7872
Pd	-1.4442	0.3854	6.0154	6.4008	0.9181	2.5323
Pt	-1.2531	0.3827	6.0154	6.3981	0.7966	4.4846
Li	-1.2564	0.3640	6.0154	6.3794	0.7987	4.5743
Be	-1.3541	0.4793	6.0154	6.4947	0.8608	3.0688
Mg	-1.3117	0.3652	6.0154	6.3806	0.8339	3.8635
Al	-1.3161	0.3737	6.0154	6.3891	0.8366	3.7832
Ga	-1.2737	0.3816	6.0154	6.3969	0.8097	4.2548
In	-1.2016	0.3725	6.0154	6.3878	0.7639	5.3126
Si	-1.3139	0.4671	6.0154	6.4825	0.8352	3.4972
Ge	-1.2829	0.4291	6.0154	6.4445	0.8155	3.9629
Sn	-1.2564	0.3670	6.0154	6.3823	0.7987	4.5275
Pb	-1.1754	0.3955	6.0154	6.4109	0.7472	5.5949
Sb	-1.2357	0.3636	6.0154	6.3790	0.7855	4.8321
Te	-1.2379	0.3705	6.0154	6.3859	0.7869	4.7672
B	-1.3484	0.6622	6.0154	6.6776	0.8572	2.6423

Table C. 6 ΔH^M, S^σ, ΔS^{ideal}, ΔS^M, $\Delta\eta/\eta_0$ and critical cooling rate for $Ti_{39}Zr_{60}X_1$ alloy (in SI units).

$Ti_{39}Zr_{60}X_1$						
X	**ΔH^M J/mol (10^4)**	**S^σ J/mol.K**	**ΔS^{ideal} J/mol.K**	**ΔS^M J/mol.K**	**$\Delta\eta/\eta_0$**	**R_c K/s (10^5)**
None	-1.2695	0.3653	5.5927	5.9580	0.8070	5.5554
Ag	-1.1198	0.3677	5.9813	6.3490	0.7119	6.9412
Au	-1.1310	0.3681	5.9813	6.3495	0.7190	6.6695
Zn	-1.2602	0.3772	5.9813	6.3585	0.8011	4.5240
Cd	-1.2315	0.3593	5.9813	6.3407	0.7829	4.9966
Cu	-1.2016	0.4111	5.9813	6.3924	0.7638	5.2330
Hg	-1.2223	0.3605	5.9813	6.3418	0.7770	5.1013
Sc	-1.2651	0.3653	5.9813	6.3466	0.8042	4.5125
Y	-1.2243	0.4107	5.9813	6.3920	0.7782	4.8814
La	-1.2264	0.4499	5.9813	6.4312	0.7796	4.6635
Hf	-1.2627	0.3596	5.9813	6.3409	0.8027	4.5286
V	-1.2929	0.3983	5.9813	6.3796	0.8219	4.0260
Nb	-1.2438	0.3703	5.9813	6.3516	0.7906	4.7743
Cr	-1.3253	0.4219	5.9813	6.4032	0.8425	3.5737
Mo	-1.2814	0.3849	5.9813	6.3662	0.8146	4.2058
W	-1.2749	0.3837	5.9813	6.3651	0.8105	4.2681
Mn	-1.2579	0.3883	5.9813	6.3696	0.7996	4.5134
Re	-1.2420	0.3817	5.9813	6.3631	0.7895	4.7201
Fe	-1.2781	0.4249	5.9813	6.4063	0.8125	4.1068
Ru	-1.2615	0.3915	5.9813	6.3729	0.8019	4.4376
Os	-1.2691	0.3876	5.9813	6.3690	0.8067	4.3267
Co	-1.2835	0.4211	5.9813	6.4024	0.8159	4.0534
Ir	-1.2690	0.3863	5.9813	6.3676	0.8067	4.3318
Ni	-1.2834	0.4231	5.9813	6.4044	0.8159	4.0475
Pd	-1.4294	0.3816	5.9813	6.3630	0.9086	2.7011
Pt	-1.2378	0.3789	5.9813	6.3602	0.7868	4.7904
Li	-1.2419	0.3600	5.9813	6.3413	0.7895	4.8741
Be	-1.3397	0.4757	5.9813	6.4570	0.8517	3.2679
Mg	-1.2981	0.3610	5.9813	6.3423	0.8252	4.1076
Al	-1.3019	0.3698	5.9813	6.3512	0.8276	4.0278
Ga	-1.2586	0.3777	5.9813	6.3591	0.8001	4.5422
In	-1.1845	0.3681	5.9813	6.3494	0.7530	5.7092
Si	-1.2993	0.4635	5.9813	6.4448	0.8260	3.7266
Ge	-1.2672	0.4254	5.9813	6.4067	0.8055	4.2371
Sn	-1.2402	0.3627	5.9813	6.3440	0.7884	4.8514
Pb	-1.1568	0.3909	5.9813	6.3722	0.7353	6.0410
Sb	-1.2185	0.3595	5.9813	6.3409	0.7746	5.1912
Te	-1.2215	0.3666	5.9813	6.3479	0.7765	5.1099
B	-1.3339	0.6586	5.9813	6.6399	0.8480	2.8149

Table C. 7 ΔH^M, S^σ, ΔS^{ideal}, ΔS^M, $\Delta\eta/\eta_0$ and critical cooling rate for $Ti_{68}Co_{31}X_1$ alloy (in SI units).

$Ti_{68}Co_{31}X_1$						
X	**ΔH^M J/mol (10^4)**	**S^σ J/mol.K**	**ΔS^{ideal} J/mol.K**	**ΔS^M J/mol.K**	**$\Delta\eta/\eta_0$**	**R_c K/s (10^7)**
None	-0.1193	0.8795	5.2093	6.0888	0.1002	3.1960
Ag	-0.0158	0.8593	5.5791	6.4383	0.0133	3.7550
Au	-0.0619	0.8591	5.5791	6.4382	0.0519	3.2420
Zn	-0.1092	0.8582	5.5791	6.4372	0.0917	2.8493
Cd	-0.0714	0.8834	5.5791	6.4625	0.0599	3.1233
Cu	-0.0644	0.8729	5.5791	6.4520	0.0541	3.2280
Hg	-0.1076	0.8681	5.5791	6.4471	0.0904	2.8068
Sc	-0.1215	0.9130	5.5791	6.4921	0.1020	2.6491
Y	-0.1934	1.0237	5.5791	6.6027	0.1624	1.9685
La	-0.2427	1.1012	5.5791	6.6803	0.2038	1.6013
Hf	-0.3622	0.8865	5.5791	6.4656	0.3042	1.2909
V	-0.0957	0.8656	5.5791	6.4447	0.0804	2.9559
Nb	-0.3184	0.8584	5.5791	6.4375	0.2674	1.5142
Cr	-0.1448	0.8800	5.5791	6.4591	0.1216	2.5249
Mo	-0.4884	0.8599	5.5791	6.4390	0.4102	0.9066
W	-0.5138	0.8595	5.5791	6.4386	0.4314	0.8332
Mn	-0.1167	0.8611	5.5791	6.4401	0.0980	2.7825
Re	-0.3938	0.8590	5.5791	6.4381	0.3307	1.1956
Fe	-0.1323	0.8822	5.5791	6.4612	0.1111	2.6166
Ru	-0.3539	0.8624	5.5791	6.4415	0.2972	1.3558
Os	-0.3664	0.8608	5.5791	6.4399	0.3077	1.2963
Zr	-0.3503	0.8795	5.5791	6.4586	0.2942	1.3407
Ir	-0.3656	0.8603	5.5791	6.4394	0.3070	1.2994
Ni	-0.1194	0.8809	5.5791	6.4599	0.1002	2.7222
Pd	-0.3438	0.8590	5.5791	6.4381	0.2887	1.4002
Pt	-0.1270	0.8584	5.5791	6.4375	0.1067	2.6663
Li	-0.0536	0.8700	5.5791	6.4491	0.0450	3.3590
Be	-0.1485	0.9228	5.5791	6.5018	0.1247	2.4342
Mg	-0.1286	0.8954	5.5791	6.4744	0.1080	2.6303
Al	-0.1021	0.8585	5.5791	6.4376	0.0857	2.9211
Ga	-0.0998	0.8582	5.5791	6.4373	0.0838	2.9290
In	-0.1781	0.9223	5.5791	6.5014	0.1496	2.2047
Si	-0.0833	0.9123	5.5791	6.4914	0.0700	2.9777
Ge	-0.1164	0.8825	5.5791	6.4616	0.0977	2.7397
Sn	-0.2102	0.9032	5.5791	6.4823	0.1765	2.0275
Pb	-0.3157	0.9808	5.5791	6.5599	0.2651	1.3877
Sb	-0.3070	0.8725	5.5791	6.4516	0.2578	1.5474
Te	-0.2270	0.8598	5.5791	6.4389	0.1906	1.9847
B	-0.3334	1.1028	5.5791	6.6819	0.2800	1.2326

Table C. 8 ΔH^M, S^σ, ΔS^{ideal}, ΔS^M, $\Delta\eta/\eta_0$ and critical cooling rate for $Ti_{67}Co_{32}X_1$ alloy (in SI units).

$Ti_{67}Co_{32}X_1$						
X	**ΔH^M J/mol (10^4)**	**S^σ J/mol.K**	**ΔS^{ideal} J/mol.K**	**ΔS^M J/mol.K**	**$\Delta\eta/\eta_0$**	**R_c K/s (10^7)**
None	-0.1193	0.8795	5.2093	6.0888	0.1002	3.1960
Ag	-0.0162	0.8780	5.6424	6.5204	0.0136	3.5986
Au	-0.0627	0.8778	5.6424	6.5202	0.0527	3.1030
Zn	-0.1019	0.8767	5.6424	6.5191	0.0856	2.7948
Cd	-0.0712	0.9027	5.6424	6.5451	0.0598	2.9973
Cu	-0.0641	0.8911	5.6424	6.5335	0.0538	3.1012
Hg	-0.1081	0.8870	5.6424	6.5295	0.0908	2.6888
Sc	-0.1206	0.9327	5.6424	6.5751	0.1013	2.5468
Y	-0.1929	1.0444	5.6424	6.6868	0.1620	1.8893
La	-0.2421	1.1226	5.6424	6.7650	0.2033	1.5364
Hf	-0.3619	0.9058	5.6424	6.5482	0.3039	1.2394
V	-0.0945	0.8839	5.6424	6.5263	0.0794	2.8473
Nb	-0.3178	0.8771	5.6424	6.5195	0.2669	1.4554
Cr	-0.1440	0.8981	5.6424	6.5406	0.1209	2.4298
Mo	-0.4880	0.8783	5.6424	6.5207	0.4098	0.8713
W	-0.5134	0.8780	5.6424	6.5204	0.4311	0.8007
Mn	-0.1162	0.8795	5.6424	6.5219	0.0976	2.6749
Re	-0.3929	0.8775	5.6424	6.5199	0.3299	1.1507
Fe	-0.1317	0.9003	5.6424	6.5427	0.1106	2.5163
Ru	-0.3537	0.8807	5.6424	6.5232	0.2970	1.3021
Os	-0.3662	0.8792	5.6424	6.5216	0.3075	1.2448
Zr	-0.3499	0.9153	5.6424	6.5577	0.2939	1.2872
Ir	-0.3656	0.8788	5.6424	6.5212	0.3070	1.2472
Ni	-0.1188	0.8990	5.6424	6.5414	0.0998	2.6176
Pd	-0.3416	0.8775	5.6424	6.5199	0.2869	1.3527
Pt	-0.1275	0.8769	5.6424	6.5193	0.1070	2.5558
Li	-0.0534	0.8891	5.6424	6.5315	0.0449	3.2244
Be	-0.1477	0.9407	5.6424	6.5831	0.1241	2.3426
Mg	-0.1274	0.9148	5.6424	6.5572	0.1070	2.5316
Al	-0.1011	0.8772	5.6424	6.5196	0.0849	2.8108
Ga	-0.0996	0.8768	5.6424	6.5192	0.0837	2.8126
In	-0.1784	0.9421	5.6424	6.5845	0.1498	2.1122
Si	-0.0824	0.9303	5.6424	6.5727	0.0692	2.8663
Ge	-0.1157	0.9006	5.6424	6.5430	0.0972	2.6352
Sn	-0.2097	0.9228	5.6424	6.5652	0.1761	1.9478
Pb	-0.3161	1.0012	5.6424	6.6436	0.2655	1.3283
Sb	-0.3067	0.8916	5.6424	6.5340	0.2575	1.4859
Te	-0.2262	0.8786	5.6424	6.5210	0.1900	1.9088
B	-0.3343	1.1206	5.6424	6.7630	0.2807	1.1804

APPENDIX D

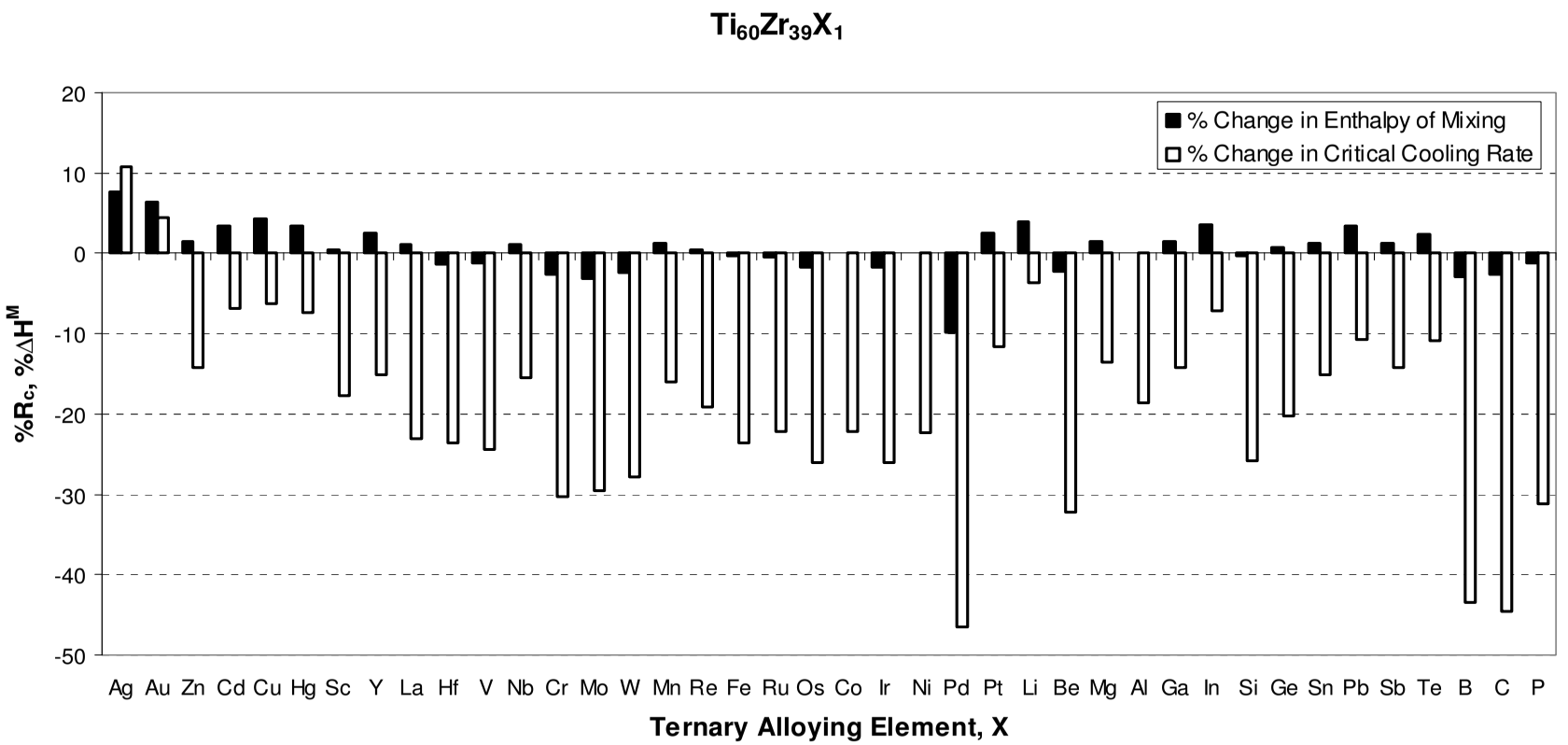

Figure D. 1 Percent changes in critical cooling rate and enthalpy of mixing for $Ti_{60}Zr_{40}$ binary alloy upon addition of 1 at % of X element instead of Zr.

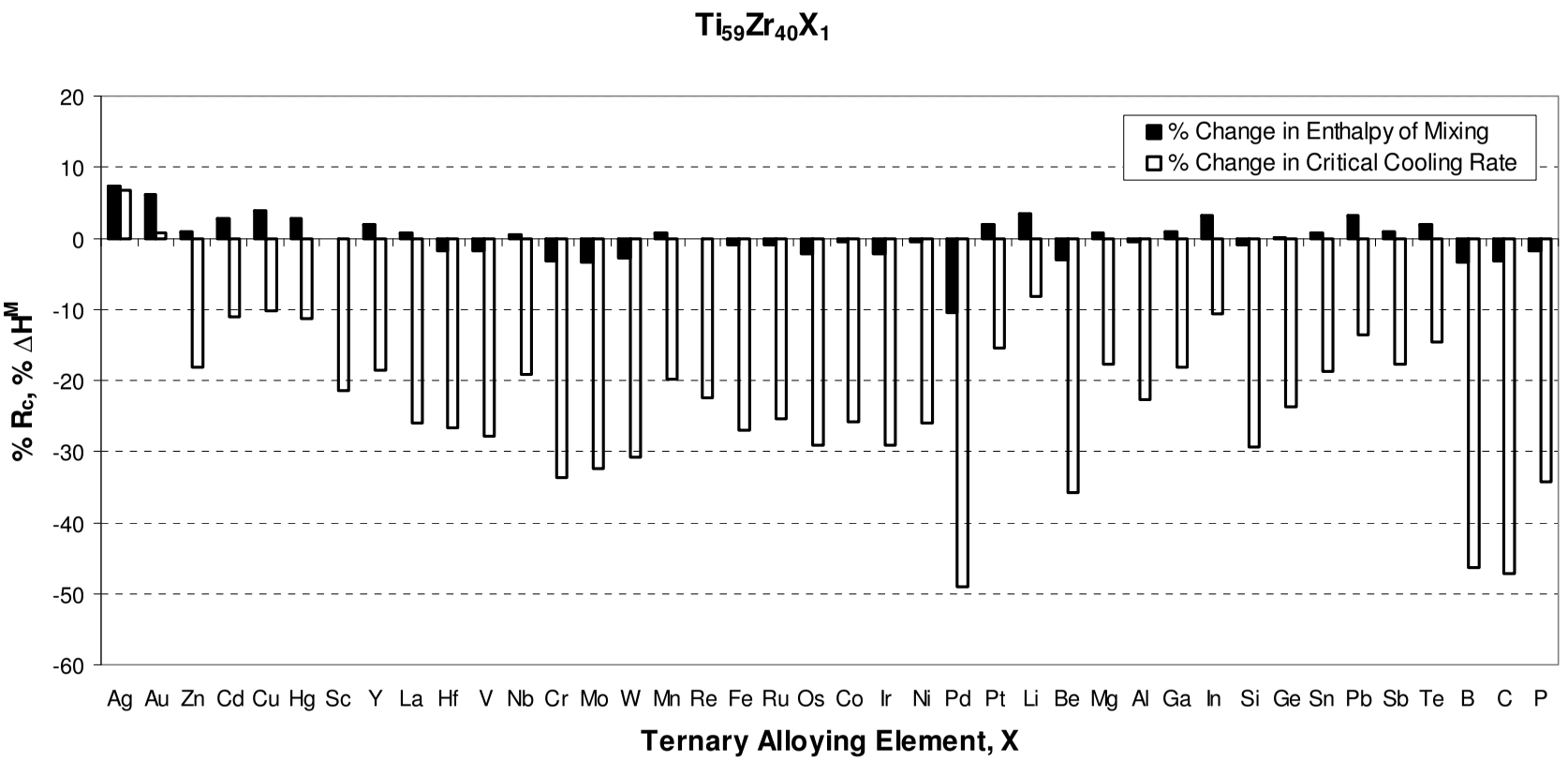

Figure D. 2 Percent changes in critical cooling rate and enthalpy of mixing for $Ti_{60}Zr_{40}$ binary alloy upon addition of 1 at % of X element instead of Ti.

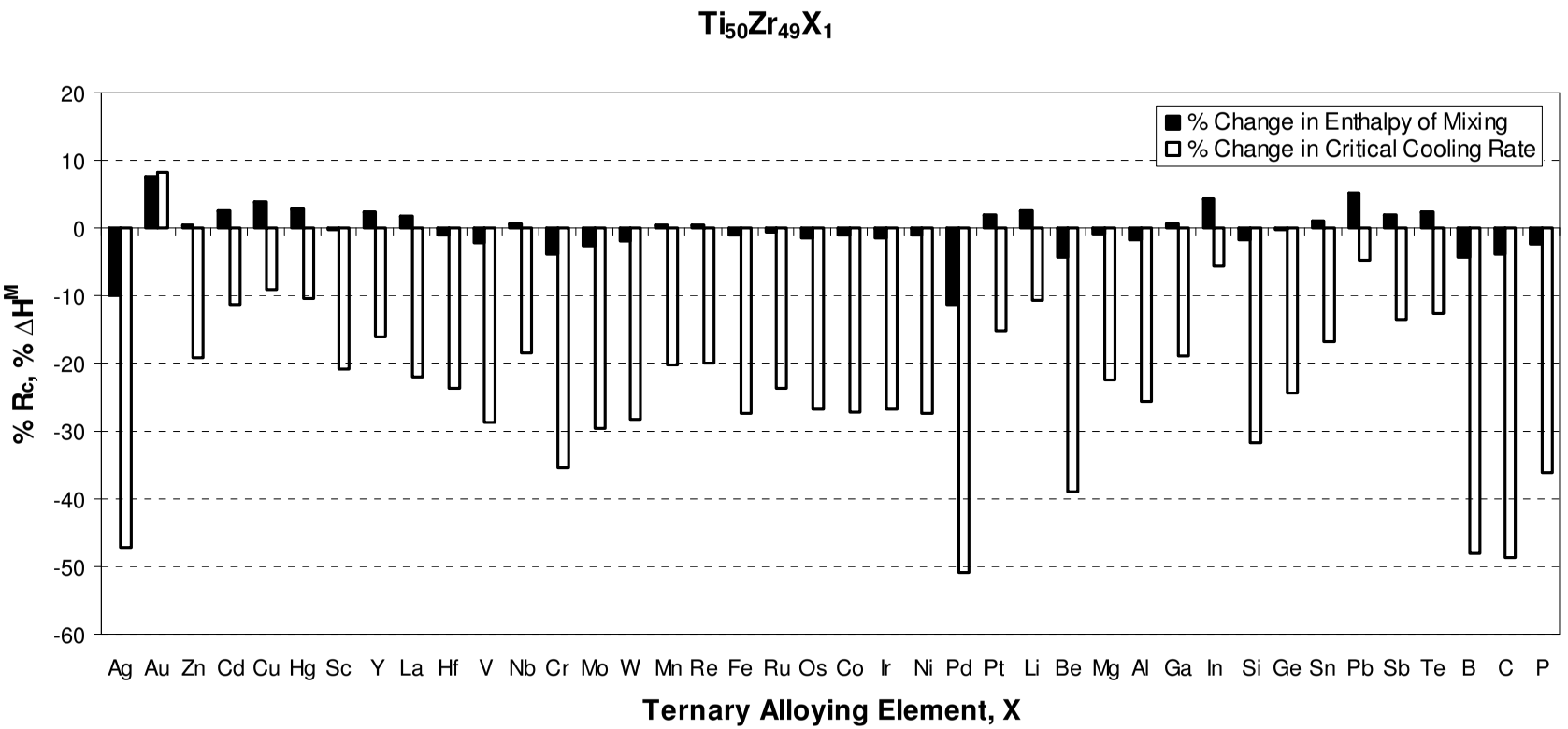

Figure D. 3 Percent changes in critical cooling rate and enthalpy of mixing for $Ti_{50}Zr_{50}$ binary alloy upon addition of 1 at % of X element instead of Zr.

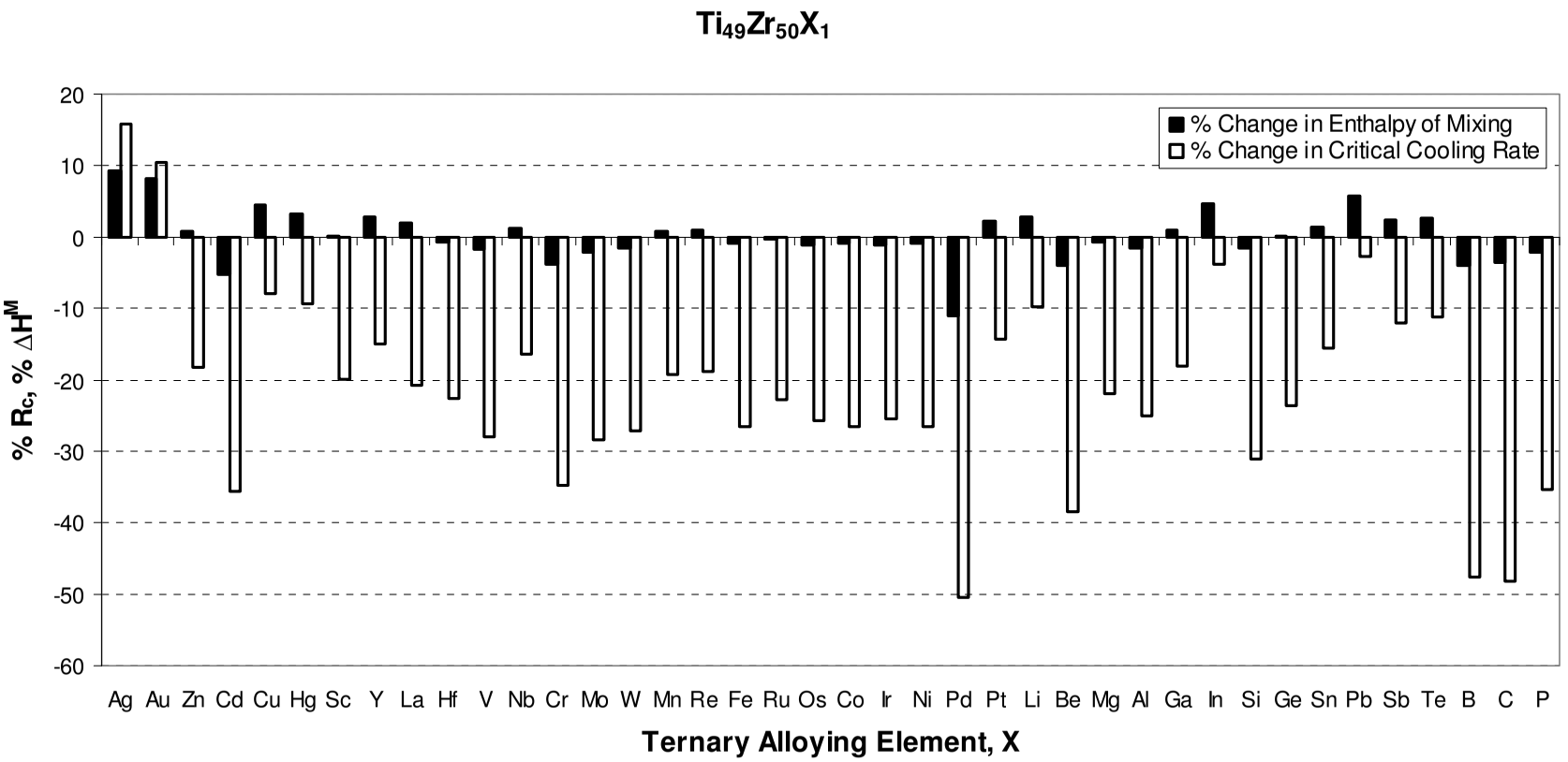

Figure D. 4 Percent changes in critical cooling rate and enthalpy of mixing for $Ti_{50}Zr_{50}$ binary alloy upon addition of 1 at % of X element instead of Ti.

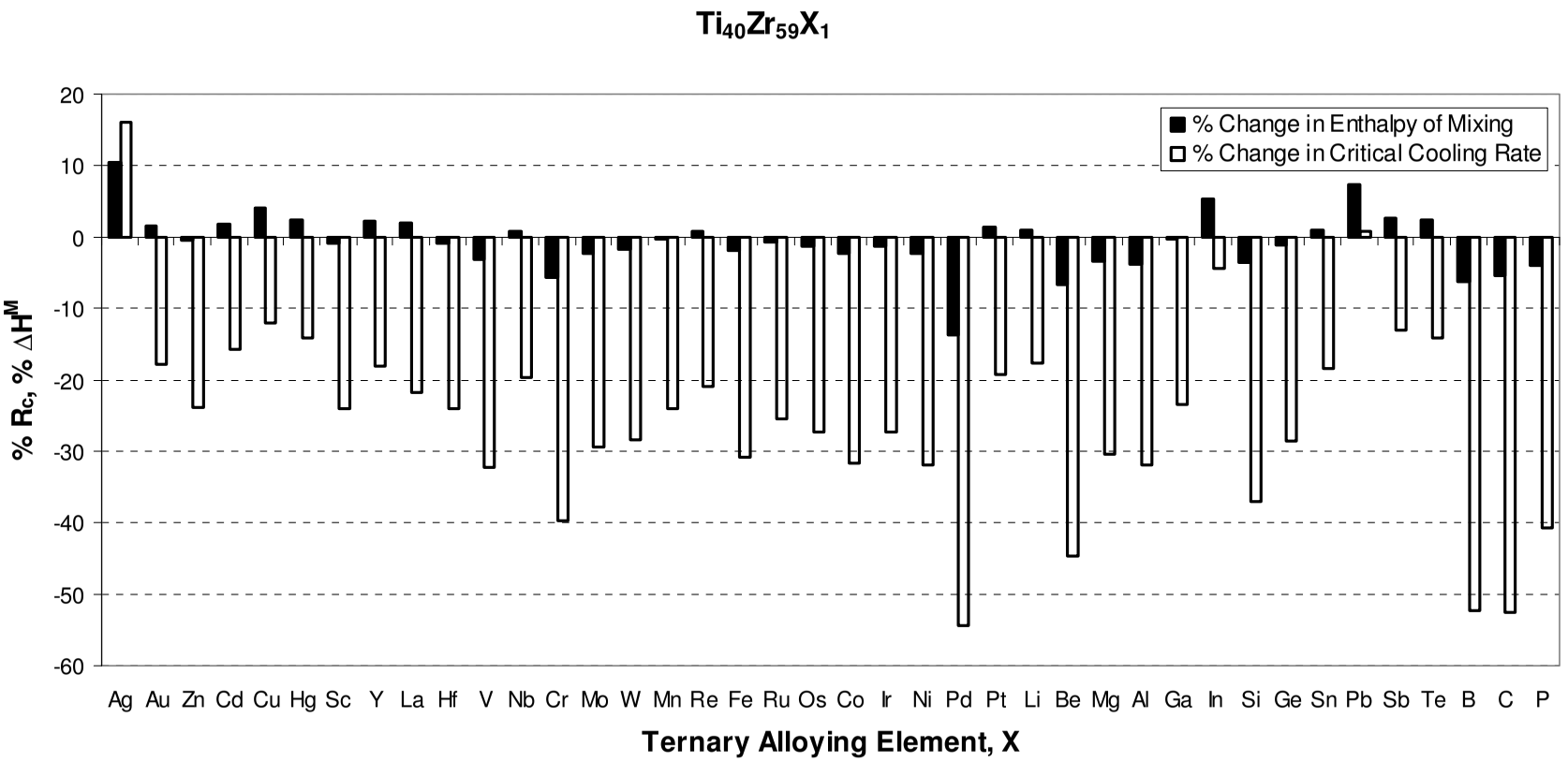

Figure D. 5 Percent changes in critical cooling rate and enthalpy of mixing for $Ti_{40}Zr_{60}$ binary alloy upon addition of 1 at % of X element instead of Zr.

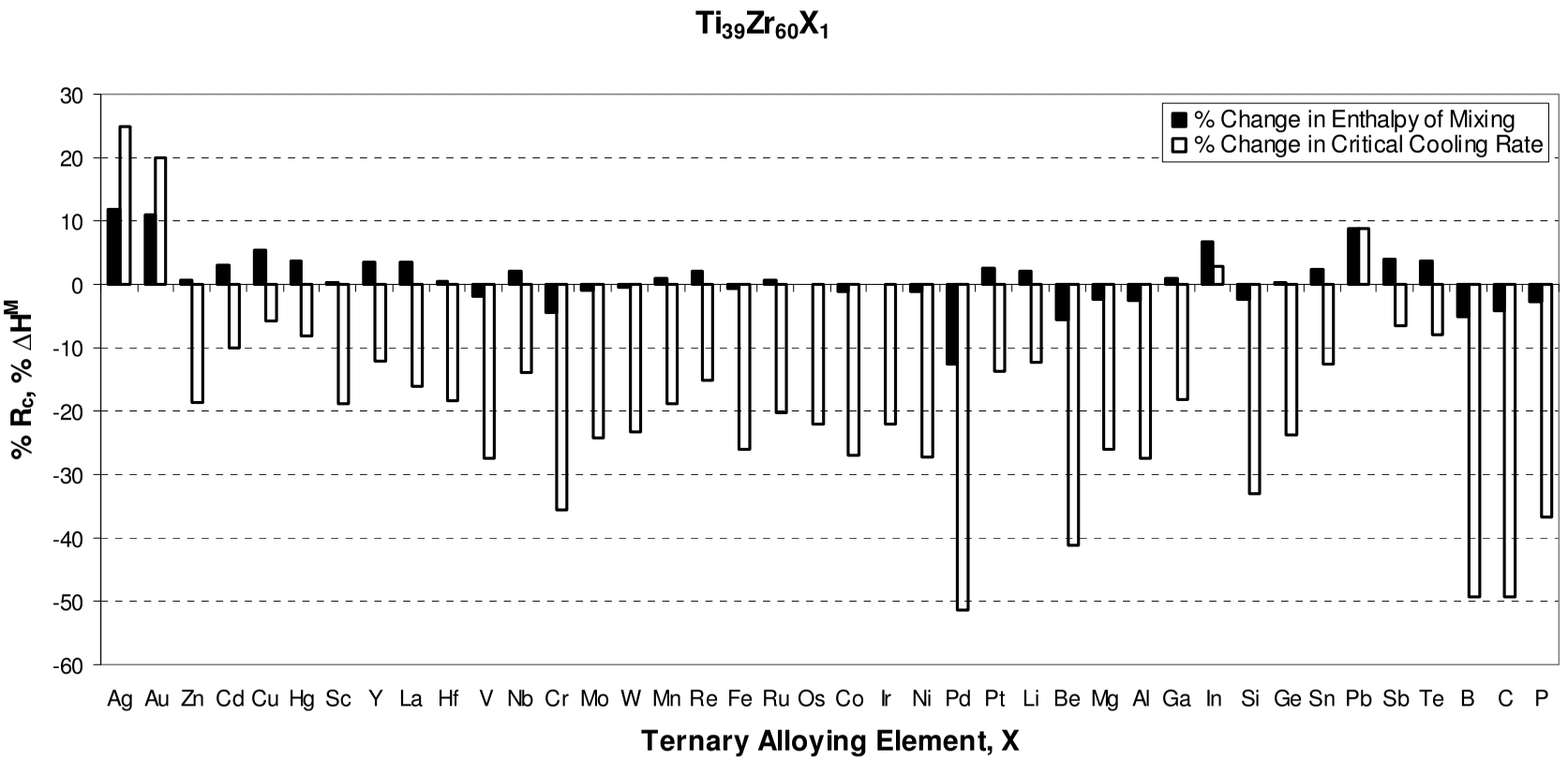

Figure D. 6 Percent changes in critical cooling rate and enthalpy of mixing for $Ti_{40}Zr_{60}$ binary alloy upon addition of 1 at % of X element instead of Ti.

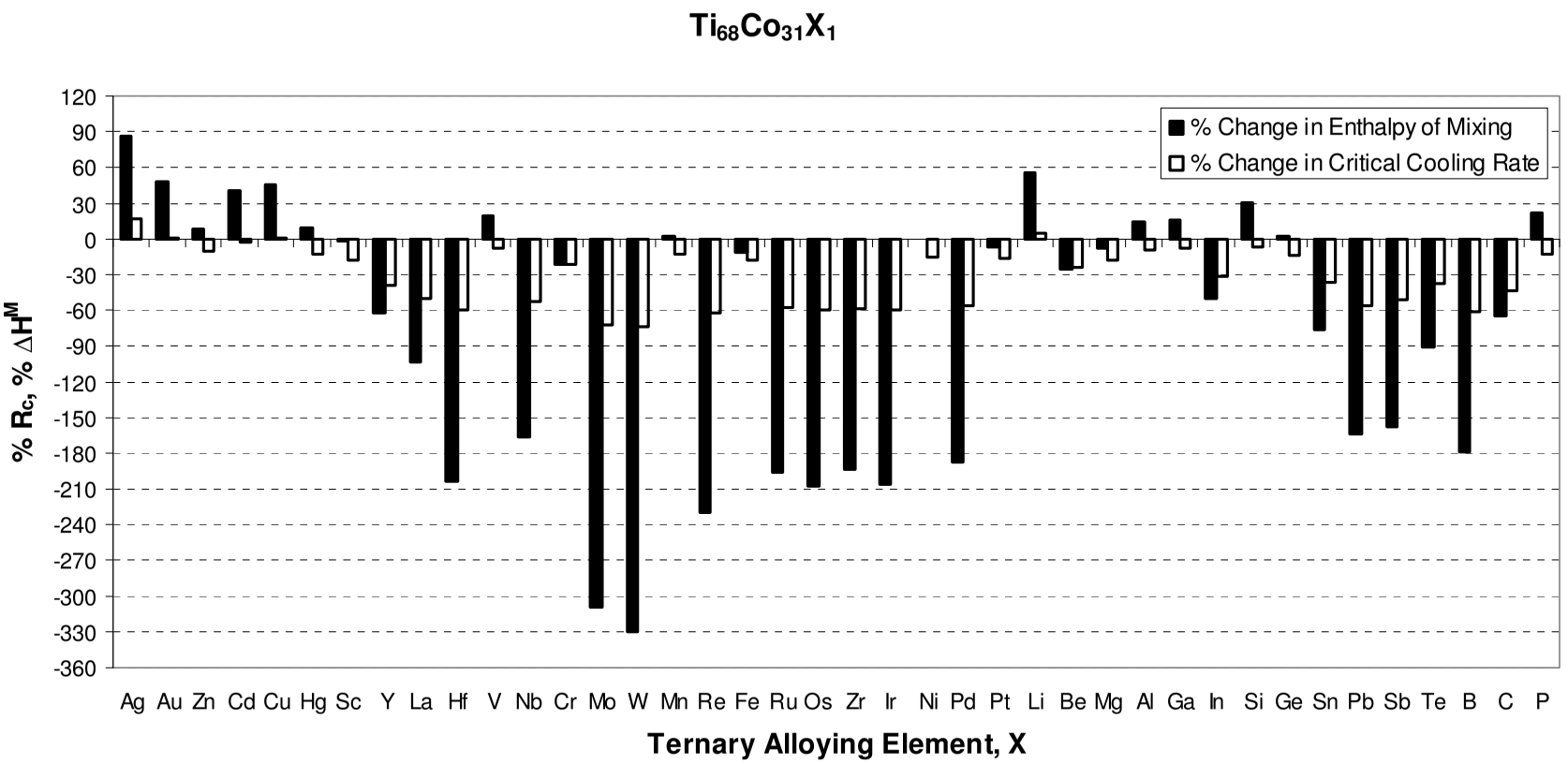

Figure D. 7 Percent changes in critical cooling rate and enthalpy of mixing for $Ti_{68}Co_{32}$ binary alloy upon addition of 1 at % of X element instead of Co.

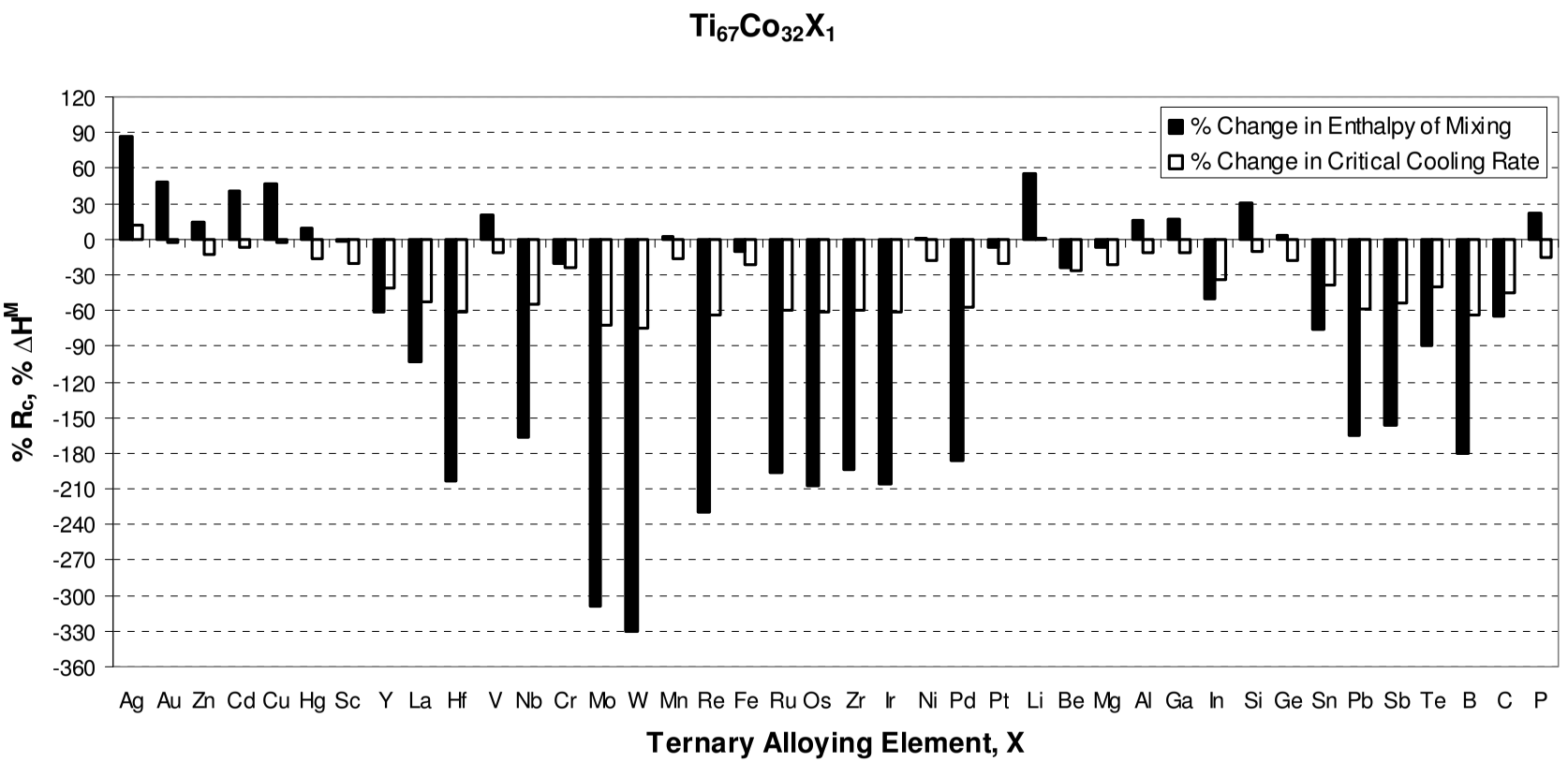

Figure D. 8 Percent changes in critical cooling rate and enthalpy of mixing for $Ti_{68}Co_{32}$ binary alloy upon addition of 1 at % of X element instead of Ti.